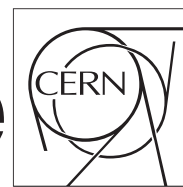


The Compact Muon Solenoid Experiment

CMS Draft Note

Mailing address: CMS CERN, CH-1211 GENEVA 23, Switzerland



2023/01/30

Archive Hash: 7d1c8f0-D

Archive Date: 2023/01/05

EFT interpretation of the top-quark-antiquark spin density matrix using the Run II dataset

Andre Zimermann-Santos, Alexander Grohsjean, Christian Schwanenberger¹ and Afiq Anuar²

¹ DESY

² CERN

Abstract

The multi-differential measurement of the spin-density matrix in the top-pair production is used to constrain the contributions of EFT couplings relevant to the top-pair production in the hadronic channel. The minimum χ^2 estimate of the normalised effective multi-differential cross-sections are used to set the constraints. A mapping between two basis of operators is verified in order to produce EFT predictions via Monte Carlo generation using the `dim6top` model. A posterior translation of the EFT limits using the same map also allows constraints to be given in terms of the two alternative EFT bases of operators.

This box is only visible in draft mode. Please make sure the values below make sense.

PDFAuthor:

Andre Zimermann-Santos

PDFTitle:

EFT interpretation of the top-quark-antiquark spin density matrix using the full Run II dataset

PDFSubject:

CMS

PDFKeywords:

CMS, your topics

Please also verify that the abstract does not use any user defined symbols

1 Contents

1	1	Introduction	1
2	2	Top EFT Basis Translation	4
3	2.1	MC sample for EFT map validation	7
4	2.2	Additional spin observables	8
5	3	Monte Carlo samples for EFT fit	35
6	4	EFT fit strategy	36
7	4.1	χ^2 minimisation	36
8	5	Conclusion and Outlook	37
9	6	Change Log	37
10	6.1	v1 to v2	37
11	A	Quantum field theory relations	38
12	A.1	Gamma matrices	38
13	A.2	Projection operators	39
14	A.3	Chiral decomposition of bilinears	39
15	B	A map between experiment-based EFT coefficients and Wilson Coefficients	40
16	B.1	Operators in $gg \rightarrow t\bar{t}$	41
17	B.2	Four-fermion operators in $q\bar{q} \rightarrow t\bar{t}$	48
18	B.3	Basis validation via Monte Carlo generation	52
19	C	Additional Information	56
20	C.1	Additional Spin Observables	56
21	C.2	Interpolation weights	70

23 1 Introduction

The aim of this study is to provide an EFT interpretation of the complete top quark-antiquark spin density matrix with two charged leptons in their final states with the full run-2 CMS data. For this purpose, first all relevant operators contributing to this process have to be identified and their contributions to the spin-related observables have to be understood. The final goal is to obtain constrains on all relevant dim-6 operators with their full inter-correlation. In this work those limits will be provided in two alternative EFT basis: 1) An experiment-based basis, where most EFT operators are naturally uncorrelated, being suitable for a low-dimensional fit over the EFT parameters. 2) A basis derived from the Warsaw basis used by the EFT UFO Model for Monte-Carlo (MC) generators `dim6top`. For the later, limits will be obtained from a linear map between experiment-based and the "dim6top" coefficients to be validated in this analysis note.

In order to perform a EFT fit over all EFT parameters on the CMS Data, MC templates for all EFT degrees of freedom must be provided for the measured observables. Ultimately, those are multi-differential distributions of all spin angular observables as a function of the reconstructed $t\bar{t}$ mass $M_{t\bar{t}}$ and the top scattering angle $\cos \Theta_t^*$ in the $t\bar{t}$ system. A definition of the spin angular observables can be found in [1]. The spin observables, due to angular momenta conservation, have the valuable property of being affected differently depending on the discrete symmetries present in the underlying interaction vertex producing the top pairs. This property is summarised in tab. 1. Here, we maintain the same definitions of [1] and, when convenient, new linear combinations of the spin observables are introduced, as in Section 2.2.

Discrete symmetries	Sensitive spin ang. observables
CP, P	$c_{Hel}, c_{kk} (c_{kk*}), c_{rr} (c_{rr*}), c_{nn}, c_{rk} + c_{kr} (c_{rk*} + c_{k*r})$
CP, \mathcal{P}	$b_k^1, b_r^1, b_k^2, b_r^2 (b_{k*}^a, b_{r*}^a, a = 1, 2)$
\mathcal{CP}, P	b_n^1, b_n^2
$\mathcal{CP}, \mathcal{P}$	$c_{nk} - c_{kn}, c_{nr} - c_{rn}$

Table 1: Discrete symmetries present at the of the top-pair production interaction vertex and the corresponding lepton angular observables which are affected by them. CP (P) stands for CP -even (P -even), while \mathcal{CP} (\mathcal{P}) stands for CP -odd (P -odd) interaction. For a definition of the lepton angular distribution, refer to [1]. Here, for shortness $b_i^a \equiv \cos \theta_a^i$, $c_{ij} \equiv \cos \theta_1^i \cos \theta_2^j$, $c_{Hel} \equiv \cos \varphi$, $a = 1, 2$ refers to charged leptons coming from a top (1) or an anti-top (2) decay, θ_i, θ_j , with i - or $j = k, r, n$, are the angles between charged leptons in the top pair rest frame with respect to the orthonormal basis k, r, n , following the convention of [1]. Distributions based on the modified axes k^* and r^* are equal $\pm k, \pm r$, depending on the sign of $|y_t| - |y_{\bar{t}}|$, the difference of the moduli of the top quark and antiquark rapidities in the laboratory frame. The use of the modified axes provides sensitivity to different combinations of four-quark operators.

44 Based on the identification of all relevant EFT contributions to the hadronic top pair production
 45 and neglecting the ones that affect only the pure gluon vertices, there are a total of 11 degrees
 46 of freedom that interfere with QCD at tree level[2]. Their properties in the experiment-based
 47 EFT basis are summarised in tab. 2. One can see that they cover all possible combinations of P -
 48 and CP -even and/or odd interactions. For the 4 fermion operators, they are further classified
 49 in according to their weak-isospin $I = 0$ and $I = 1$. Operators with weak-isospin 1 do not have
 50 pure P, CP -even or odd structures.

The EFT coefficients c_{tG} and c_{tG}^I parametrise the EFT interaction introduced by the non-hermitian operator

$$\mathcal{O}_{tG} = g_s \left(\bar{Q}_L \sigma^{\mu\nu} T^A t_R \right) \tilde{\varphi} G_{\mu\nu}^A. \quad (1)$$

51 The real part, c_{tG} , parametrises the coupling introduced by $\mathcal{O}_{tG} + \mathcal{O}_{tG}^\dagger$, while its imaginary part,
 52 c_{tG}^I , parametrises $\mathcal{O}_{tG} - \mathcal{O}_{tG}^\dagger$, after spontaneous symmetry breaking, where the only physical
 53 degree of freedom of the Higgs doublet $\tilde{\varphi}$ is given a vacuum expectation value $v/2$. Consider-
 54 ing that $\mathcal{O}_{tG} + \mathcal{O}_{tG}^\dagger$ introduces CP - and P -even interactions, while $\mathcal{O}_{tG} - \mathcal{O}_{tG}^\dagger$ CP - and P -odd
 55 ones, one can say that the coefficient c_{tG} parametrises CP - and P -even effects while c_{tG}^I CP - and
 56 P -odd ones. The full picture of the CP and P effects at differential cross-section level is more
 57 convolved. In order to see that, note from EFT Lagrangians in tab. 2 that c_{tG} and c_{tG}^I introduce the
 58 Feynman diagrams shown in fig. 1. They do not only interfere with standard SM $t\bar{t}$ production
 59 but also introduce quadratic pure EFT contributions.

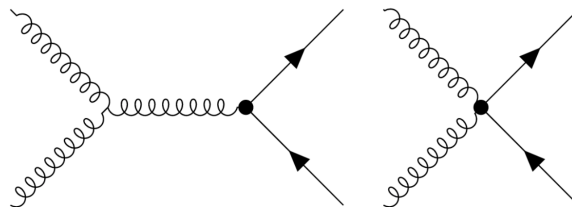


Figure 1: EFT interactions parametrised by the Wilson Coefficients c_{tG} and c_{tG}^I in $t\bar{t}$ production, which give rise to a EFT amplitude $\mathcal{M}_{c_{tG}^{(I)}}$.

Wilson-coefficients	EFT Lagragian	EFT Vertices	Disc. symmetries
$c_{tG} / \Lambda^2 (\propto \hat{\mu}_t)$	$g_s \frac{v}{\sqrt{2}} (\bar{t}\sigma^{\mu\nu} T^A t) G_{\mu\nu}^A$		CP, P
$c_{tG}^I / \Lambda^2 (\propto \hat{d}_t)$	$g_s \frac{v}{\sqrt{2}} (\bar{t}\sigma^{\mu\nu} \gamma_5 T^A t) G_{\mu\nu}^A$		$\mathcal{CP}, \mathcal{P}'$
c_{--} / Λ^2	$i(\bar{t}\gamma^\mu \gamma_5 T^A D^\nu t) G_{\mu\nu}^A + h.c.$	$gt\bar{t}, ggt\bar{t}$	$\mathcal{CP}, \mathcal{P}'$
c_{-+} / Λ^2	$i(\bar{t}\gamma^\mu T^A D^\nu t) G_{\mu\nu}^A - i h.c.$		\mathcal{CP}, P
c_{VV} / Λ^2	$(\bar{q}\gamma^\mu T^A q)(\bar{t}\gamma_\mu T^A t)$		CP, P, $I = 0$
c_{VA} / Λ^2	$(\bar{q}\gamma^\mu T^A q)(\bar{t}\gamma_\mu \gamma_5 T^A t)$		CP, $\mathcal{P}', I = 0$
c_{AV} / Λ^2	$(\bar{q}\gamma^\mu \gamma_5 T^A q)(\bar{t}\gamma_\mu T^A t)$		CP, $\mathcal{P}', I = 0$
c_{AA} / Λ^2	$(\bar{q}\gamma^\mu \gamma_5 T^A q)(\bar{t}\gamma_\mu \gamma_5 T^A t)$	$q\bar{q}t\bar{t}$	CP, P, $I = 0$
c_1 / Λ^2	$\left[(\bar{q}\gamma^\mu T^A \sigma_3 q)(\bar{t}\gamma_\mu T^A t) + (\bar{q}\gamma^\mu \gamma_5 T^A \sigma_3 q)(\bar{t}\gamma_\mu T^A t) \right]$		CP, $I = 1$
c_2 / Λ^2	$\left[(\bar{q}\gamma^\mu \gamma_5 T^A \sigma_3 q)(\bar{t}\gamma_\mu \gamma_5 T^A t) - (\bar{q}\gamma^\mu \gamma_5 T^A \sigma_3 q)(\bar{t}\gamma_\mu T^A t) \right]$		CP, $I = 1$
c_3 / Λ^2	$\left[(\bar{q}\gamma^\mu T^A \sigma_3 q)(\bar{t}\gamma_\mu \gamma_5 T^A t) + (\bar{q}\gamma^\mu \gamma_5 T^A \sigma_3 q)(\bar{t}\gamma_\mu T^A t) \right]$		CP, $I = 1$

Table 2: EFT degrees of freedom (Wilson-coefficients in the first column and operators in the second one) entering at the hadronic top pair production at tree level, together with the vertices they may introduce (third column) and their properties with respect to the discrete symmetries CP, P and weak-isospin I (fourth column). CP (P) stands for CP-even (P-even), while \mathcal{CP} (\mathcal{P}') stands for CP-odd (P-odd) behaviour.

c_i/Λ^2	Disc. symmetries	Sensitive spin ang. obs.
c_{tG} / Λ^2	CP, P	$c_{Hel}, c_{kk}, c_{rr}, c_{nn}, c_{rk} + c_{kr}$
c_{tG}^I / Λ^2	$\mathcal{CP}, \mathcal{P}$	$c_{nk} - c_{kn}, c_{nr} - c_{rn}$
c_{VV} / Λ^2	CP, P	$c_{kk}, c_{rr}, c_{nn}, c_{rk} + c_{kr},$
c_{VA} / Λ^2	CP, \mathcal{P}	$b_k^a, b_r^a, (a = 1, 2)$
c_{AV} / Λ^2	CP, \mathcal{P}	$b_{k*}^a, b_{r*}^a, (a = 1, 2)$
c_{AA} / Λ^2	CP, P	$c_{kk*}, c_{rr*}, c_{rk*} + c_{k*r}$
c_1 / Λ^2	CP	$c_{Hel}, c_{kk}, c_{rr}, c_{nn}, c_{rk} + c_{kr},$
c_3 / Λ^2	CP	$b_k^a, b_r^a, (a = 1, 2)$
$(c_1 - c_2 - c_3) / \Lambda^2$	CP	$b_{k*}^a, b_{r*}^a, (a = 1, 2)$

Table 3: Linear EFT couplings (first column) and the corresponding discrete symmetries at differential cross-section level (second column), which determine the sensitive lepton angular observables (third column). CP (P) stands for CP -even (P -even), while \mathcal{CP} (\mathcal{P}) stands for CP -odd (P -odd) behaviour. For a definition of the lepton angular distribution, refer to [1]. Here, for shortness $b_i^a \equiv \cos \theta_a^i$, $c_{ij} \equiv \cos \theta_1^i \cos \theta_2^j$, $c_{Hel} \equiv \cos \varphi$. $a = 1, 2$ refers to charged leptons coming from a top (1) or an anti-top (2) decay. θ_i, θ_j , with i - or $j = k, r, n$ are the angles between charged leptons in the top pair rest frame with respect to the orthonormal basis k, r, n , following the convention of [1].

For the general mechanism of how it works, consider arbitrary EFT operators c_i 's. The squared matrix element is given by

$$|\mathcal{M}_{EFT}|^2(z) = |\mathcal{M}_{SM}|^2(z) + \sum_i \frac{c_i}{\Lambda^2} 2\text{Re}\mathcal{M}_{SM}^\dagger(z)\mathcal{M}_{c_i}(z) + \sum_{i,j} \frac{c_i c_j}{\Lambda^4} 2\text{Re}\mathcal{M}_{c_i}^\dagger(z)\mathcal{M}_{c_j}(z). \quad (2)$$

where z are all parton's four-momenta. The squared amplitude $|\mathcal{M}_{SM}|^2$ contains all the Standard Model $t\bar{t}$ processes. Feynman diagrams, such as the ones in fig. 1 will enter in the squared matrix element as \mathcal{M}_{c_i} . Hence, $\mathcal{M}_{SM}^\dagger \mathcal{M}_{c_i}$ gives the SM-EFT interference terms and $\mathcal{M}_{c_i}^\dagger \mathcal{M}_{c_j}$ are pure EFT quadratic contributions. The QCD $t\bar{t}$ production vertices are CP -, P -even in the SM. Therefore the SM amplitudes considered in this work introduces only P - and CP -even effects. Because terms with a given P - and CP - symmetry when multiplied by a P - and CP -even one will maintain their original symmetry, $\mathcal{M}_{SM}^\dagger \mathcal{M}_{c_i}$ effectively introduces P -, CP - effects of \mathcal{M}_{c_i} , i.e. those parametrised by c_i . By similar arguments, the symmetries introduced by the quadratic pure EFT terms can be found. In fact, they are not necessarily the same as the ones introduced by the interference terms. For example, for a CP -, P -odd coupling, such as c_{tG}^I , the SM-interference adds CP -, P -odd effects while its squared contribution $(c_{tG}^I/\Lambda^2)^2 |\mathcal{M}_{c_{tG}^I}|^2$, having squared CP -, P -odd contributions, results in CP -, P -even effects. Knowing that differential cross-sections are proportional to the squared matrix elements, expected effects on observables can be put together by these means. In the spin observables they are summarised for the interference terms in tab. 3, and for quadratic terms containing identical Wilson Coefficients in tab. 4.

2 Top EFT Basis Translation

Fixed-order theory calculations predicting the EFT effects of the operators relevant to our study are limited. For example, in [2] they are only available for differential 1-D observables and are based on the linear approximation, i.e. the quadratic EFT terms are completely neglected. Therefore, we can only rely on the prediction of multi-differential distributions using MC techniques to fully capture the EFT effects. This is challenging because, on the one hand, the

$(c_i/\Lambda^2)^2$	Disc. symmetries	Sensitive spin ang. obs.
$(c_{tG} / \Lambda^2)^2$	CP, P	$c_{Hel}, c_{kk}, c_{rr}, c_{nn}, c_{rk} + c_{kr}$
$(c_{tG}^I / \Lambda^2)^2$	CP, P	$c_{Hel}, c_{kk}, c_{rr}, c_{nn}, c_{rk} + c_{kr}$
$(c_{VV} / \Lambda^2)^2$	CP, P	$c_{Hel}, c_{kk}, c_{rr}, c_{nn}, c_{rk} + c_{kr}$
$(c_{VA} / \Lambda^2)^2$	CP, P	$c_{Hel}, c_{kk}, c_{rr}, c_{nn}, c_{rk} + c_{kr}$
$(c_{AV} / \Lambda^2)^2$	CP, P	$c_{Hel}, c_{kk}, c_{rr}, c_{nn}, c_{rk} + c_{kr}$
$(c_{AA} / \Lambda^2)^2$	CP,P	$c_{Hel}, c_{kk}, c_{rr}, c_{nn}, c_{rk} + c_{kr}$
$(c_1 / \Lambda^2)^2$	CP	$c_{Hel}, c_{kk}, c_{kk*}, c_{rr}, c_{nn}, c_{rk*} + c_{k*}$
$(c_3 / \Lambda^2)^2$	CP	$c_{Hel}, b_{k*}^a, b_{r*}^a \quad (a = 1, 2), c_{kk}, c_{rr}, c_{nn}, c_{rk} + c_{kr},$ $c_{Hel}, b_k^a, b_r^a \quad (a = 1, 2), c_{kk}, c_{rr}, c_{nn}, c_{rk} + c_{kr},$
$((c_1 - c_2 - c_3) / \Lambda^2)^2$	CP	

Table 4: Squared EFT couplings (first column) and the corresponding discrete symmetries of their differential cross-section terms (second column), which determine the sensitive lepton angular observables (third column). CP (P) stands for CP -even (P -even), while \mathcal{CP} (\mathcal{P}) stands for CP -odd (P -odd) behaviour. CP (P) stands for CP -even (P -even), while \mathcal{CP} (\mathcal{P}) stands for CP -odd (P -odd) behaviour. For a definition of the lepton angular distribution, refer to [1]. Here, for shortness $b_i^a \equiv \cos \theta_a^i$, $c_{ij} \equiv \cos \theta_1^i \cos \theta_2^j$, $c_{Hel} \equiv \cos \varphi$. $a = 1, 2$ refers to charged leptons coming from a top (1) or an anti-top (2) decay. θ_i, θ_j , with i - or $j = k, r, n$ are the angles between charged leptons in the top pair rest frame with respect to the orthonormal basis k, r, n , following the convention of [1].

82 experiment-based coefficients basis in tab. 2 naturally uncorrelates their Wilson coefficients
 83 by looking at the right observables. On the other hand, there are not UFO EFT models imple-
 84 mented in terms of the experiment-based coefficients for MC generators. The MC models are
 85 usually parametrised in an EFT basis derived from the Warsaw basis of the dim-6 operators
 86 with added gauge symmetries assumptions, as it is the case of `dim6top`. However, in such
 87 bases the four-fermion operators introduce mixed CP -, P - odd effects, affecting a larger number
 88 of the spin observables. For this reason, EFT operators are all intercorrelated in these bases
 89 and a fit would have to take that into account. We aim to tackle this issue by first finding a
 90 valid EFT mapping between the two bases. Then, one can use the map to do MC predictions
 91 for the experiment-based EFT parameters, while providing as input to the MC generators the
 92 correct combination of `dim6top` parameters that results in the experiment-based EFT coupling
 93 of interest.

Following theoretical studies done by the authors of this AN, based on [2], [3], [4], we summarise the following basis translation between the Wilson coefficients of the Warsaw-basis

based operators and the experiment-based operators.

$$c_{-+} = \sum_{a=1,2} (c_{uG}^{I(a3)} - c_{uG}^{I(3a)})/2, \quad (3)$$

$$c_{--} = c_{tG}^I + \sum_{a=1,2} (c_{uG}^{I(a3)} + c_{uG}^{I(3a)})/2, \quad (4)$$

$$c_{VV} = (c_{tq}^8 + c_{Qq}^{(8,1)})/2 + (c_{tu}^8 + c_{td}^8 + c_{Qu}^8 + c_{Qd}^8)/4, \quad (5)$$

$$c_{AA} = -(c_{tq}^8 - c_{Qq}^{(8,1)})/2 + (c_{tu}^8 + c_{td}^8 - c_{Qu}^8 - c_{Qd}^8)/4, \quad (6)$$

$$c_{VA} = (c_{tq}^8 - c_{Qq}^{(8,1)})/2 + (c_{tu}^8 + c_{td}^8 - c_{Qu}^8 - c_{Qd}^8)/4, \quad (7)$$

$$c_{AV} = -(c_{tq}^8 + c_{Qq}^{(8,1)})/2 + (c_{tu}^8 + c_{td}^8 + c_{Qu}^8 + c_{Qd}^8)/4, \quad (8)$$

$$c_1 = (c_{tu}^8 - c_{td}^8)/2 + (c_{Qu}^8 - c_{Qd}^8)/2 + c_{Qq}^{(8,3)}, \quad (9)$$

$$c_2 = (c_{tu}^8 - c_{td}^8)/2 - (c_{Qu}^8 - c_{Qd}^8)/2 + c_{Qq}^{(8,3)}, \quad (10)$$

$$c_3 = (c_{tu}^8 - c_{td}^8)/2 - (c_{Qu}^8 - c_{Qd}^8)/2 - c_{Qq}^{(8,3)}. \quad (11)$$

Note the convention of adding an implicit choice of scale $\Lambda = m_t/g_s$ by [2]. With that, our parameters relates by theirs by

$$\hat{c}_i = \frac{m_t^2}{g_s^2} (c_i/\Lambda^2). \quad (12)$$

Additionally, the anomalous chromo-magnetic and chromo-electric dipole moments of the top quark as in [2], can be recovered from:

$$\hat{\mu}_t = 2m_t^2 (c_{tG}/\Lambda^2), \quad (13)$$

$$\hat{d}_t = 2m_t^2 (c_{tG}^I/\Lambda^2). \quad (14)$$

$$(15)$$

With this information, limits present in that convention, such as in [1] can be converted to the

`dim6top` basis by the relations:

$$c_{uG}^{I(13)}/\Lambda^2 = \frac{g_s^2}{2m_t^2} \left(\hat{c}_{-+} + (\hat{c}_{--} - \hat{d}_t) \right), \quad (16)$$

$$c_{uG}^{I(3a)}/\Lambda^2 = -\frac{g_s^2}{2m_t^2} \left(\hat{c}_{-+} - (\hat{c}_{--} - \hat{d}_t) \right), \quad (17)$$

$$c_{tq}^8/\Lambda^2 = \frac{g_s^2}{2m_t^2} (\hat{c}_{VV} - \hat{c}_{AA} + \hat{c}_{AV} - \hat{c}_{VA}), \quad (18)$$

$$c_{Qq}^{(8,1)}/\Lambda^2 = \frac{g_s^2}{2m_t^2} (\hat{c}_{VV} + \hat{c}_{AA} - \hat{c}_{AV} - \hat{c}_{VA}), \quad (19)$$

$$c_{tu}^8/\Lambda^2 = \frac{g_s^2}{2m_t^2} (\hat{c}_{VV} + \hat{c}_{AA} + \hat{c}_{AV} + \hat{c}_{VA} + \hat{c}_1 + \hat{c}_3), \quad (20)$$

$$c_{td}^8/\Lambda^2 = \frac{g_s^2}{2m_t^2} (\hat{c}_{VV} + \hat{c}_{AA} + \hat{c}_{AV} + \hat{c}_{VA} - \hat{c}_1 - \hat{c}_3), \quad (21)$$

$$c_{Qu}^8/\Lambda^2 = \frac{g_s^2}{2m_t^2} (\hat{c}_{VV} - \hat{c}_{AA} - \hat{c}_{AV} + \hat{c}_{VA} + \hat{c}_1 - \hat{c}_2), \quad (22)$$

$$c_{Qd}^8/\Lambda^2 = \frac{g_s^2}{2m_t^2} (\hat{c}_{VV} - \hat{c}_{AA} - \hat{c}_{AV} + \hat{c}_{VA} - \hat{c}_1 + \hat{c}_2), \quad (23)$$

$$c_{Qq}^{(8,3)}/\Lambda^2 = \frac{g_s^2}{2m_t^2} (\hat{c}_2 - \hat{c}_3). \quad (24)$$

It is important to note that [2] only includes the first generation of light quarks in their analytical predictions for the experiment-based parameters. They then rely on the assumption that the EFT contributions of the first and second generation are at least of the same order, but the second generation is highly suppressed by the PDFs. For eqs. 17 and 18 where we can explicitly choose the first family of quarks, the relation between `dim6top` and their predictions is exact. For the four-quark operators, the `dim6top` predictions differ from [2] by including small corrections from the second generation of quarks in the matrix element calculation.

Details of how we found those relationship can be found in Appendix D. We verify the map with MC samples in order to use it later to produce EFT templates for our fits. The flavour-changing neutral current (FCNC) operators, parameterised by $c_{uG}^{I(13)}$ and $c_{uG}^{I(31)}$, cannot appear in $t\bar{t}$ with a single vertex within `dim6top`. Hence, we are not able to provide MC predictions for c_{-+} and c_{--} and they will be disregarded from our study.

2.1 MC sample for EFT map validation

In order to validate the coefficients translation, we need predictions based on `dim6top` that have as input all the Wilson coefficient combinations, each of which yields only one non-vanishing experiment-based EFT coefficient at a time. Since MC events give the full EFT prediction, *i.e.* both the SM-interference and the pure EFT, one must be able to extract the linear and quadratic terms from the predictions. Only by doing so, one can analyse its effects,. That is step is performed via a quadratic interpolation. Only then can one verify whether the correct CP and P properties of the experiment-based operators are recovered from the map, by looking at the correct spin observables.

The fact that the EFT description is quadratic on the Wilson coefficients (WCs) c_i 's means that for each individual EFT operator contribution, three MC templates (different values of c_i) are

sufficient to perform a quadratic interpolation. The interpolation can be done bin-by-bin based on normalised distributions to extract the shapes of the linear and quadratic EFT terms. One can use, for instance, SM as a common hypothesis for the interpolation of each EFT operator and therefore only further two MC templates are needed for each operator. We have used this information to create private MC templates for the 9 identified relevant experiment-based EFT coefficients. The process produced is 100M events of $t\bar{t} \rightarrow W^+ bW^- \bar{b}$ from a proton-proton collision in which the $W^{+(-)}$ decays into $\ell^+ \bar{\nu}_\ell (\ell^- \nu_\ell)$. Top-pairs are produced with LO QCD precision. The decay is fully done within `MadGraph`. Charged leptons ℓ consist of electrons and muons only and the five-quark flavour scheme for PDFs is used. The hard interaction is parameterised by the parton density functions (PDFs) provided by the library `LHAPDF 6.2.1` [5]. The hadronisation and parton shower steps were performed using `PYTHIA 8` [6]. The production and decay matrix elements were fully computed by `MadGraph5_aMC@NLO 2.6.1` [7] for the SM hypothesis. This was used as the baseline for event generation and the matrix element reweighting method from `MadGraph` was used to generate the 9×2 necessary EFT templates for the theory space interpolation.

The samples are analysed at parton level and the normalised differential distributions are computed. The linear and quadratic EFT contributions in the top pair production extracted from the histograms via quadratic interpolation are shown in figs. 2 to ???. There one can see how they compare with our the SM prediction at LO QCD accuracy. Once, the interpolation is performed, one can extrapolate the predictions for the full phase space of Wilson coefficients. In order to see a clear sensitivity, shown as a clear shape variation, we extrapolate our templates to artificially large values of the experiment-based coefficients ($c/\Lambda^2 = 15$). One can see that the linear and quadratic contributions recover the effects summarised in tabs. 3 and 4. Because samples were generated in `MadGraph` with the combinations of `dim6top-WCs` which result in the pure EFT experiment-based EFT coefficients, the correct behaviour recovered plots validates the translation between the `dim6top` and the experiment-based parameters.

2.2 Additional spin observables

Motivated by the definition of $c_{Hel} = c_{kk} + c_{rr} + c_{nn}$, we have also present the results in terms of variations of the distributions mentioned in 2 which are linearly related to them, but have the experimental advantage in the unfolded measurements of having a linear shape. Those linearly related to c_{kk} , c_{rr} , c_{nn} are

$$c_{Han} = c_{kk} - c_{rr} - c_{nn} \text{ (hardness is flipped)}, \quad (25)$$

$$c_{Sca} = -c_{kk} + c_{rr} - c_{nn} \text{ (scatering plane is flipped)}, \quad (26)$$

$$c_{Tra} = -c_{kk} + c_{rr} - c_{nn} \text{ (transverse plane is flipped)}, \quad (27)$$

$$c_{kk*L} = -c_{kk*} - c_{rr} - c_{nn}, \quad (28)$$

$$c_{rr*} = -c_{kk} - c_{rr*} - c_{nn}, \quad (29)$$

$$(30)$$

those linearly related with 10 cross-terms $c_{ij} \pm c_{ij}$ are

$$c_{nr}^\pm = -c_{kk} - (c_{nr} \pm c_{nr}), \quad (31)$$

$$c_{nk}^\pm = -c_{rr} - (c_{nk} \pm c_{nk}), \quad (32)$$

$$c_{rk}^\pm = -c_{nn} - (c_{rk} \pm c_{kr}), \quad (33)$$

$$c_{rk*}^\pm = -c_{nn} - (c_{rk*} \pm c_{k*r}), \quad (34)$$

$$c_{r*k}^\pm = -c_{nn} - (c_{r*k} \pm c_{kr*}). \quad (35)$$

$$(36)$$

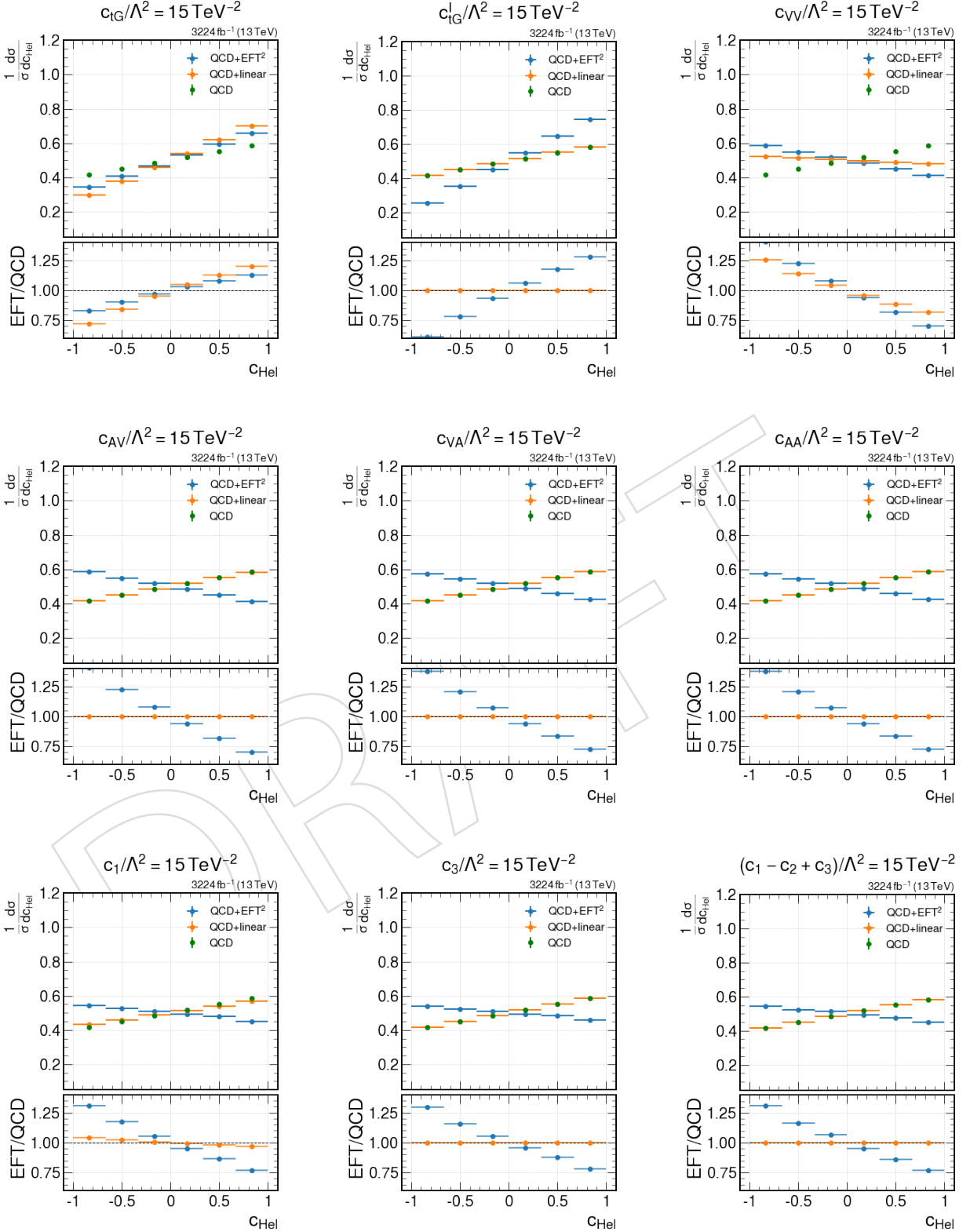


Figure 2: Lepton angular distribution showing the linear and quadratic contributions of each experiment-based EFT coefficients compared to the LO-SM contribution.

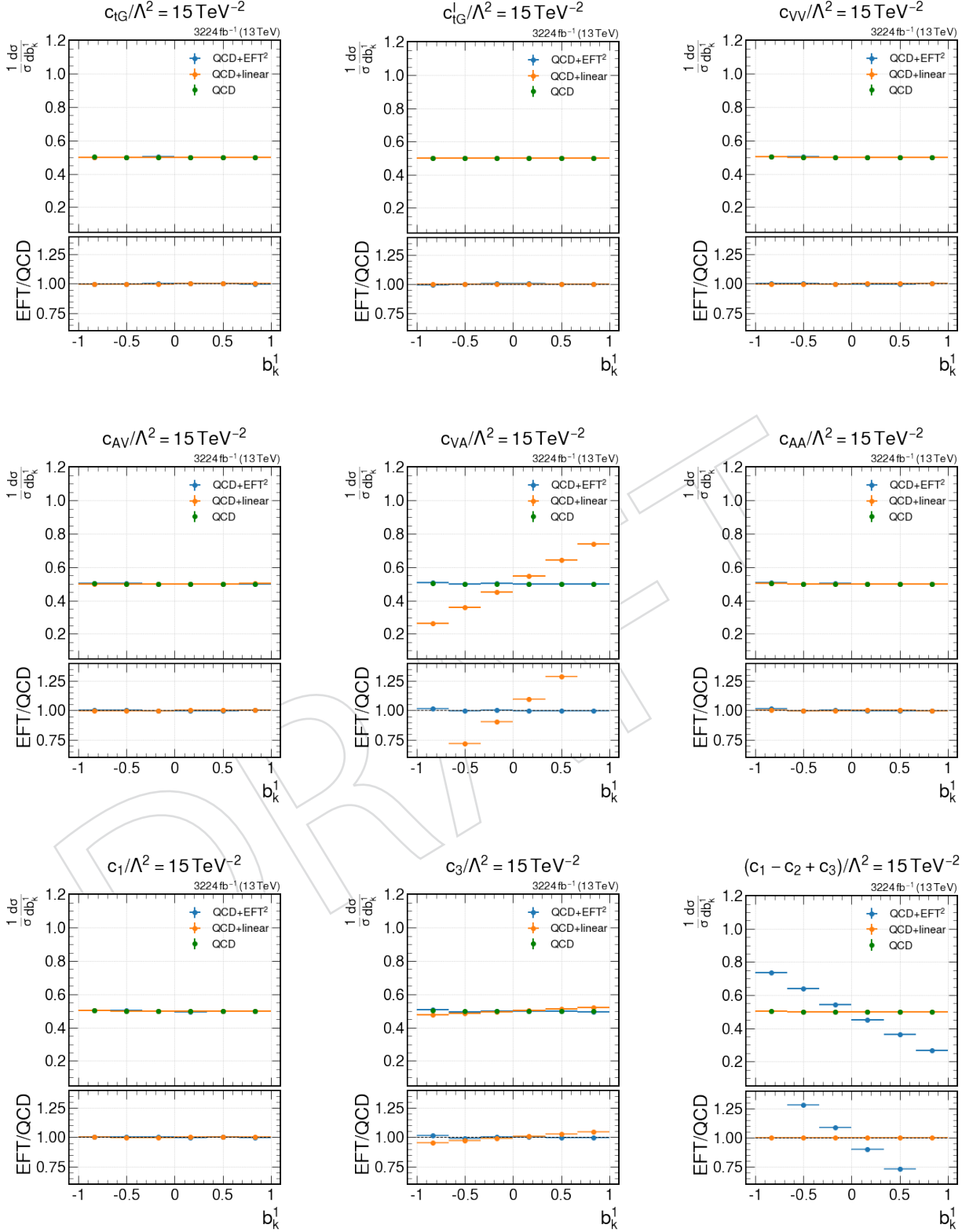


Figure 3: Lepton angular distribution showing the linear and quadratic contributions of each experiment-based EFT coefficients compared to the LO-SM contribution.

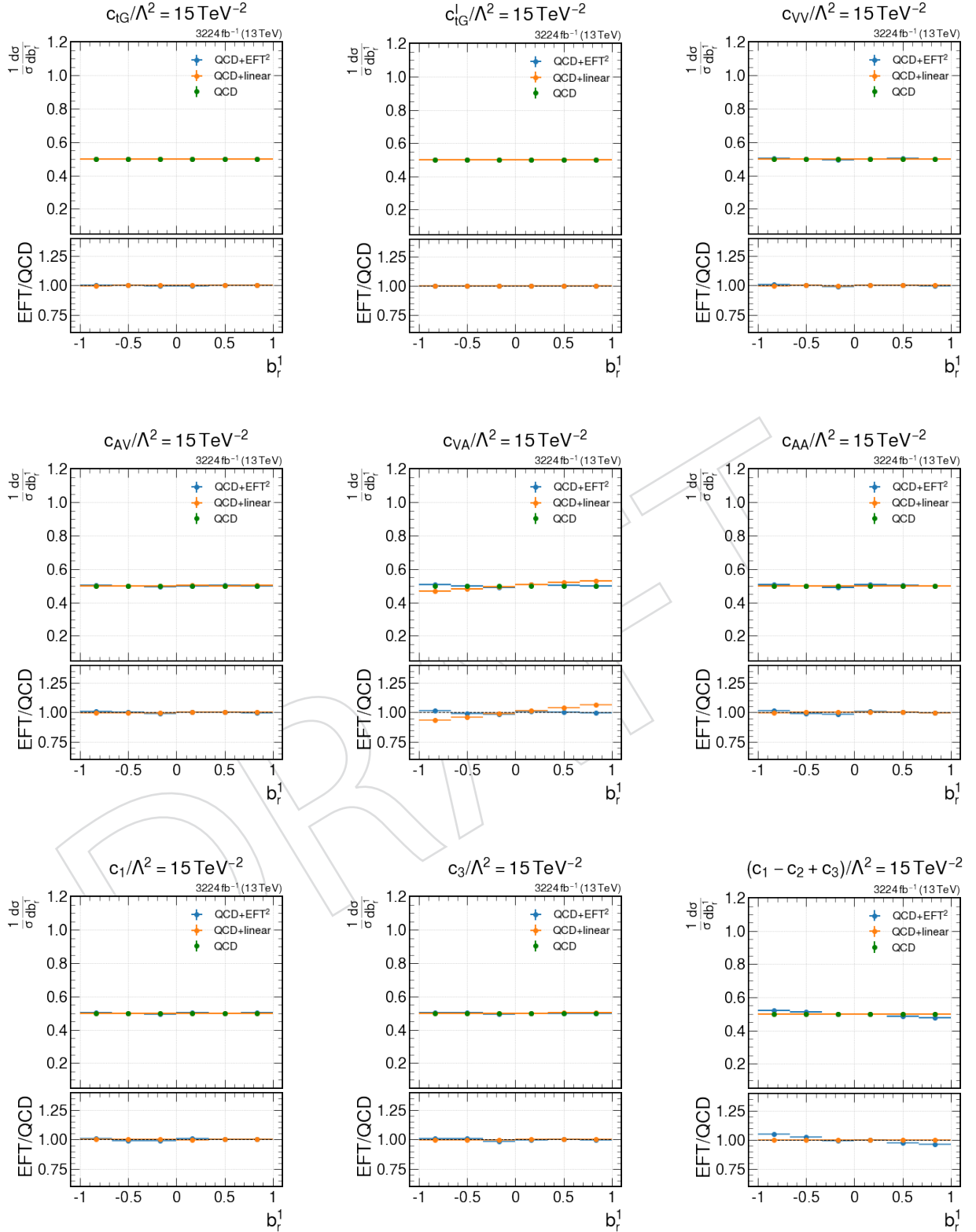


Figure 4: Lepton angular distribution showing the linear and quadratic contributions of each experiment-based EFT coefficients compared to the LO-SM contribution.

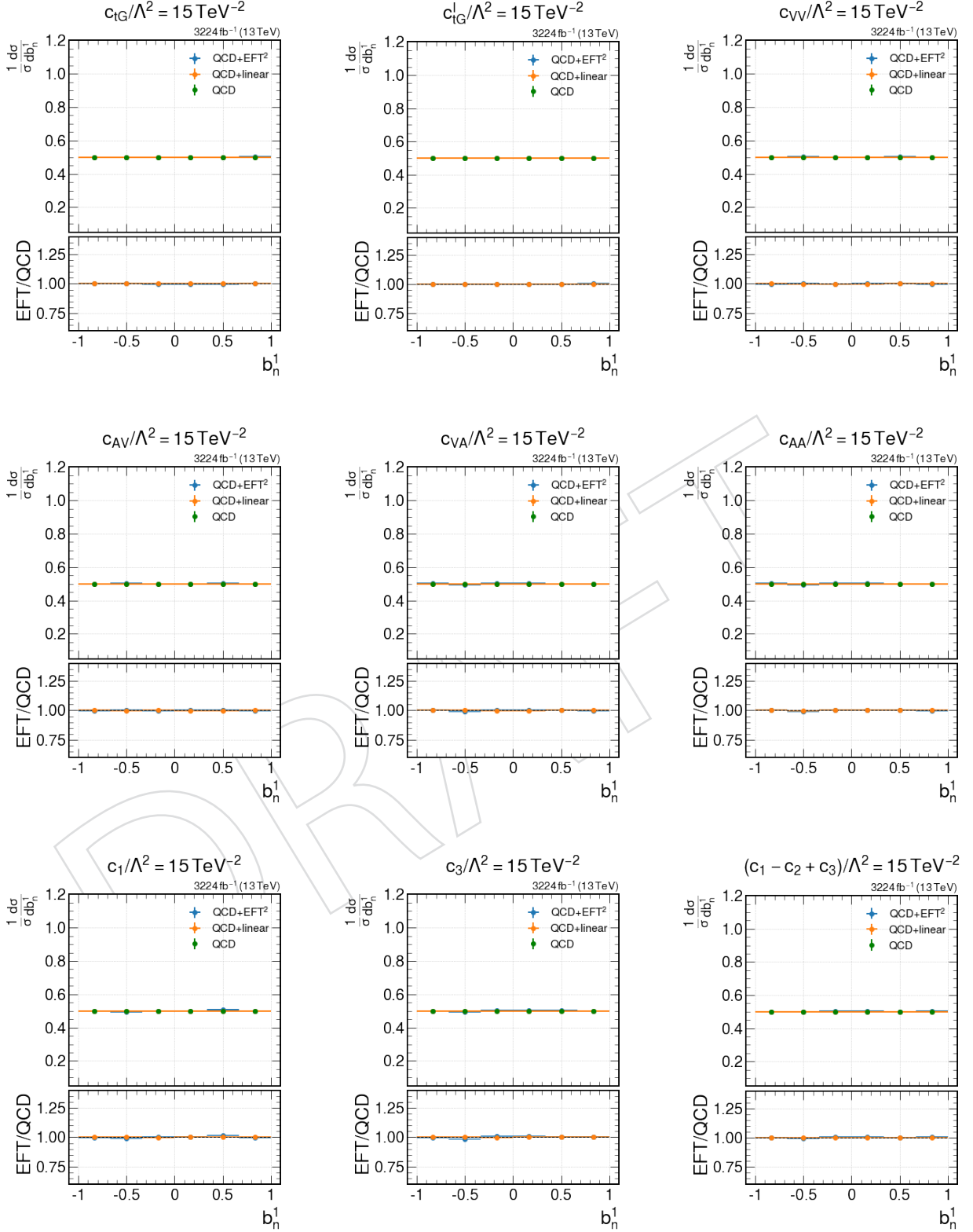


Figure 5: Lepton angular distribution showing the linear and quadratic contributions of each experiment-based EFT coefficients compared to the LO-SM contribution.

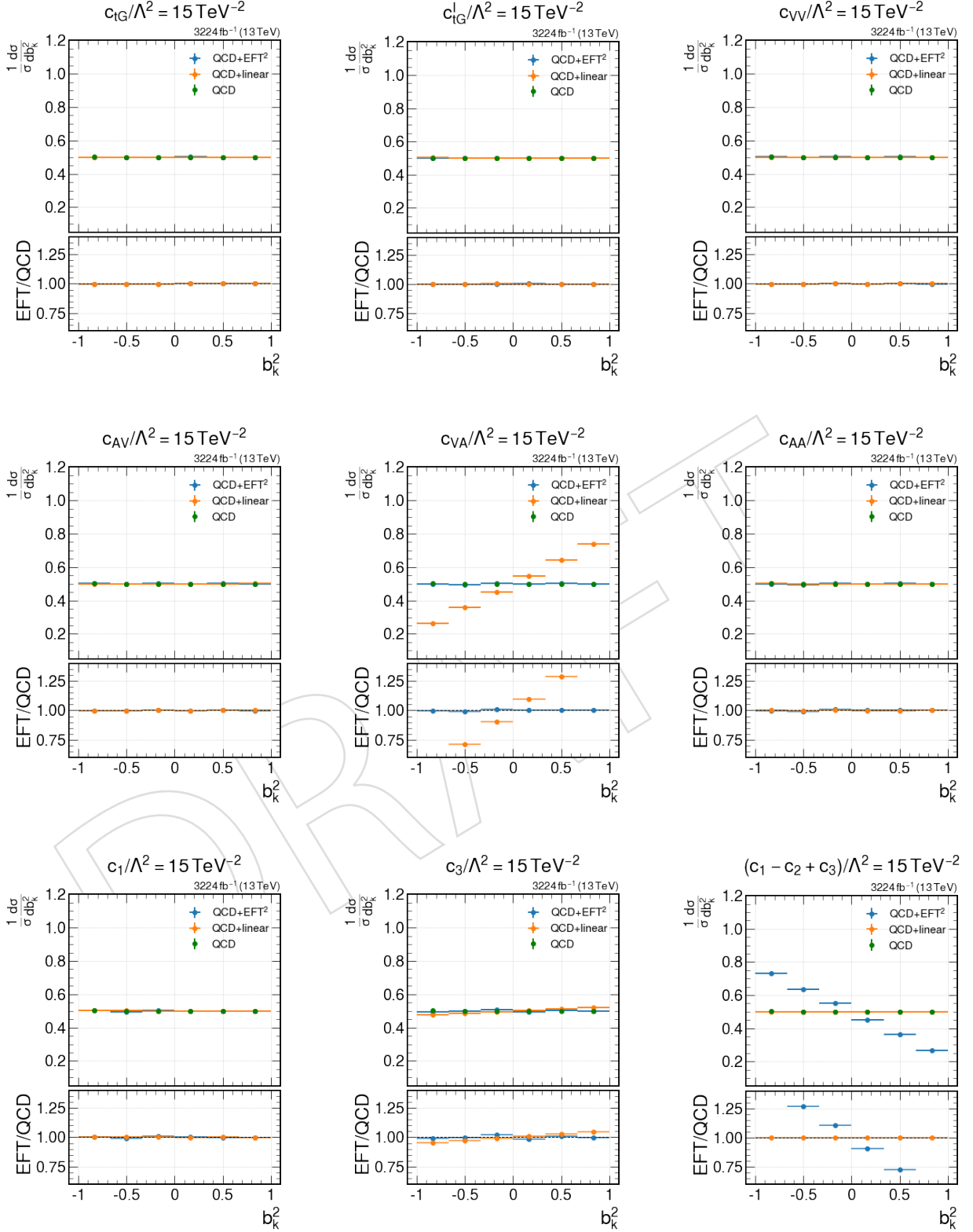


Figure 6: Lepton angular distribution showing the linear and quadratic contributions of each experiment-based EFT coefficients compared to the LO-SM contribution.

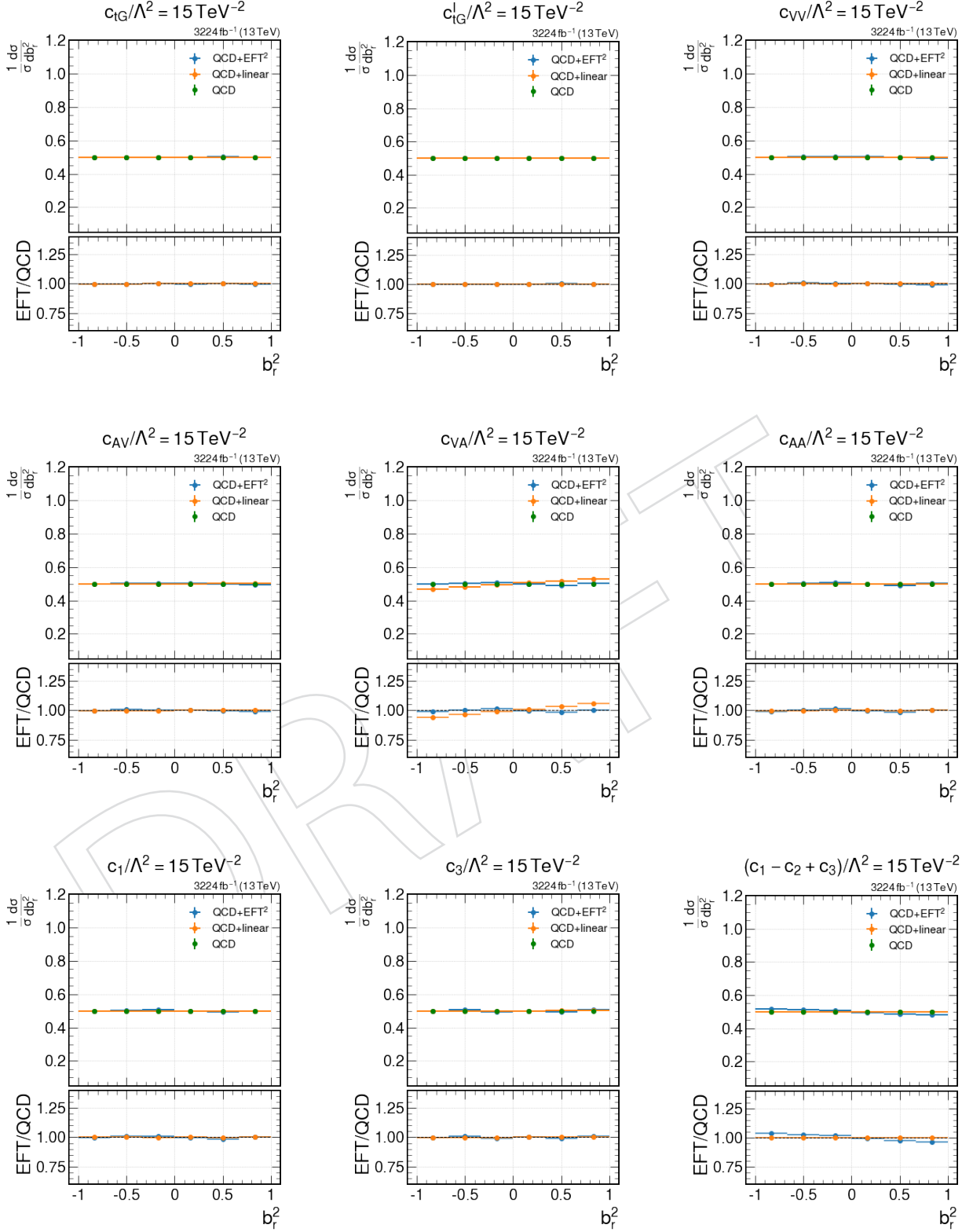


Figure 7: Lepton angular distribution showing the linear and quadratic contributions of each experiment-based EFT coefficients compared to the LO-SM contribution.

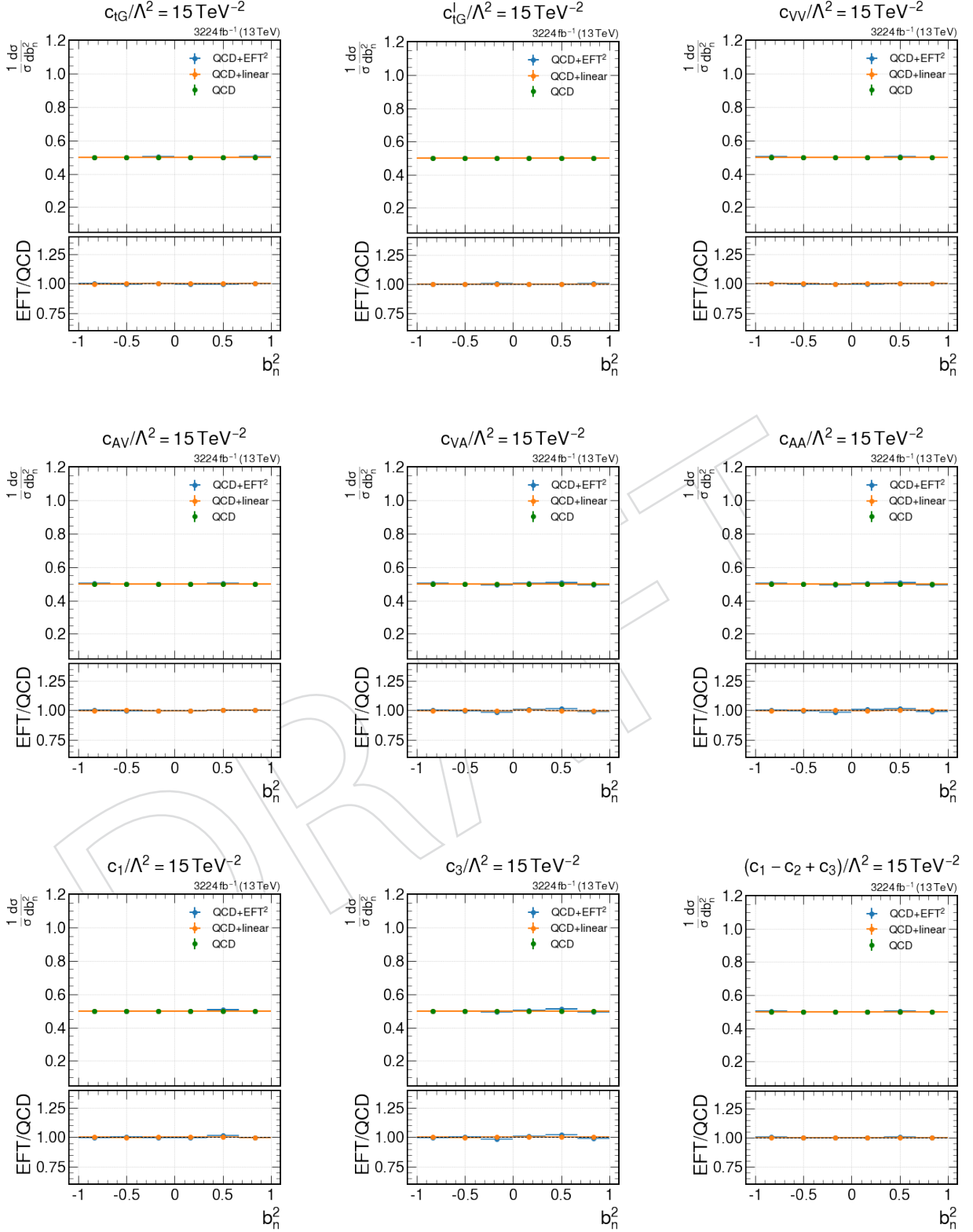


Figure 8: Lepton angular distribution showing the linear and quadratic contributions of each experiment-based EFT coefficients compared to the LO-SM contribution.

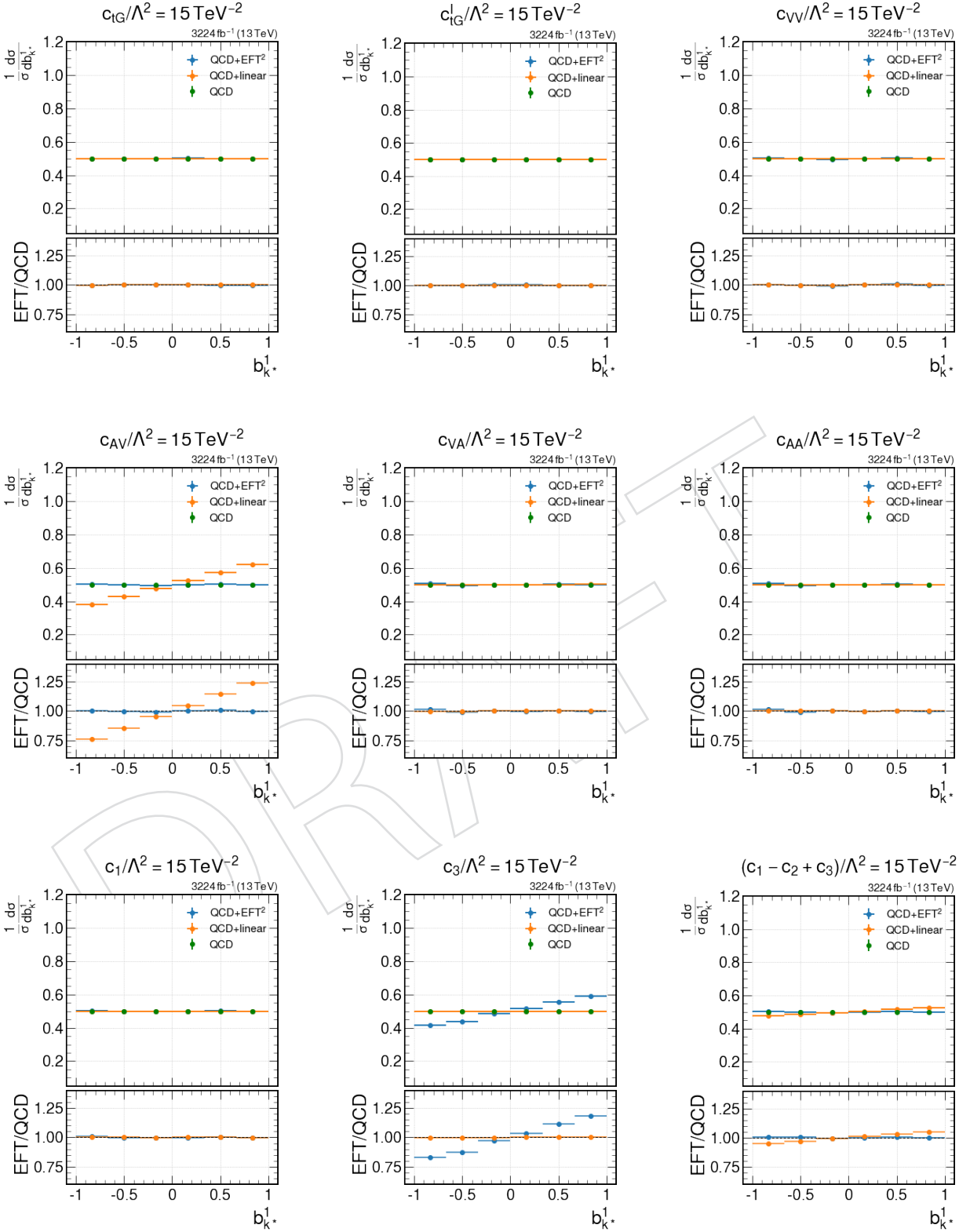


Figure 9: Lepton angular distribution showing the linear and quadratic contributions of each experiment-based EFT coefficients compared to the LO-SM contribution.

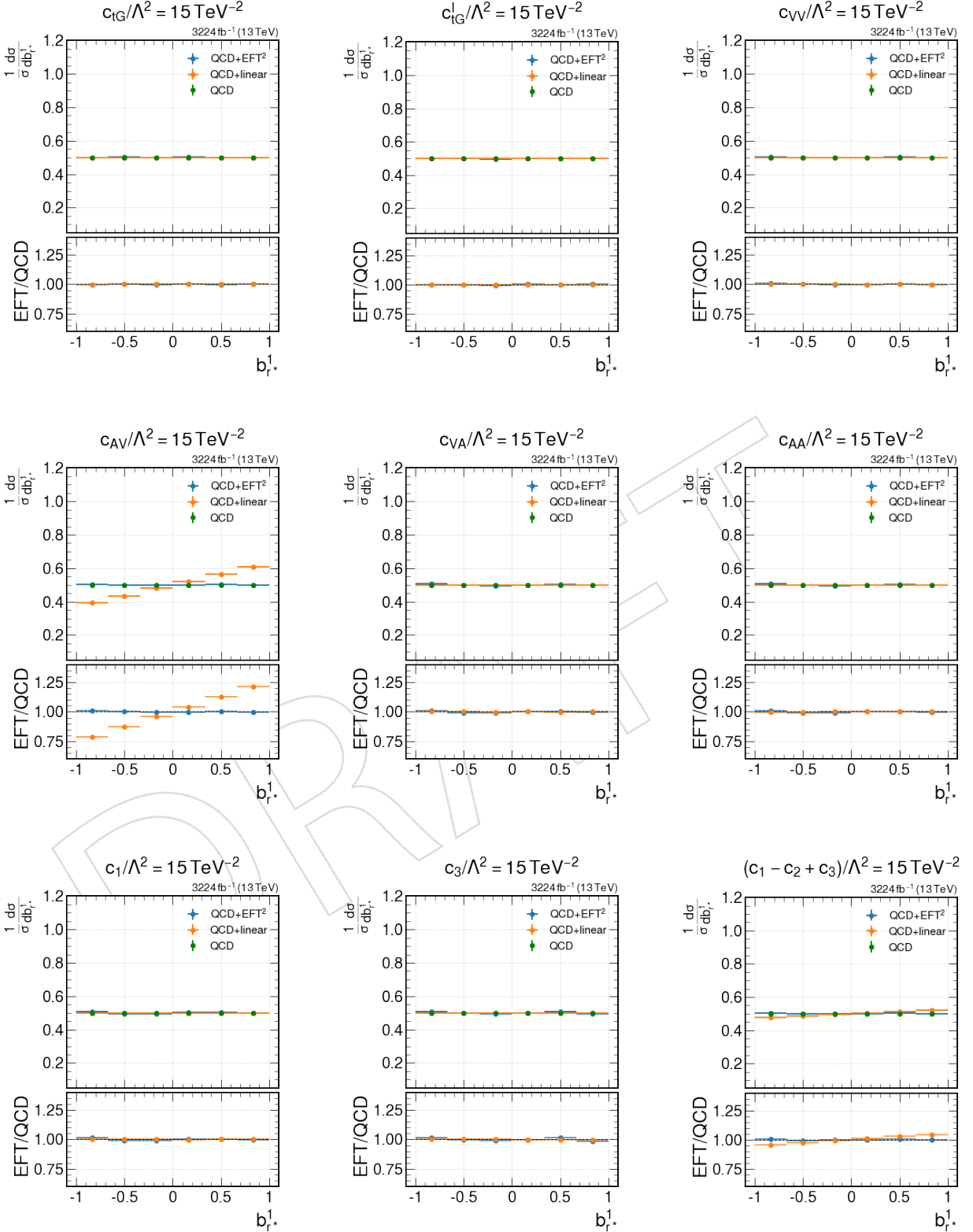


Figure 10: Lepton angular distribution showing the linear and quadratic contributions of each experiment-based EFT coefficients compared to the LO-SM contribution.

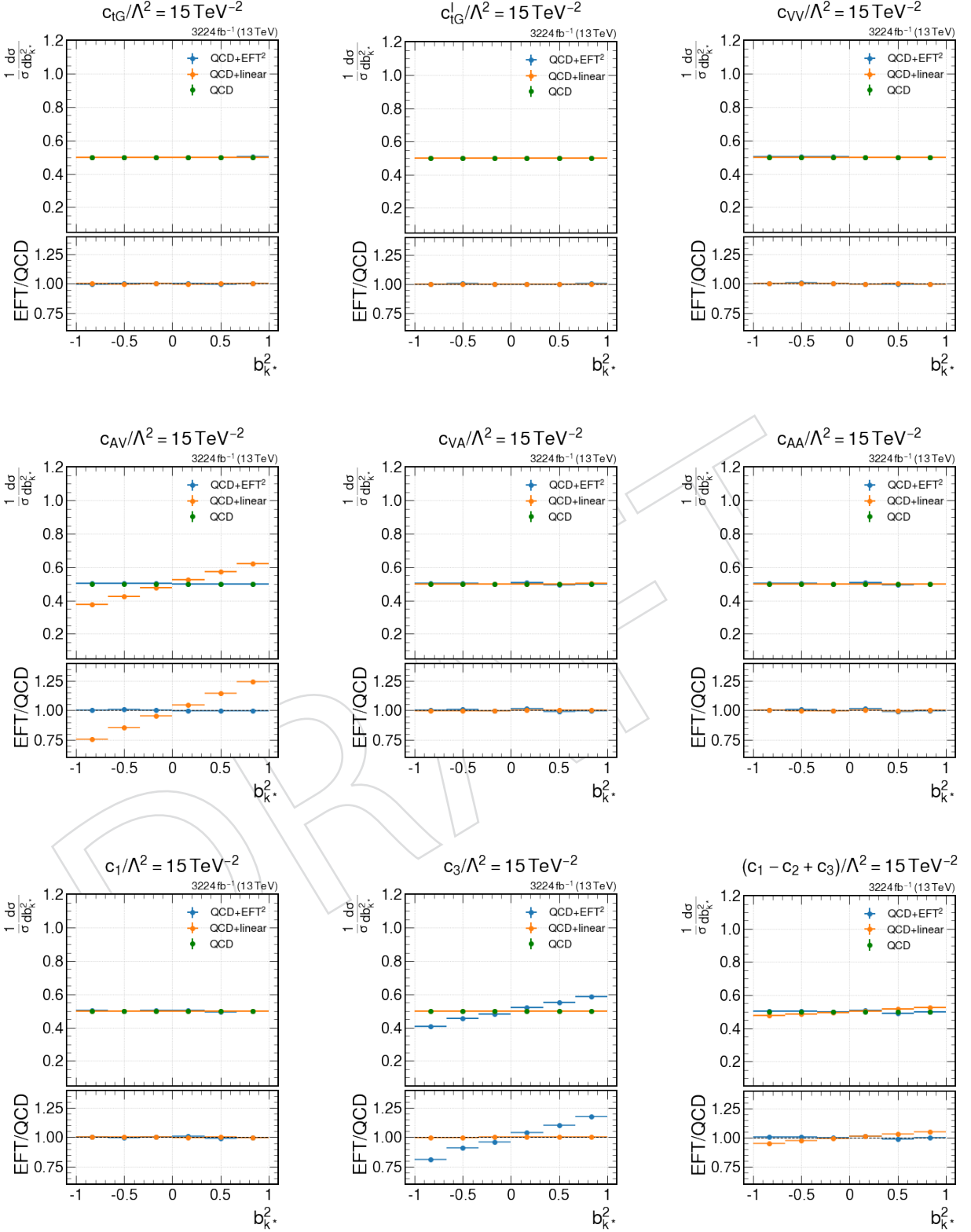


Figure 11: Lepton angular distribution showing the linear and quadratic contributions of each experiment-based EFT coefficients compared to the LO-SM contribution.

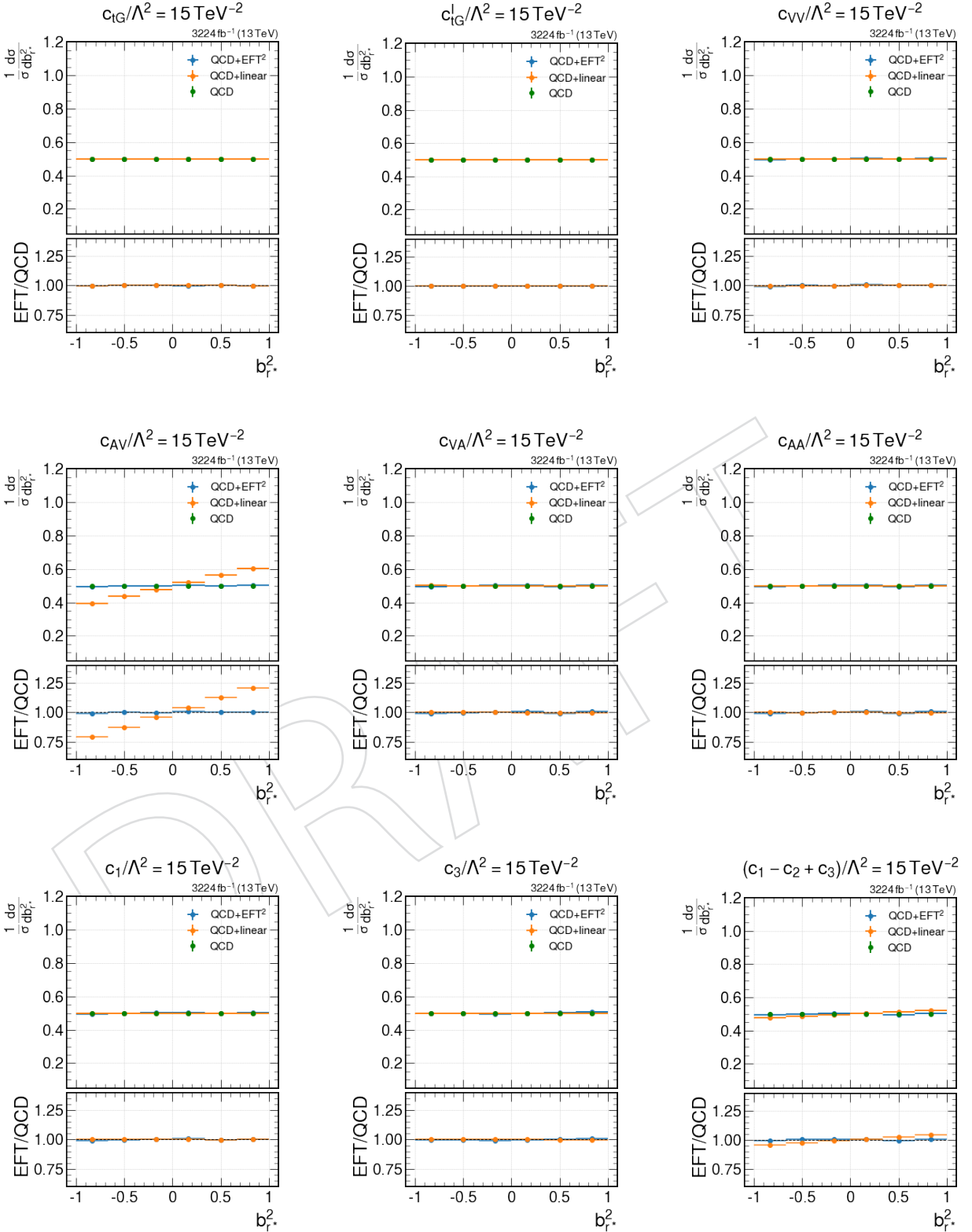


Figure 12: Lepton angular distribution showing the linear and quadratic contributions of each experiment-based EFT coefficients compared to the LO-SM contribution.

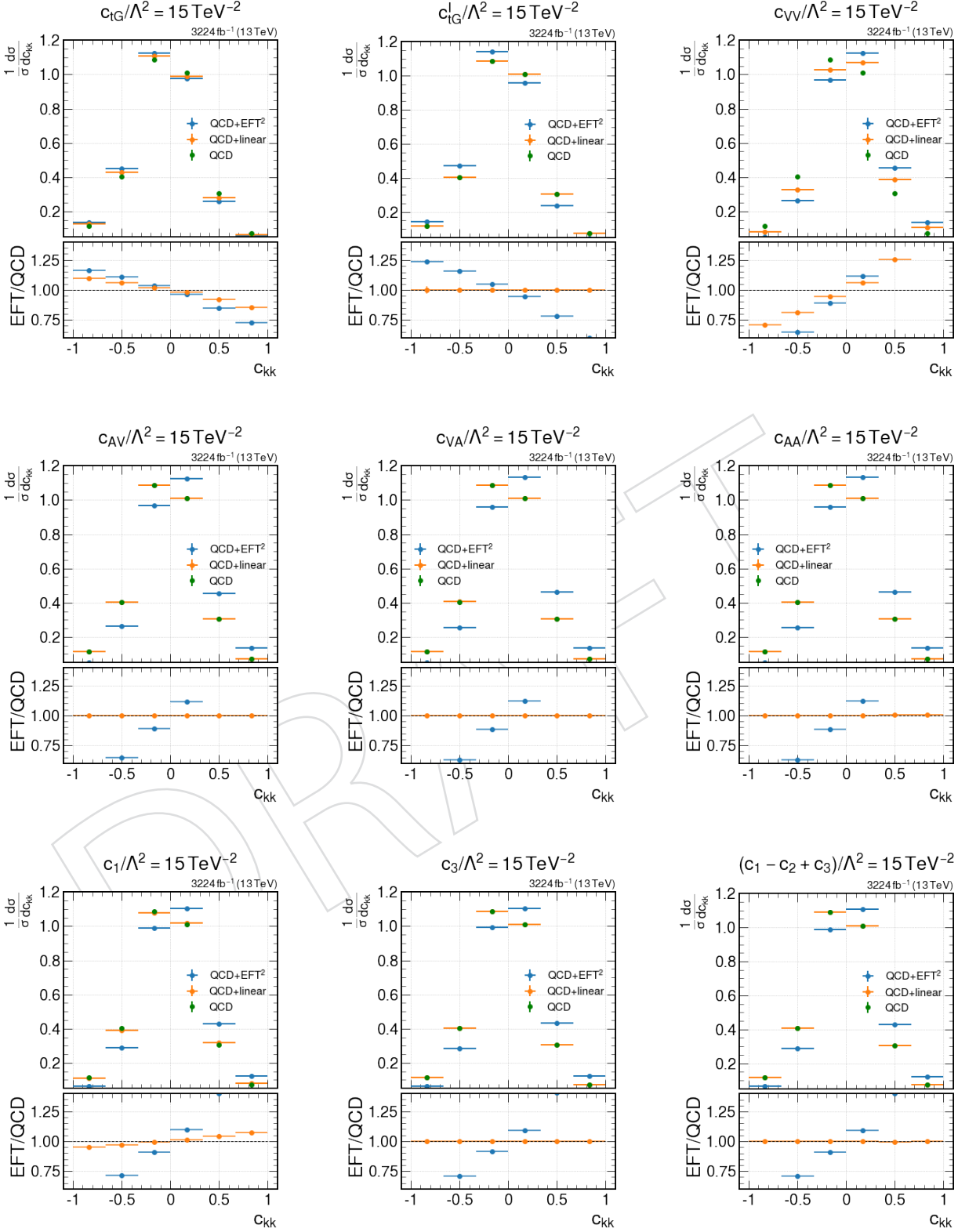


Figure 13: Lepton angular distribution showing the linear and quadratic contributions of each experiment-based EFT coefficients compared to the LO-SM contribution.

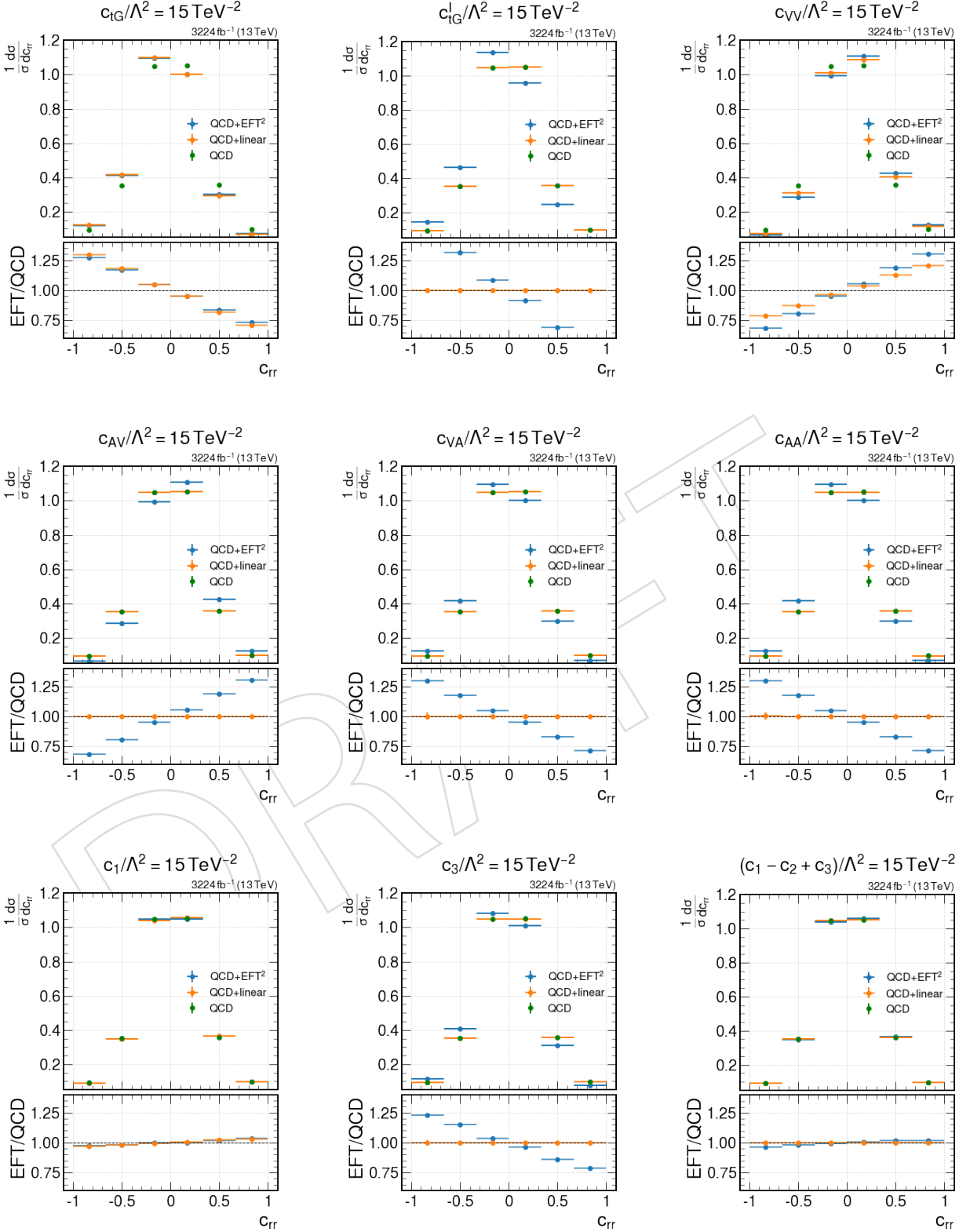


Figure 14: Lepton angular distribution showing the linear and quadratic contributions of each experiment-based EFT coefficients compared to the LO-SM contribution.

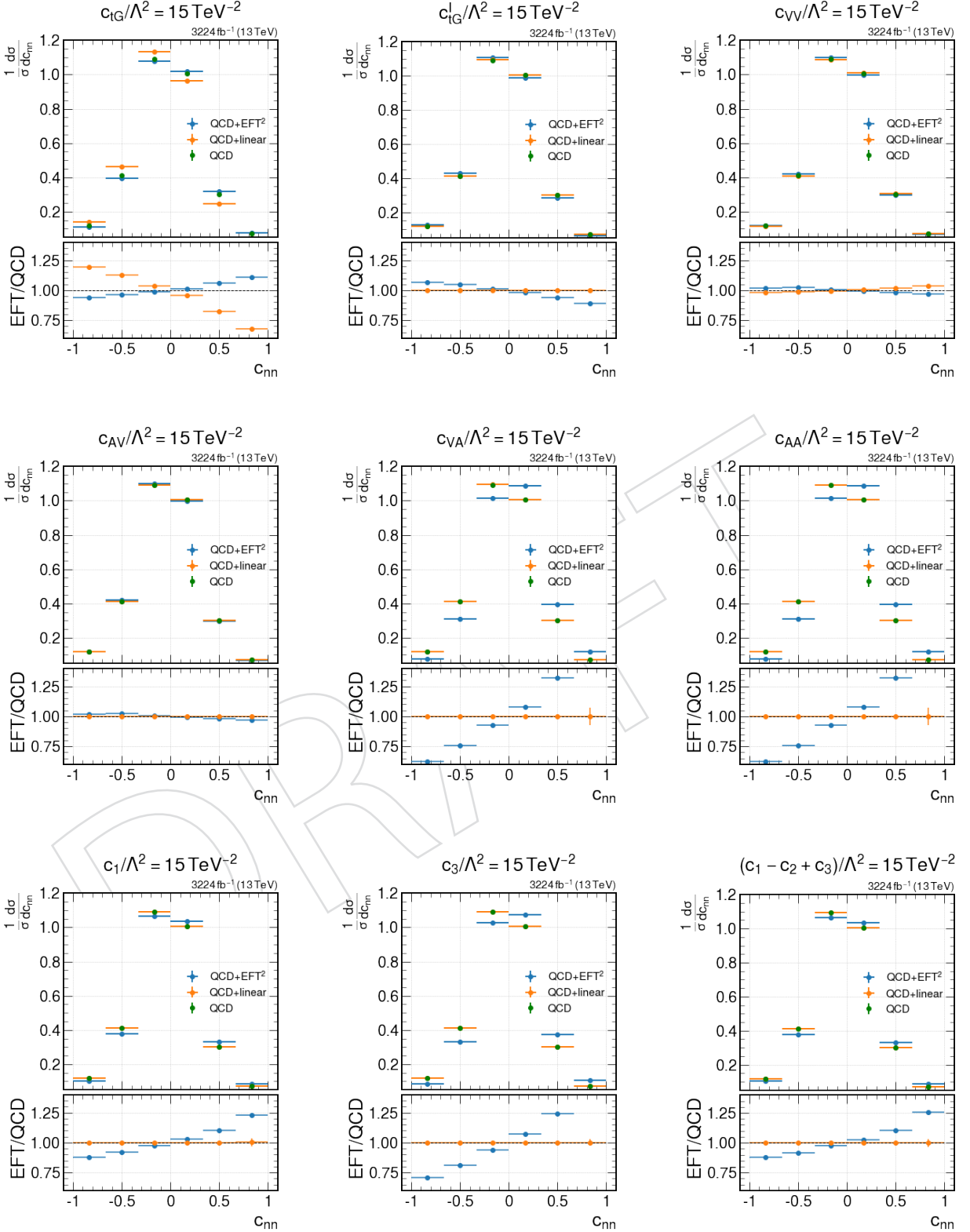


Figure 15: Lepton angular distribution showing the linear and quadratic contributions of each experiment-based EFT coefficients compared to the LO-SM contribution.

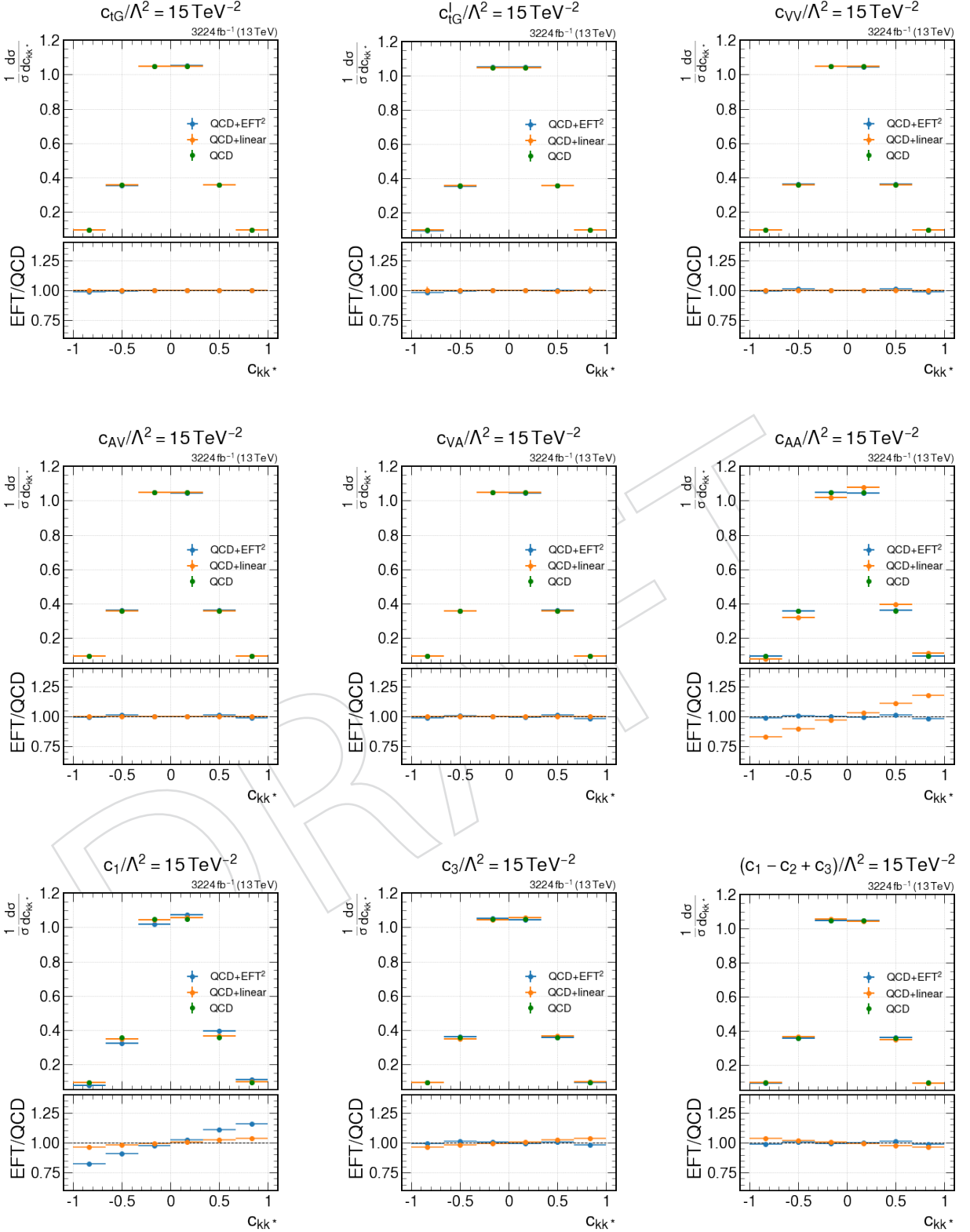


Figure 16: Lepton angular distribution showing the linear and quadratic contributions of each experiment-based EFT coefficients compared to the LO-SM contribution.

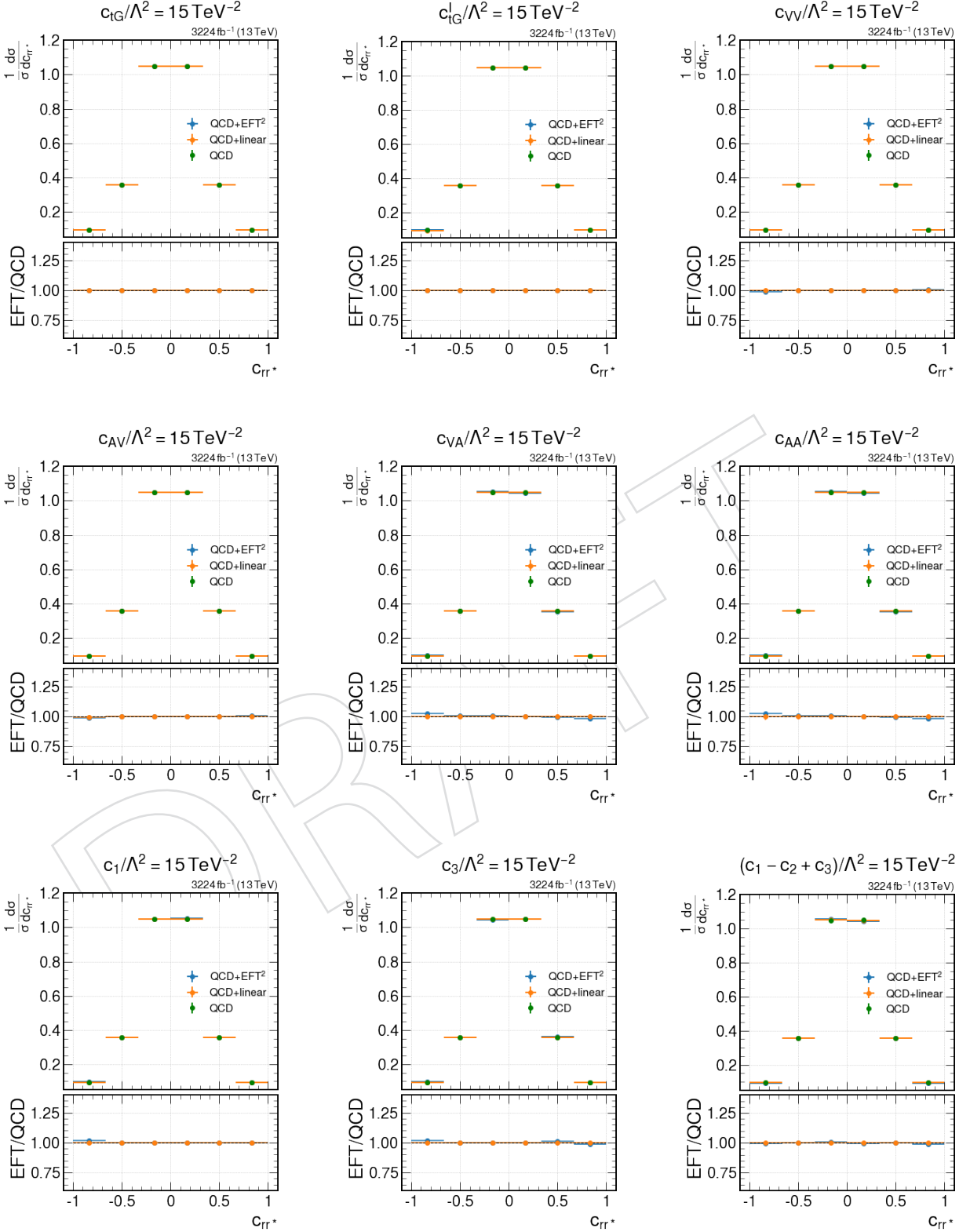


Figure 17: Lepton angular distribution showing the linear and quadratic contributions of each experiment-based EFT coefficients compared to the LO-SM contribution.

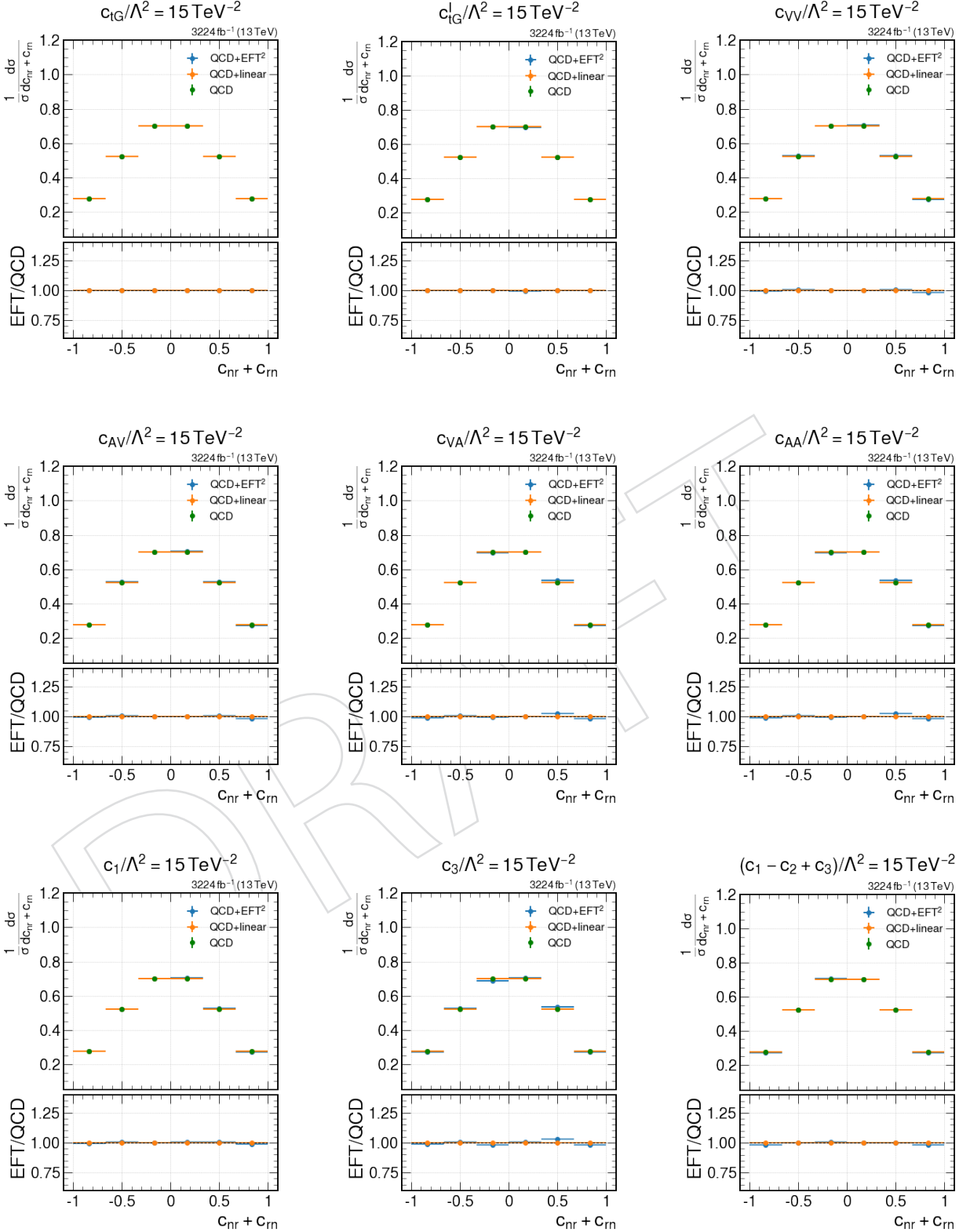


Figure 18: Lepton angular distribution showing the linear and quadratic contributions of each experiment-based EFT coefficients compared to the LO-SM contribution.

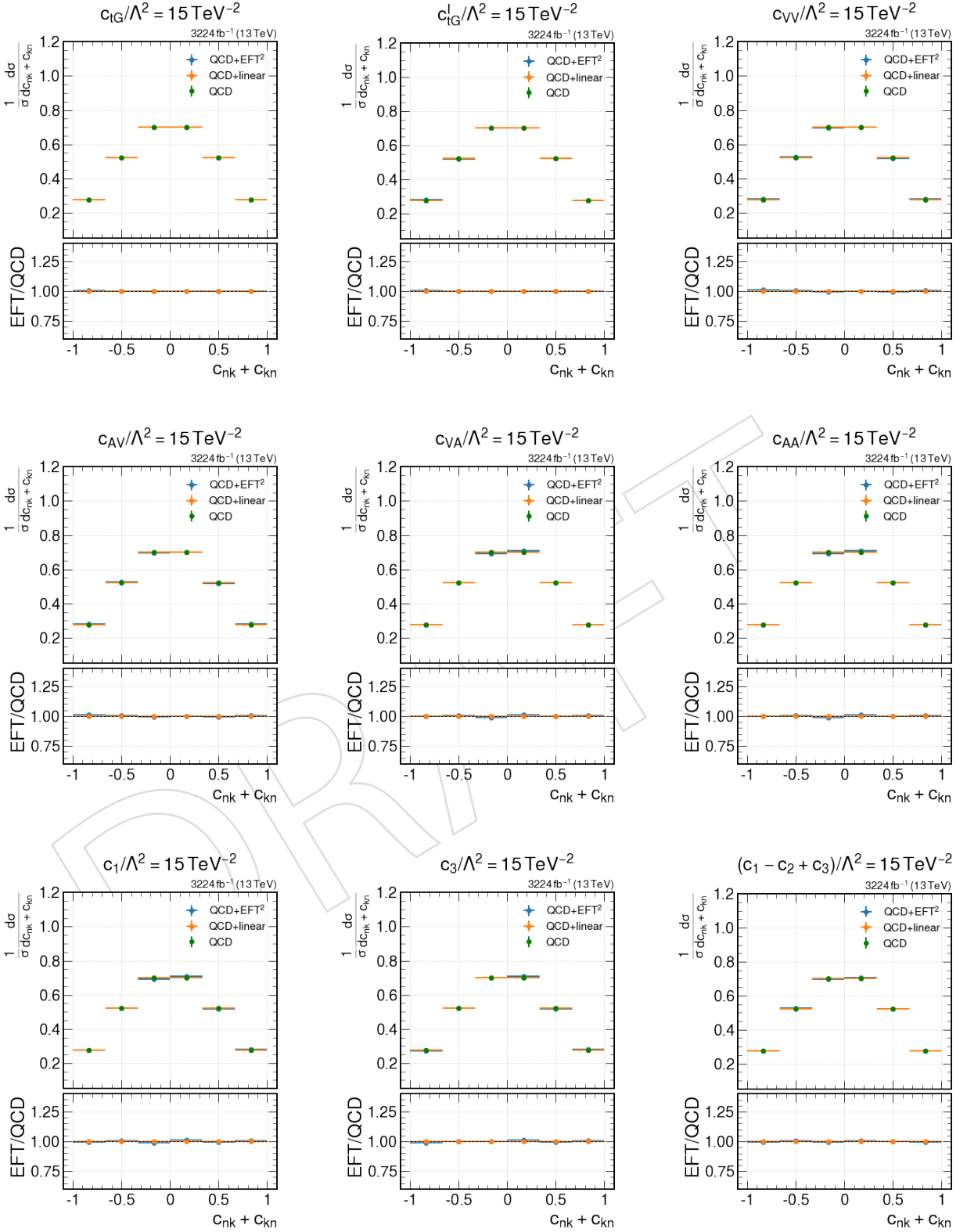


Figure 19: Lepton angular distribution showing the linear and quadratic contributions of each experiment-based EFT coefficients compared to the LO-SM contribution.

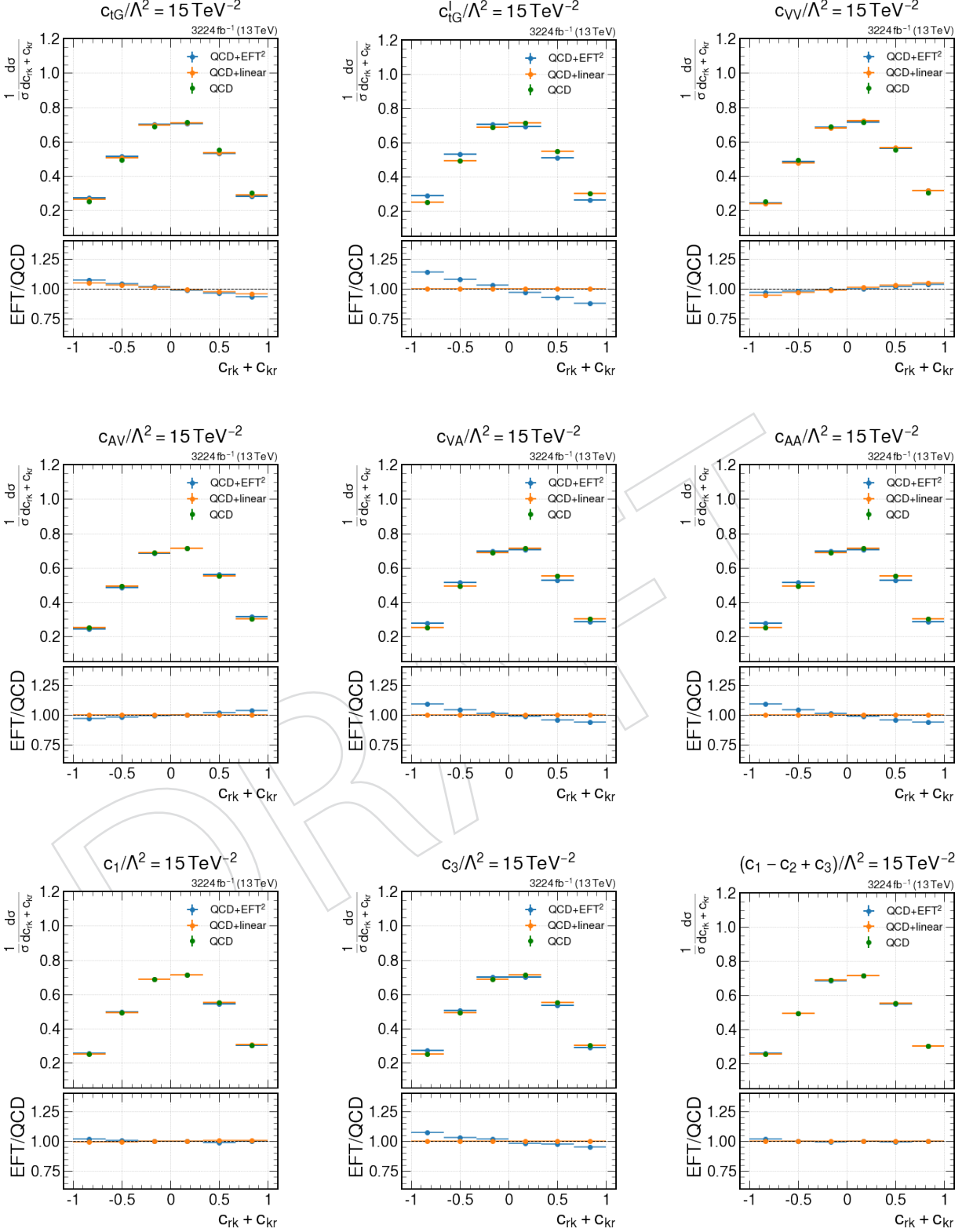


Figure 20: Lepton angular distribution showing the linear and quadratic contributions of each experiment-based EFT coefficients compared to the LO-SM contribution.

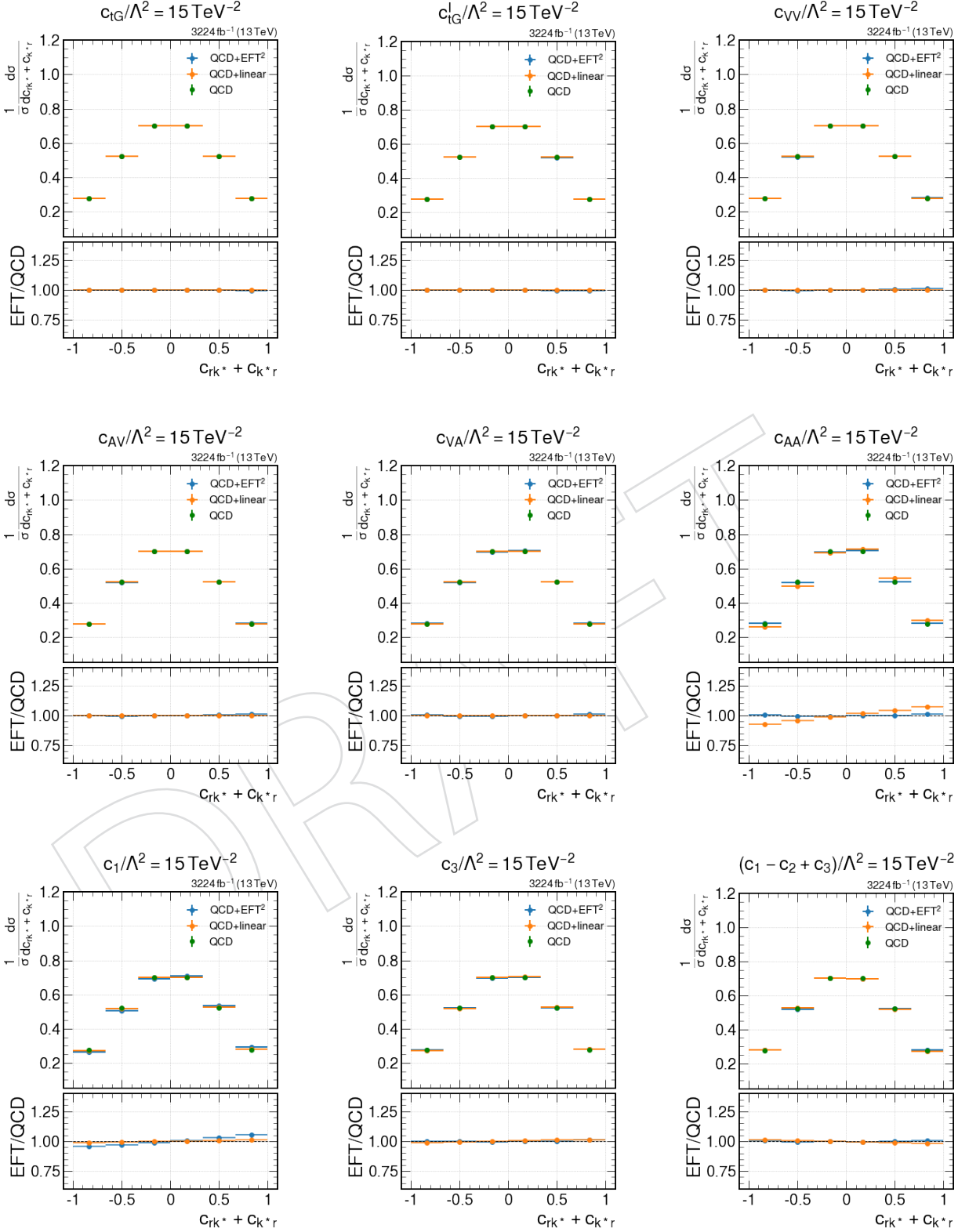


Figure 21: Lepton angular distribution showing the linear and quadratic contributions of each experiment-based EFT coefficients compared to the LO-SM contribution.

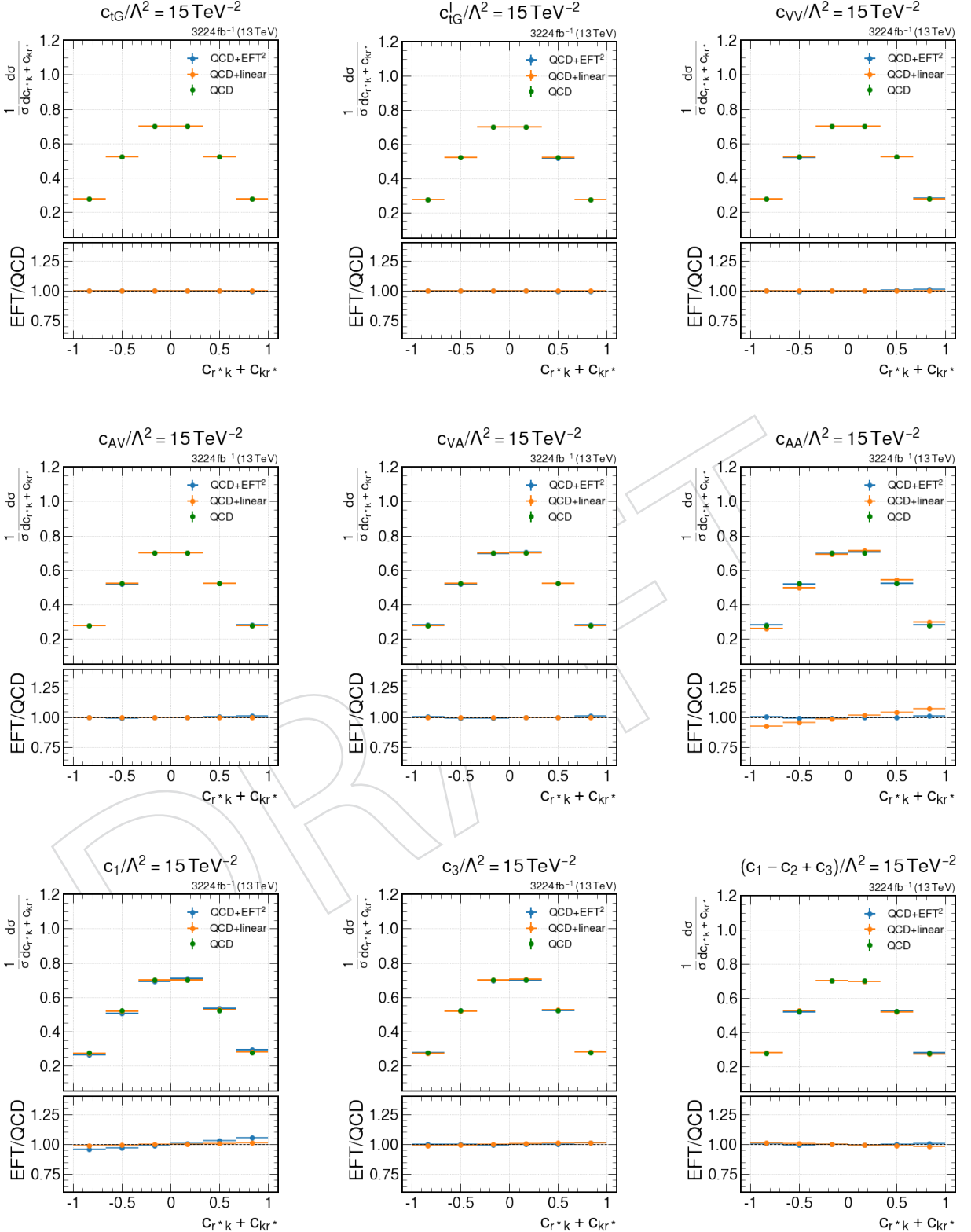


Figure 22: Lepton angular distribution showing the linear and quadratic contributions of each experiment-based EFT coefficients compared to the LO-SM contribution.

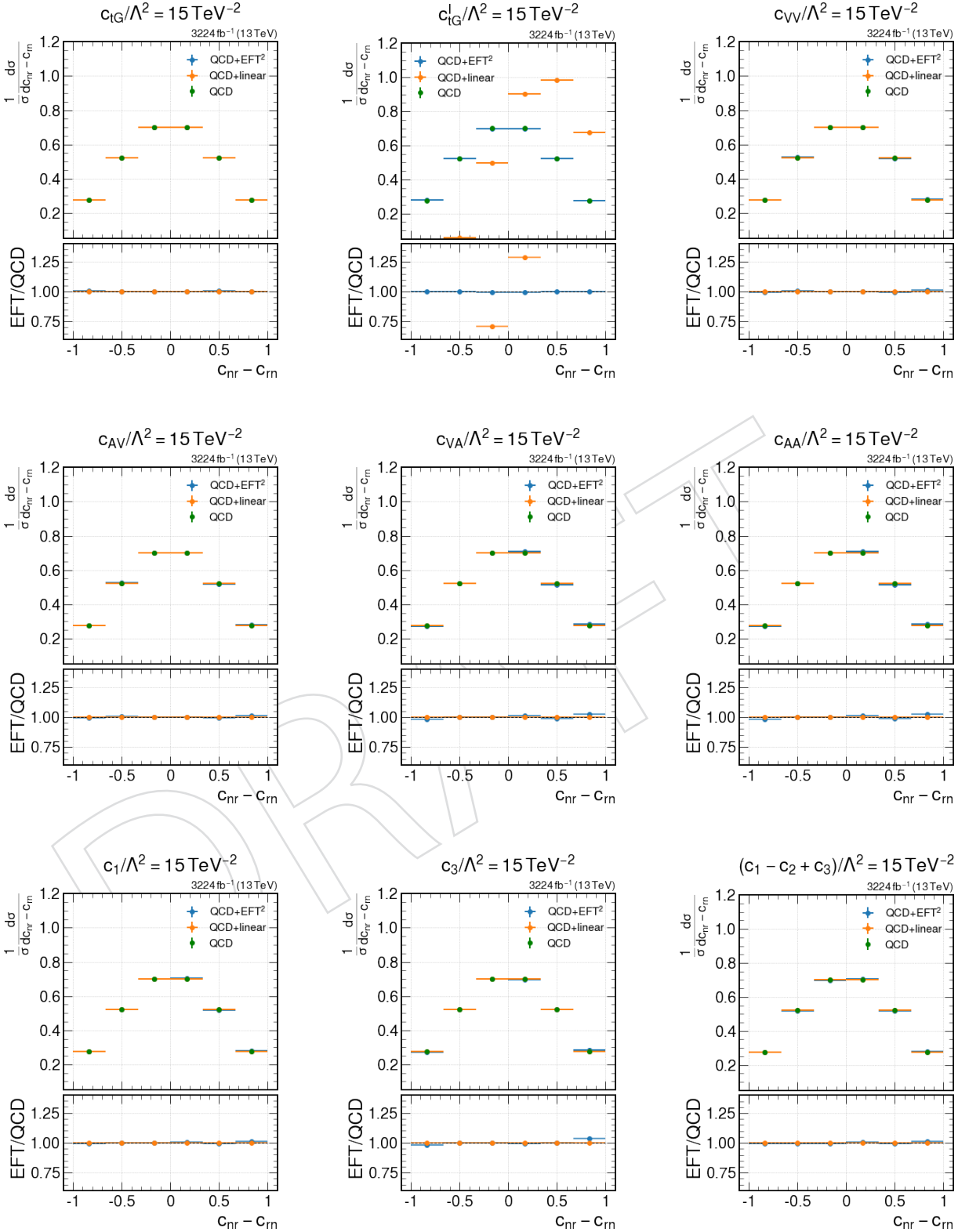


Figure 23: Lepton angular distribution showing the linear and quadratic contributions of each experiment-based EFT coefficients compared to the LO-SM contribution.

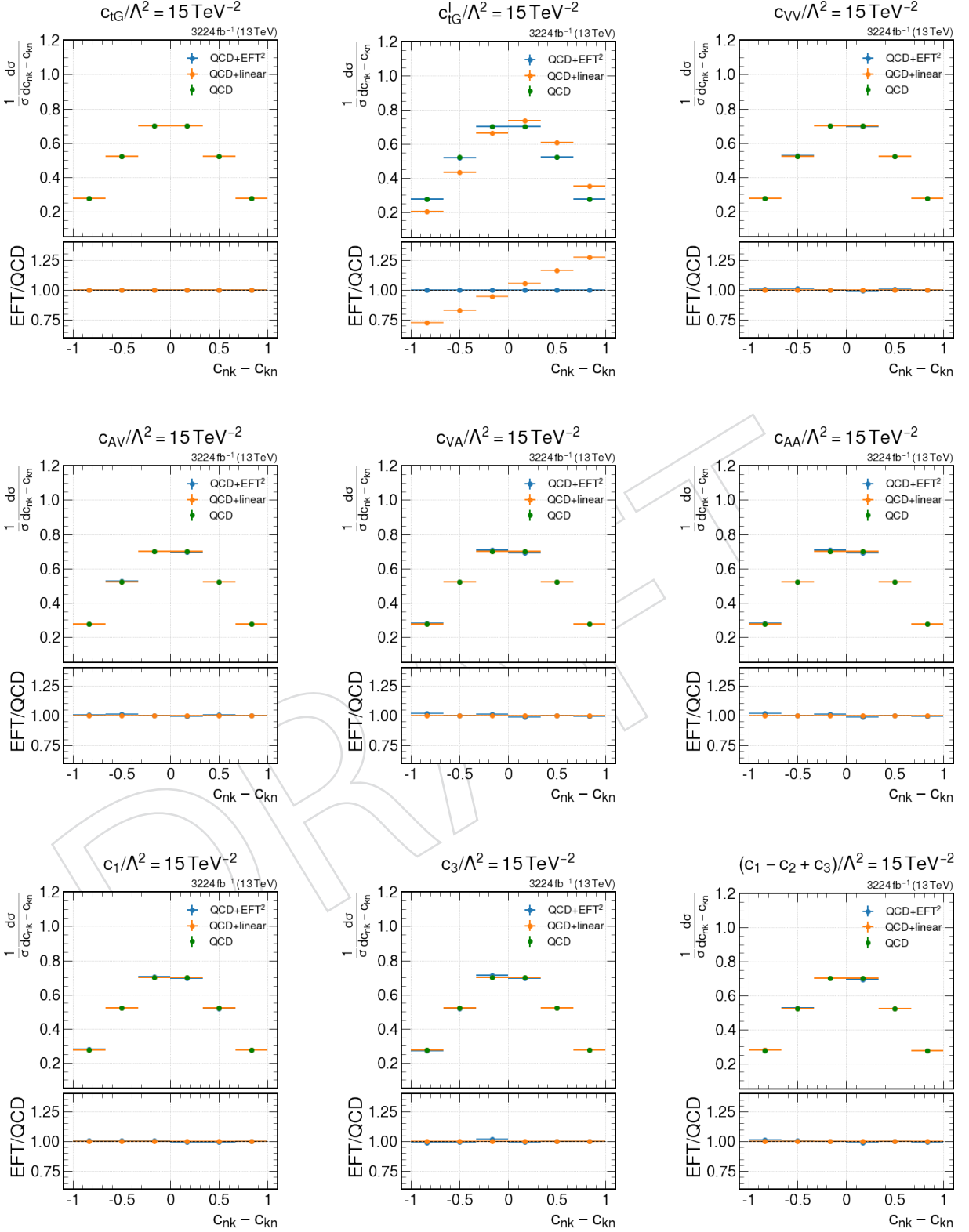


Figure 24: Lepton angular distribution showing the linear and quadratic contributions of each experiment-based EFT coefficients compared to the LO-SM contribution.

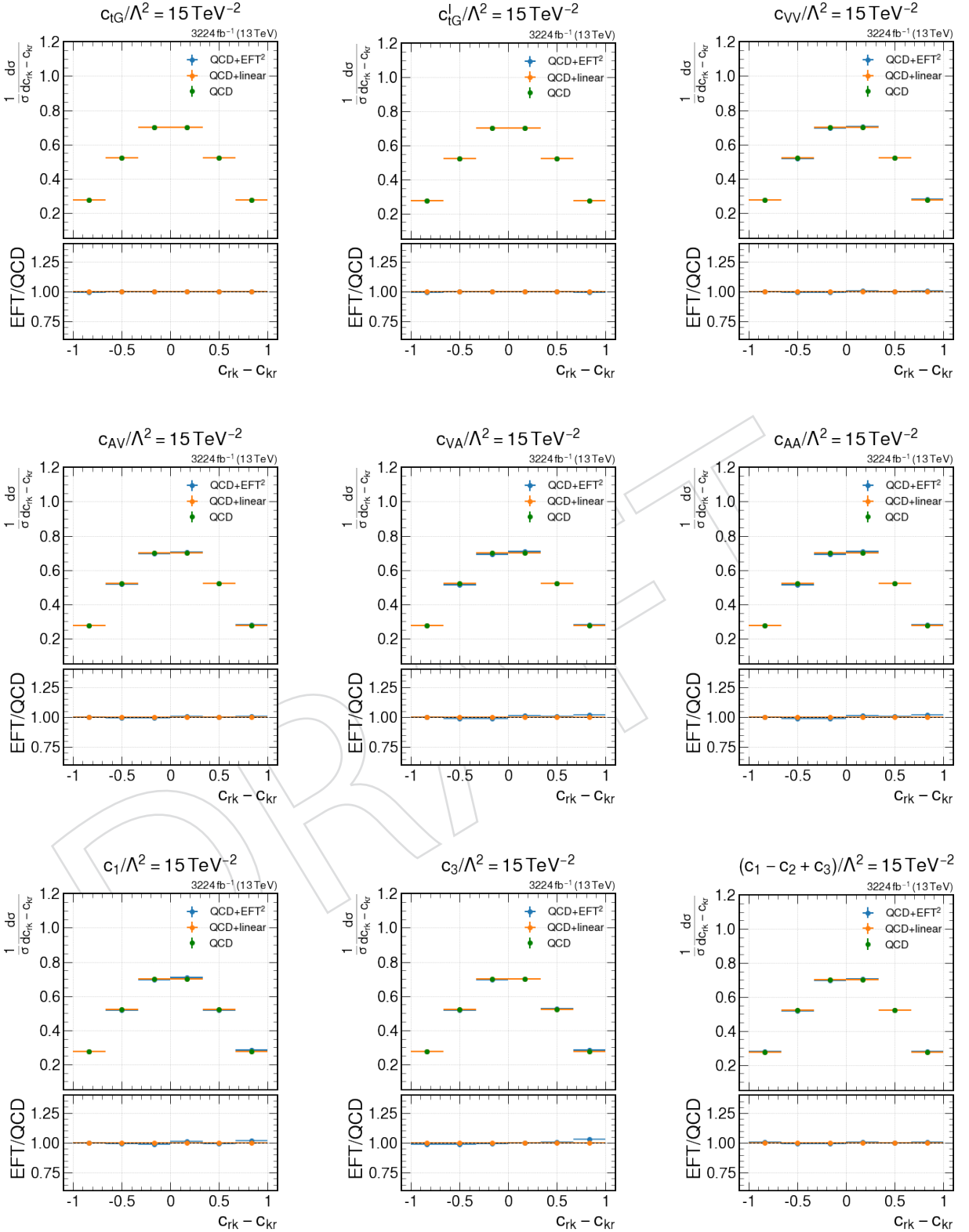


Figure 25: Lepton angular distribution showing the linear and quadratic contributions of each experiment-based EFT coefficients compared to the LO-SM contribution.

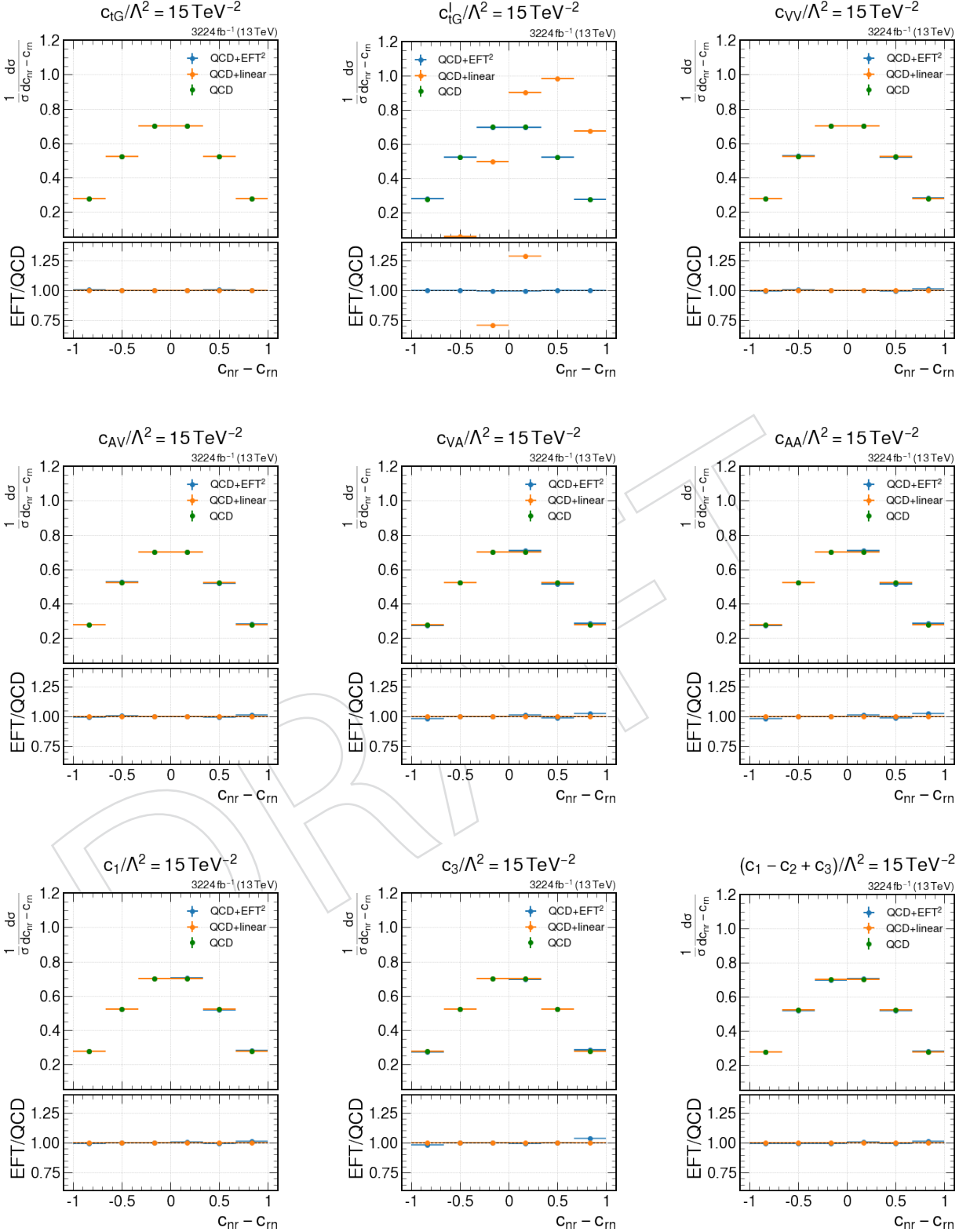


Figure 26: Lepton angular distribution showing the linear and quadratic contributions of each experiment-based EFT coefficients compared to the LO-SM contribution.

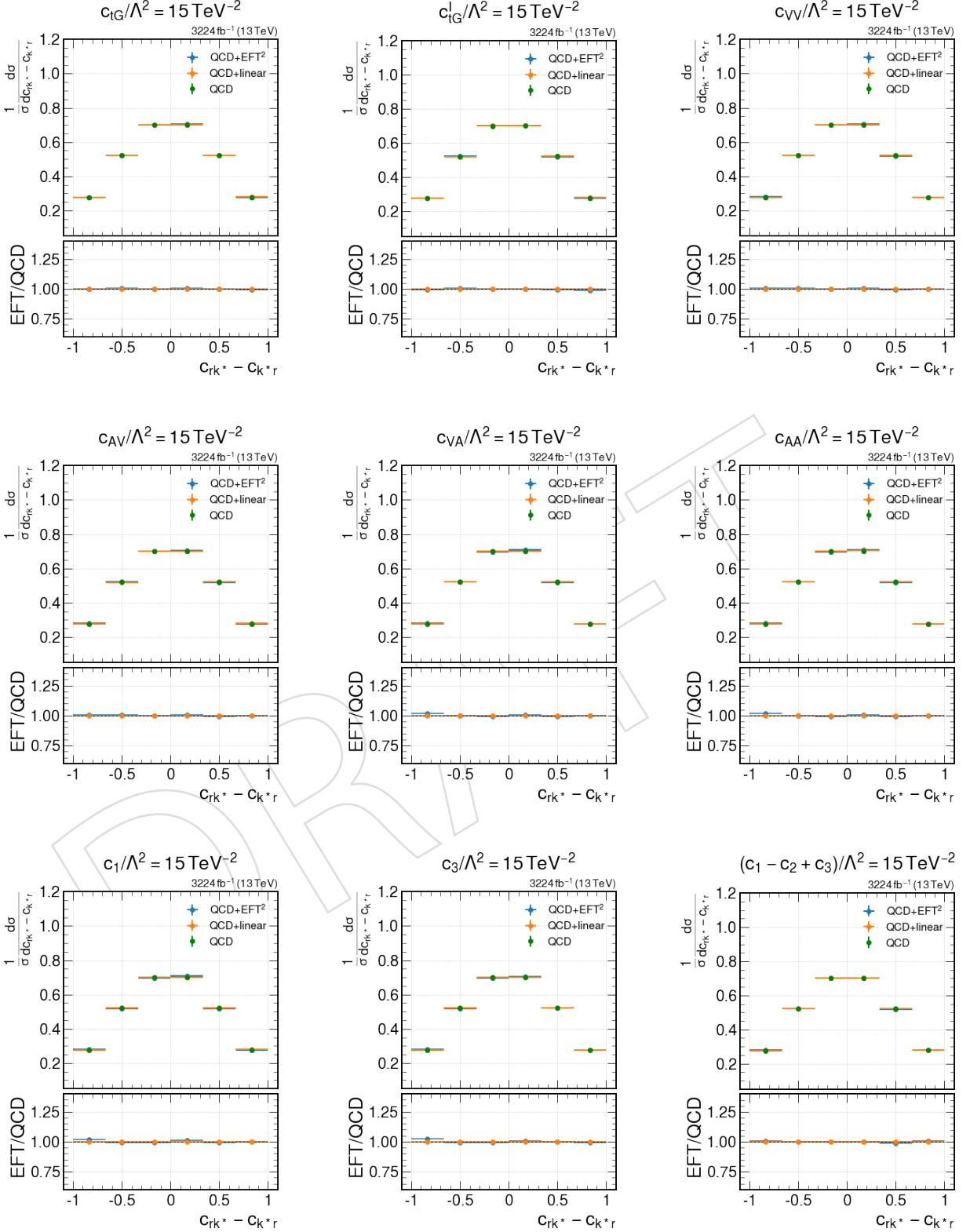


Figure 27: Lepton angular distribution showing the linear and quadratic contributions of each experiment-based EFT coefficients compared to the LO-SM contribution.

144 Differential distributions for these observables are shown in the Appendix C.1 . Observe that
 145 these angular observables, in being a linear combination of the formers, do not have their ef-
 146 fects determined by a pure CP - or P -even/odd EFT contribution. The complete set of these
 147 observables will still contain the full symmetry information of their linearly relatable observ-
 148 ables.

149 3 Monte Carlo samples for EFT fit

150 The parton-level EFT signal samples to be used in the EFT fitting are generated centrally with
 151 MadGraph5_aMC@NLO 2.6.5 [7] for the matrix element calculation and event generation and
 152 PYTHIA-8 [6] for the parton shower and hadronisation. The matrix element computed by
 153 MG corresponds to $pp \rightarrow t\bar{t}$ plus up to three additional partons, where $t\bar{t} \rightarrow W^+ b W^- \bar{b}$ and
 154 $W^{(+)} \rightarrow \ell^+ \bar{\nu}_\ell$ ($\ell^- \nu_\ell$) are fully decayed within Madgraph. Electrons, muons and tau lep-
 155 tons are considered. We use the MLM matching scheme for jet merging, which for samples
 156 containing three additional partons are competitive with NLO Powheg samples in terms of ex-
 157 perimental data agreement. The size of the samples are chosen to be equal to central samples
 158 NLO Powheg samples for dileptonic $t\bar{t}$ in order to get comparable statistics on the precision.

159 Predictions for the experiment-based EFT parameters are added with LO accuracy via the
 160 dim6top[8] model. Those predictions are computed by matrix element reweighting over a
 161 baseline where all the Wilson coefficients are set to null. We use 54 EFT reweighting points
 162 which, together with the "SM" point as baseline, are necessary to extrapolate the 9 EFT degrees
 163 of freedom over the full theory space, *i.e.* allowing all Wilson coefficients to be considered at
 164 the same time, if necessary. These 55 different theory points are called EFT benchmarks. The
 165 benchmark points were chosen so that they correspond to all possible combinations where one
 166 unique EFT parameter is set to both one positive and one negative value, while the remaining
 167 WCs are kept to zero, as well as all the possible combinations where only 2 EFT parameters
 168 are non-null (and positive). The non-null values chosen for c_{tG} and c_{tG}^I in all combinations are
 169 either -2 or 2. For the seven four fermion WCs the values chosen were -5 and 5.

170 In order to validate whether our benchmark points provide a good coverage over the theory
 171 spaces over the theory space, we have looked at their corresponding interpolation weights.
 172 Those depend only on the quadratic parametrisation of the benchmark points, being, thus, a
 173 process independent information. The validation consists of generating 1000 sets of random
 174 values for the 9 WCs and using the quadratic interpolation to determine their interpolation
 175 weights w_i . The estimative of the uncertainties is given by $\sqrt(w_i^2)$. Most weights over the -2,2
 176 range for c_{tG} and c_{tG}^I and -5,5 for the four fermion coefficients were found to be very small,
 177 ranging from 1 to 10. These weights are shown projected into the c_{tG} and c_{tG}^I parameter plane
 178 in fig. 28. The same test projected in all planes formed by the combinations of 2 WCs, *i.e.* over
 179 the full theory space is shown in the Appendix C.2.

180 Having guaranteed the good choice of benchmark points, we have also validated our bench-
 181 mark choice in terms of the kinematic and spin phase space. For that, smaller private samples
 182 of 100k events were generated using the same inputs both using reweighting and the full gen-
 183 eration via Madgraph for the combinations where one unique EFT parameter is set to both one
 184 positive and one negative value while the others are kept to zero, *i.e.* 18 EFT theory points. The
 185 agreement between the samples was validated using Rivet routines for standard kinematic
 186 observables relevant for $t\bar{t}$ as well as spin observables.

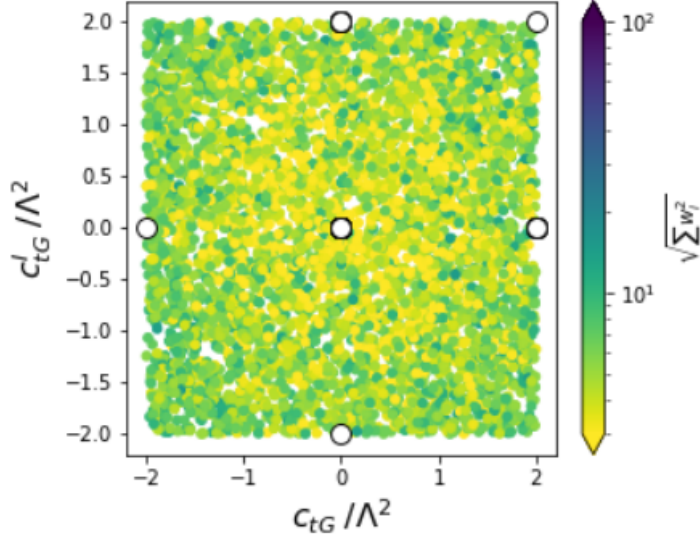


Figure 28: Interpolation weights for 1000 random test EFT hypothesis shown here as a function of c_{tG} and c_{tG}^I . White dots are the EFT benchmarks point.

187 4 EFT fit strategy

188 4.1 χ^2 minimisation

The expected observable yields calculated for the different EFT scenarios can be compared with experimental data for hypothesis testing. The fitting strategy consists of minimising the function

$$\chi^2(\vec{\theta}) = \sum_{i,j}^{N_{bins}} \left(x_{i,obs} - \hat{x}_i(\vec{\theta}) \right) \left(x_{j,obs} - \hat{x}_j(\vec{\theta}) \right) M_{ij} \quad (37)$$

189 over a range of different EFT hypotheses $\vec{\theta}$. $x_{i,obs}$ is the observed bin yield of an unfolded differential or multidifferential distribution, while $\hat{x}_i(\theta)$ is the expected yield for the same bin given 190 a EFT point θ . M_{ij} is the element in row i and column j of the inverted total covariance matrix 191 of the unfolded measurement. The total covariance matrix includes 1) statistics correlation 192 between bins of the same N-D distributions, 2) correlation between bins of different N-D 193 distributions, as well as 3) covariance matrix of all the systematics uncertainties, including variations 194 on theory parameters. In the case where θ corresponds to single EFT operator, the 1 (2) σ 195 confidence interval is determined by the range within $\Delta\chi^2 < 1$ (4) with respect to the point of 196 minimum χ^2_{min} , i.e. the point of best fit. In case of multiple operators, the $\Delta\chi^2$ corresponding to 197 1 (2) σ intervals are adapted accordingly. 198

199 EFTFitter is the code used for χ^2 minimisation [9]. The implementation was exhaustively 200 validated over the CMS note AN-18-288 [10]. Additionally, CMS public results using it the tool 201 to fit up to 2 EFT operators simultaneously were made available [1]. Because all the observ- 202 ables are unfolded at once in the measurement, with their inter- and intra- correlations taken 203 into account, the fit can make use of more than one distributions to set stringent constraints on 204 the EFT operators. The measured observables correspond to independent elements of the spin 205 density matrix, thus a continuous increase in sensitivity is expected as observables are added 206 one by one to the fit. For doing so, first the results of single observable fits are performed and 207 compared based on the width of their 2σ bands. The observable with the highest sensitivity is

208 picked and the remaining observables are added to it one by one to obtain the pair of observ-
 209 ables with the highest sensitivity (with the restriction that one of them is the best-performing
 210 single observable). This proceeds iteratively until the full set of observables is exhausted. This
 211 process work both when the observables being considered are single differential distributions
 212 as well as multi-differential distributions, for instance sets of spin observables or set of spin
 213 observables measured as a function function of $m_{t\bar{t}}$ and/or $\cos \Theta_t^*$ bins.

214 5 Conclusion and Outlook

215 In this note the validation of a basis map allowing MC predictions of experiment-based EFT
 216 parameters is presented. It used `dim6top` parameters for EFT inputs in the MC generators.
 217 EFT contributions in the experiment-based basis has the advantage of affecting an indepen-
 218 dent subset of observables depending on the discrete symmetries (CP, P, weak isospin) and
 219 Lorentz (Vector/ Axial-vector) properties of the EFT operators. As a result, operators affecting
 220 different subset of multi-D observables are naturally uncorrelated and the dimensionality of
 221 the EFT fit is reduced. EFT signal samples for top pair production with LO + 3 jets accuracy are
 222 being centrally prepared by CMS. The samples can be interpolated over the full theory space to
 223 produce EFT-template over a range of WCs needed for the EFT fit. A validated χ^2 fit strategy
 224 is presented here to perform the fit of every over each set of correlated EFT operators. The
 225 constrains on on experiment-based WCs, together with the basis map, will allow EFT limits to
 226 be presented in terms of `dim6top` parameters with their full correlation taken into account. As
 227 soon as 1) Unfolded distributions 2) Covariance matrices containing statistical correlations 3)
 228 Systematics covariance matrices with breakdown per source are available by the measurement
 229 team (AN-20-037), our strategy will be applies to produce to the measured multi-differential
 230 cross-sections to produce expected results.

231 6 Change Log

232 6.1 v1 to v2

- 233 • Changed anomalous coupling to experiment-based EFT coefficients to make clear
 234 that we are referring to a complete set of dim-6 EFT operators.
- 235 • Information to clarify the goals, the EFT predictions and the EFT fit goals was added
 236 to the introduction so that L3 EFT conveners' comments were addressed. Several
 237 sentences were also rephrased.
- 238 • Table 1 divided into 4, i.e. table 1 shows the sensitive observables considering a
 239 given P,CP symmetry, table 2 shows details on the EFT degrees of freedom in t,
 240 tables 3 and 4 shows which observables are affected by the linear and quadratic EFT
 241 contributions, respectively, as requested by the L3 EFT conveners.
- 242 • Eq. 1 : gs was added to the Otg definition to make clear we are using ctG normalised
 243 by gs. Explanation below eq. 1 was rephrased.
- 244 • Eq. 2: was generalised to N EFT parameter.
- 245 • Explanation about Eq. 2 was rephrased to explain better the CP,P effects introduced
 246 by the experiment-based coefficients. Eq. 3 was misleading and hence removed.
- 247 • Subsection 2.1 was promoted to Section 2.
- 248 • Eq. 3 and 4 were added a Summation in order to present them in their most general
 249 form.

- 250 • Eq. 12,13,14 were added to make clear how our experiment-based coefficients relate
251 with the one from our theory reference.
- 252 • Eq. 15 to 26 were added to present how the EFT limits published by CMS for 2016
253 data could be converted to the dim6top basis, as suggested by the L3 EFT conveners.
- 254 • Explanation about the reweighting step and quadratic interpolation for the private
255 samples used in the basis map was rephrased.
- 256 • Plots of observables $b_i^a + b_i^a$ and $b_a - b_i^a$ were removed because these observables are
257 not going to be used in the measurement and do not add relevant information for the
258 basis translation. Plots that did not directly contribute to the basis map validation
259 were removed from subsection 2.1 Top EFT
- 260 • Basis Map and moved to Section D.1 Additional Spin Observables.
- 261 • SM changed to LO QCD in the explanation about the private samples as well as all
262 related figs, for clarity.
- 263 • Cosmetic changes on Figs. 2 to 27. SM label changed to QCD for clarity.
- 264 • In Section 2.1, additional information on the translation of the EFT parameters was
265 included as well as some sentences rephrased to address L2 EFT convener comment.
- 266 • Observable definitions of eq. 15 to 26 (in v2 eqs 25 to 36) were moved to a separate
267 sub-section 2.2.
- 268 • Subsection 2.2 EFT Signal Sample was promoted to Section 3 Monte Carlo samples
269 for EFT fit. Explanation about samples reweighting was rephrased and informa-
270 tion on the reweighting validation was added. Plot of the interpolation weights for
271 accessing theory space coverage was added.
- 272 • Section 3 - ζ Section EFT fit strategy: Information on the covariance matrices added.
273 Rephrasing the explanation of the evolution of sensitivity when adding observables
274 into the fit. Benchmarks fits using published covariance matrices with CMS data
275 from 2016 were pushed out to avoid confusion.
- 276 • Section Conclusion and Outlook is written.
- 277 • Appendix B EFT operators entering in the top decay is pushed out of the AN because
278 the study is not complete.
- 279 • Appendix C Additional information was added. It contains 1) plots of additional
280 spin observables 2) Plots of interpolation weights

281 A Quantum field theory relations

282 A.1 Gamma matrices

Their defining property is

$$\{ \gamma^\mu, \gamma^\nu \} \equiv 2\eta^{\mu\nu}, \quad (38)$$

where $\eta^{\mu\nu}$ is the Minkowski metric. A product of all γ^μ 's is conventionally defined as

$$\gamma_5 \equiv i\gamma^0\gamma^1\gamma^2\gamma^3. \quad (39)$$

The commutator of γ^μ 's defines an antisymmetric tensor

$$\sigma^{\mu\nu} \equiv \frac{i}{2} [\gamma^\mu, \gamma^\nu]. \quad (40)$$

In this work the following properties of the γ^μ 's are going to be used

$$(\gamma^\mu)^\dagger = \gamma^0 \gamma^\mu \gamma^0, \quad (41)$$

$$(\gamma_5)^\dagger = \gamma_5, \quad (42)$$

$$(\sigma^{\mu\nu})^\dagger = \gamma^0 \sigma^{\mu\nu} \gamma^0. \quad (43)$$

From them, it also follows that

$$(\gamma^0)^2 = 1, \quad (44)$$

$$(\gamma_5)^2 = 1. \quad (45)$$

283 A.2 Projection operators

Projection operators are defined as

$$P_R = \frac{(1 + \gamma_5)}{2}, P_L = \frac{(1 - \gamma_5)}{2}, \quad (46)$$

so that chiral components can be obtained by acting on spinors

$$\psi_{R/L} = P_{R/L}\psi, \quad (47)$$

$$\bar{\psi}_{R/L} = \bar{\psi}P_{L/R}. \quad (48)$$

It follows that ψ_R and ψ_L are eigenvectors of γ_5 :

$$\gamma_5 \psi_R = +\psi_R, \quad (49)$$

$$\gamma_5 \psi_L = -\psi_L. \quad (50)$$

From their definition, projection operators obey additional properties that are extensively used in this work

$$P_{R/L}^2 = P_{R/L}, \quad (51)$$

$$P_R P_L = P_L P_R = 0, \quad (52)$$

$$P_{R/L} \gamma^\mu = \gamma^\mu P_{L/R}, \quad (53)$$

$$P_{R/L} \sigma^{\mu\nu} = \sigma^{\mu\nu} P_{R/L}, \quad (54)$$

$$P_{R/L} \sigma^{\mu\nu} \gamma_5 = \sigma^{\mu\nu} \gamma_5 P_{L/R}. \quad (55)$$

$$(56)$$

284 A.3 Chiral decomposition of bilinears

Decompositions of bilinears that we have used in this study to separate their chirality are summarised here.

$$\bar{\psi}^{(a)} \gamma^\mu \psi = \bar{\psi}_R^{(a)} \gamma^\mu \psi_R^{(b)} + \bar{\psi}_L^{(a)} \gamma^\mu \psi_L^{(b)}, \quad (57)$$

$$\bar{\psi}^{(a)} \gamma^\mu D^\nu \psi^{(b)} = \bar{\psi}_R^{(a)} \gamma^\mu D^\nu \psi_R^{(b)} + \bar{\psi}_L^{(a)} \gamma^\mu D^\nu \psi_L^{(b)}, \quad (58)$$

$$\bar{\psi}^{(a)} \sigma^{\mu\nu} \psi^{(b)} = \bar{\psi}_R^{(a)} \sigma^{\mu\nu} \psi_L^{(b)} + \bar{\psi}_L^{(a)} \sigma^{\mu\nu} \psi_R^{(b)}, \quad (59)$$

$$\bar{\psi}^{(a)} \sigma^{\mu\nu} \gamma_5 \psi^{(b)} = \bar{\psi}_L^{(a)} \sigma^{\mu\nu} \psi_R^{(b)} - \bar{\psi}_R^{(a)} \sigma^{\mu\nu} \psi_L^{(b)}. \quad (60)$$

One can show that they hold by using projection operators P_R , P_L and their properties:

$$\begin{aligned}
 \bar{\psi}^{(a)} \gamma^\mu \psi &= (\bar{\psi}_R^{(a)} + \bar{\psi}_L^{(a)}) \gamma^\mu (\psi_R^{(b)} + \psi_L^{(b)}) \\
 &= \bar{\psi}_R^{(a)} \gamma^\mu \psi_R^{(b)} + \bar{\psi}_R^{(a)} \gamma^\mu \psi_L^{(b)} + \bar{\psi}_L^{(a)} \gamma^\mu \psi_R^{(b)} + \bar{\psi}_L^{(a)} \gamma^\mu \psi_L^{(b)} \\
 &= \bar{\psi}_R^{(a)} \gamma^\mu \psi_R^{(b)} + \bar{\psi}^{(a)} P_L \gamma^\mu P_L \psi^{(b)} + \bar{\psi}^{(a)} P_R \gamma^\mu P_R \psi^{(b)} + \bar{\psi}_L^{(a)} \gamma^\mu \psi_L^{(b)} \\
 &= \bar{\psi}_R^{(a)} \gamma^\mu \psi_R^{(b)} + \bar{\psi}^{(a)} \gamma^\mu P_R P_L \psi^{(b)} + \bar{\psi}^{(a)} \gamma^\mu P_L P_R \psi^{(b)} + \bar{\psi}_L^{(a)} \gamma^\mu \psi_L^{(b)} \\
 &= \bar{\psi}_R^{(a)} \gamma^\mu \psi_R^{(b)} + \bar{\psi}_L^{(a)} \gamma^\mu \psi_L^{(b)},
 \end{aligned} \tag{61}$$

$$\begin{aligned}
 \bar{\psi}^{(a)} \gamma^\mu D^\nu \psi^{(b)} &= (\bar{\psi}_R^{(a)} + \bar{\psi}_L^{(a)}) \gamma^\mu D^\nu (\psi_R^{(b)} + \psi_L^{(b)}) \\
 &= \bar{\psi}_R^{(a)} \gamma^\mu D^\nu \psi_R^{(b)} + \bar{\psi}_R^{(a)} \gamma^\mu D^\nu \psi_L^{(b)} + \bar{\psi}_L^{(a)} \gamma^\mu D^\nu \psi_R^{(b)} + \bar{\psi}_L^{(a)} \gamma^\mu D^\nu \psi_L^{(b)} \\
 &= \bar{\psi}_R^{(a)} \gamma^\mu D^\nu \psi_R^{(b)} + \bar{\psi}^{(a)} P_L \gamma^\mu D^\nu P_L \psi^{(b)} + \bar{\psi}^{(a)} P_R \gamma^\mu D^\nu P_R \psi^{(b)} + \bar{\psi}_L^{(a)} \gamma^\mu D^\nu \psi_L^{(b)} \\
 &= \bar{\psi}_R^{(a)} \gamma^\mu D^\nu \psi_R^{(b)} + \bar{\psi}^{(a)} \gamma^\mu D^\nu P_R P_L \psi^{(b)} + \bar{\psi}^{(a)} \gamma^\mu P_L P_R \psi^{(b)} + \bar{\psi}_L^{(a)} \gamma^\mu D^\nu \psi_L^{(b)} \\
 &= \bar{\psi}_R^{(a)} \gamma^\mu D^\nu \psi_R^{(b)} + \bar{\psi}_L^{(a)} \gamma^\mu D^\nu \psi_L^{(b)},
 \end{aligned} \tag{62}$$

$$\begin{aligned}
 \bar{\psi}^{(a)} \sigma^{\mu\nu} \psi^{(b)} &= (\bar{\psi}_R^{(a)} + \bar{\psi}_L^{(a)}) \sigma^{\mu\nu} (\psi_R^{(b)} \psi_L^{(b)}) \\
 &= \bar{\psi}_R^{(a)} \sigma^{\mu\nu} \psi_R^{(b)} + \bar{\psi}_R^{(a)} \sigma^{\mu\nu} \psi_L^{(b)} + \bar{\psi}_L^{(a)} \sigma^{\mu\nu} \psi_R^{(b)} + \bar{\psi}_L^{(a)} \sigma^{\mu\nu} \psi_L^{(b)} \\
 &= \bar{\psi}^{(a)} P_L \sigma^{\mu\nu} P_R \psi^{(b)} + \bar{\psi}_R^{(a)} \sigma^{\mu\nu} \psi_L^{(b)} + \bar{\psi}_L^{(a)} \sigma^{\mu\nu} \psi_R^{(b)} + \bar{\psi}^{(a)} P_R \sigma^{\mu\nu} P_L \psi^{(b)} \\
 &= \bar{\psi}^{(a)} \sigma^{\mu\nu} P_L P_R \psi^{(b)} + \bar{\psi}_R^{(a)} \sigma^{\mu\nu} \psi_L^{(b)} + \bar{\psi}_L^{(a)} \sigma^{\mu\nu} \psi_R^{(b)} + \bar{\psi}^{(a)} \sigma^{\mu\nu} P_R P_L \psi^{(b)} \\
 &= \bar{\psi}_R^{(a)} \sigma^{\mu\nu} \psi_L^{(b)} + \bar{\psi}_L^{(a)} \sigma^{\mu\nu} \psi_R^{(b)},
 \end{aligned} \tag{63}$$

$$\begin{aligned}
 \bar{\psi}^{(a)} \sigma^{\mu\nu} \gamma_5 \psi^{(b)} &= (\bar{\psi}_R^{(a)} + \bar{\psi}_L^{(a)}) \sigma^{\mu\nu} \gamma_5 (\psi_R^{(b)} + \psi_L^{(b)}) \\
 &= (\bar{\psi}_R^{(a)} + \bar{\psi}_L^{(a)}) \sigma^{\mu\nu} \gamma_5 (\gamma_5 \psi_R^{(b)} - \gamma_5 \psi_L^{(b)}) \\
 &= (\bar{\psi}_R^{(a)} + \bar{\psi}_L^{(a)}) \sigma^{\mu\nu} (\psi_R^{(b)} - \psi_L^{(b)}) \\
 &= \bar{\psi}_R^{(a)} \sigma^{\mu\nu} \psi_R^{(b)} - \bar{\psi}_R^{(a)} \sigma^{\mu\nu} \psi_L^{(b)} + \bar{\psi}_L^{(a)} \sigma^{\mu\nu} \psi_R^{(b)} - \bar{\psi}_L^{(a)} \sigma^{\mu\nu} \psi_L^{(b)} \\
 &= \bar{\psi}^{(a)} P_L \sigma^{\mu\nu} P_R \psi^{(b)} - \bar{\psi}^{(a)} P_L \sigma^{\mu\nu} P_L \psi^{(b)} + \bar{\psi}^{(a)} P_R \sigma^{\mu\nu} P_R \psi^{(b)} - \bar{\psi}^{(a)} P_R \sigma^{\mu\nu} P_L \psi^{(b)} \\
 &= \bar{\psi}^{(a)} \sigma^{\mu\nu} P_L P_R \psi^{(b)} - \bar{\psi}_R^{(a)} \sigma^{\mu\nu} \psi_L^{(b)} + \bar{\psi}_L^{(a)} \sigma^{\mu\nu} \psi_R^{(b)} - \bar{\psi}^{(a)} \sigma^{\mu\nu} P_R P_L \psi^{(b)} \\
 &= \bar{\psi}_L^{(a)} \sigma^{\mu\nu} \psi_R^{(b)} - \bar{\psi}_R^{(a)} \sigma^{\mu\nu} \psi_L^{(b)}.
 \end{aligned} \tag{64}$$

285 B A map between experiment-based EFT coefficients and Wilson 286 Coefficients

287 In this study we aim at providing a suitable basis translation between Wilson Coefficients from
288 a EFT basis of operators conventionally used by UFO models for Monte Carlo generators (e.g.

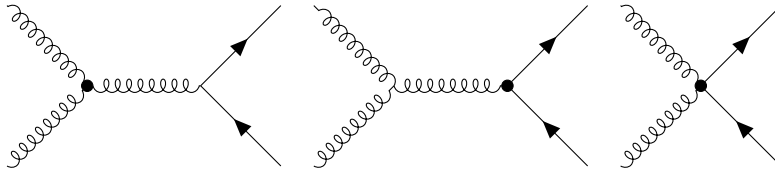


Figure 29: Feynman diagrams showing EFT vertices from dimension-6 operators contributing to top pair production via gluon fusion.

289 `dim6top` [8] and `SMEFT@NLO`[11]), as well as for usual EFT interpretations of LHC data¹, and
 290 the experiment-based EFT coefficients's basis used in the context of phenomenological studies
 291 of top spin correlations[2].

292 B.1 Operators in $gg \rightarrow t\bar{t}$

293 For hadronic top pair production via gluon fusion EFT operators insertions are allowed in the
 294 pure gluon vertex as well as the quark-gluon vertices, as shown in Figure 29). Pure gluonic in-
 295 insertions are highly constrained by multi-jet production[12],[13]. They lie beyond the sensitivity
 296 in top pair production, hence they are disregarded in this study. Operators in the $gt\bar{t}$ vertex,
 297 which parametrises the anomalous chromo-magnetic and chromo-eletric dipole moments of
 298 the top-quark, and in $ggt\bar{t}$ vertex are left.

299 B.1.1 Chromo-magnetic and chromo-eletric dipole moments of top quarks

The real, dimensionless parameters $\hat{\mu}_t$ and \hat{d}_t denote the anomalous chromo-magnetic (CMDM) and chromo-electric (CEDM) dipole moments of the top quark. They relate to the real and imaginary parts of the Wilson coefficient of the operator added into the $gt\bar{t}$ vertex[2]

$$\mathcal{O}_{CDM} = \left[\left(\tilde{\phi} \bar{Q}_L \right) \sigma^{\mu\nu} T^A t_R \right] G_{\mu\nu}^A. \quad (65)$$

where $Q_L = (t_L, b_L)$, $\tilde{\phi} = i\sigma_2 \phi^\dagger = (\phi_0^*, -\phi_-)$ is the charged conjugated Higgs doublet and $G_{\mu\nu}^A = \partial_\mu G_\nu^A - \partial_\nu G_\mu^A - g_s f^{abc} G_\mu^b G_\nu^c$. The operator \mathcal{O}_{tG} implemented in `dim6top` and `SMEFT@NLO` relates with \mathcal{O}_{CDM} via a normalisation by g_s :

$$\mathcal{O}_{tG} = g_s \mathcal{O}_{CDM}. \quad (66)$$

Additionally, we know that the translation between their Wilson coefficients is given by

$$\hat{\mu}_t = \frac{2m_t^2}{\Lambda^2} \text{Re} \left[c_{tg} \right], \quad (67)$$

$$\hat{d}_t = \frac{2m_t^2}{\Lambda^2} \text{Im} \left[c_{tg} \right], \quad (68)$$

We check if the above holds starting by noticing that, after spontaneous symmetry breaking, the only physical degree of freedom left in the Higgs doublet acquires a vacuum expectation value $\langle \phi \rangle = \frac{v}{\sqrt{2}}$. Therefore, the following simplification occurs:

$$\tilde{\phi} \bar{Q}_L = (\phi_0^*, -\phi_-) \cdot (t_L, b_L) \xrightarrow{v.e.v.} \frac{1}{\sqrt{2}} (v, 0) \cdot (t_L, b_L) = \frac{v}{\sqrt{2}} t_L. \quad (69)$$

¹Such basis can be obtained directly from the so-called Warsaw basis[?], normally with some additional symmetry assumption, for example, $U(2)_q \times U(2)_u \times U(2)_d$ flavour symmetry among quarks of the first and second generation. The latter is justified from the fact that at the LHC top-quark observables are largely blind to the light quark flavours with same quantum numbers. In order to see how these operators and their coefficients translates to the Warsaw Basis refer to Appendix C and Table 1 of [8]

\mathcal{O}_{CDM} is non-hermitian, therefore its contribution to the effective Lagrangian must be of the form

$$\mathcal{L}_{eff} = \left(\frac{C_{CDM}}{\Lambda^2} \mathcal{O}_{CDM} + h.c. \right). \quad (70)$$

In order to find $\mathcal{O}_{CDM}^\dagger$ we use the set of properties ²

$$T^{a\dagger} = T^A, \quad (71)$$

$$G_{\mu\nu}^{a*} = G_{\mu\nu}^a, \quad (72)$$

$$\gamma_0^\dagger = \gamma_0, \quad (73)$$

$$\sigma^{\mu\nu\dagger} = \gamma_0 \sigma^{\mu\nu} \gamma_0, \quad (74)$$

$$(\gamma_0)^2 = 1, \quad (75)$$

so that

$$\begin{aligned} \mathcal{O}_{CDM}^\dagger &= \left(\bar{t}_L \sigma^{\mu\nu} T^A t_R \right)^\dagger G_{\mu\nu}^{a*} \\ &= \left(t_R^\dagger \sigma^{\mu\nu\dagger} T^{a\dagger} (\bar{t}_L)^\dagger \right) G_{\mu\nu}^a \\ &= \left(t_R^\dagger \gamma_0 \sigma^{\mu\nu\dagger} \gamma_0 T^a \gamma_0^\dagger t_L \right) G_{\mu\nu}^a \\ &= \left(t_R^\dagger \gamma_0 \sigma^{\mu\nu} T^A t_L \right) G_{\mu\nu}^a \\ &= \left(\bar{t}_R \sigma^{\mu\nu} T^A t_L \right) G_{\mu\nu}^a. \end{aligned} \quad (76)$$

Using the expression for $\mathcal{O}_{CDM}^\dagger$, the effective Lagrangian can be further simplified

$$\begin{aligned} \mathcal{L}_{eff} &= \left(\frac{C_{CDM}}{\Lambda^2} \mathcal{O}_{CDM} + h.c. \right) \\ &= \frac{\nu}{\sqrt{2}\Lambda^2} \left[C_{CDM} \left(\bar{t}_L \sigma^{\mu\nu} T^A t_R \right) G_{\mu\nu}^A + C_{CDM}^* \left(\bar{t}_R \sigma^{\mu\nu} T^A t_L \right) G_{\mu\nu}^A \right] \\ &= \frac{\nu}{\sqrt{2}\Lambda^2} \left[C_{CDM} \left(\bar{t}_R P_R \sigma^{\mu\nu} T^A P_R t \right) G_{\mu\nu}^A + C_{CDM}^* \left(\bar{t}_L P_L \sigma^{\mu\nu} T^A P_L t \right) G_{\mu\nu}^A \right] \\ &= \frac{\nu}{\sqrt{2}\Lambda^2} \left[C_{CDM} \left(\bar{t}_R \sigma^{\mu\nu} T^A P_R^2 t \right) G_{\mu\nu}^A + C_{CDM}^* \left(\bar{t}_L \sigma^{\mu\nu} T^A P_L^2 t \right) G_{\mu\nu}^A \right] \\ &= \frac{\nu}{\sqrt{2}\Lambda^2} \left[C_{CDM} \left(\bar{t}_R \sigma^{\mu\nu} T^A t_R \right) G_{\mu\nu}^A + C_{CDM}^* \left(\bar{t}_L \sigma^{\mu\nu} T^A t_L \right) G_{\mu\nu}^A \right] \\ &= \frac{\nu}{\sqrt{2}\Lambda^2} \left[\bar{t}_R \sigma^{\mu\nu} T^A \left(C_{CDM} t_R + C_{CDM}^* t_L \right) G_{\mu\nu}^A \right], \end{aligned} \quad (77)$$

where we additionally used that

$$P_{R/L} = \frac{(1 \pm \gamma_5)}{2} \Rightarrow \psi_{R/L} = P_{R/L} \psi, \quad (78)$$

$$P_R^2 = P_R \text{ and } P_L^2 = P_L, \quad (79)$$

$$[P_{R/L}, \sigma^{\mu\nu}] = 0 \quad (80)$$

²In red is not verified, but it assumes that the gluon field G_μ^A is real.

For complex valued C_{CDM} one can rewrite the same Lagragian alternatively as

$$\mathcal{L}_{eff} = \frac{\text{Re}[C_{CDM}]}{\Lambda^2} \left(\mathcal{O}_{CDM} + \mathcal{O}_{CDM}^\dagger \right) + i \frac{\text{Im}[C_{CDM}]}{\Lambda^2} \left(\mathcal{O}_{CDM} - \mathcal{O}_{CDM}^\dagger \right) \quad (81)$$

$$= \frac{\nu}{\sqrt{2}\Lambda^2} \left[\text{Re}[C_{CDM}] \left(\bar{t}\sigma^{\mu\nu} T^A (t_R + t_L) G_{\mu\nu}^a \right) + i\text{Im}[C_{CDM}] \left(\bar{t}\sigma^{\mu\nu} T^A (t_R - t_L) G_{\mu\nu}^a \right) \right]. \quad (82)$$

Using the eigenvalues relations $\gamma_5 t_R = t_R$ and $\gamma_5 t_L = -t_L$ to insert γ_5 in the second term of (82), we have

$$\mathcal{L}_{eff} = \frac{\nu}{\sqrt{2}\Lambda^2} \left[\text{Re}[C_{CDM}] (\bar{t}\sigma^{\mu\nu} T^A t) G_{\mu\nu}^A + \text{Im}[C_{CDM}] i(\bar{t}\sigma^{\mu\nu} \gamma_5 T^A t) G_{\mu\nu}^A \right] \quad (83)$$

Comparing it with equation (3.5) of [2], knowing that in their convention the QCD quark gluon interaction ($\mathcal{L} = -g_s \bar{q} \gamma^\mu T^A q G_\mu^A$) adds an additional minus sign with respect to the dim6top [8], one can read-off the correspondence

$$\frac{g_s}{2m_t} \hat{\mu}_t = \frac{\nu}{\sqrt{2}\Lambda^2} \text{Re}[C_{CDM}], \quad (84)$$

$$\frac{g_s}{2m_t} \hat{d}_t = \frac{\nu}{\sqrt{2}\Lambda^2} \text{Im}[C_{CDM}]. \quad (85)$$

Additional simplifications can still be done. The mass of a fermion is given by the strength of its respective Yukawa interaction, i.e.

$$g_f = \sqrt{2}m_f/\nu. \quad (86)$$

Furthermore, it is known that the coupling strength is related with the top Yukawa term in the Yukawa matrix by $y_t = g_t/g_t^{SM}$. On the other hand, top mass measurements[14],[15] combined with eq. (86) gives $g_t^{SM} \approx 1$. Lastly, both dim6top and SMEFT@NLO assume both $y_t = 1$, which is in accordance with experimental bounds [16]. Therefore, in this context, one can safely assume $g_t \approx 1$ and use $m_t = \nu/\sqrt{2}$ to reduce the relations to

$$g_s \hat{\mu}_t = \frac{2m_t^2}{\Lambda^2} \text{Re}[C_{CDM}], \quad (87)$$

$$g_s \hat{d}_t = \frac{2m_t^2}{\Lambda^2} \text{Im}[C_{CDM}]. \quad (88)$$

³⁰⁰ Considering that \mathcal{O}_{tG} is normalised by g_s , we know that $c_{tG} = C_{CDM}/g_s$. Therefore the translation obtained agrees with eq. (67) and (68).

³⁰² B.1.2 Additional CP-violating degrees of freedom in $gg \rightarrow t\bar{t}$

Reference [2] shows two additional operators involving two quarks and up to three gluons

$$\mathcal{O}_{gt} = \left[\bar{t}_R \gamma^\mu T^A D^\nu t_R \right] G_{\mu\nu}^A, \quad (89)$$

$$\mathcal{O}_{gQ} = \left[\bar{Q}_L \gamma^\mu T^A D^\nu Q_L \right] G_{\mu\nu}^A. \quad (90)$$

³⁰³ where $D_\mu = \partial_\mu + ig_s T^A G_\mu^A$. These operators are non-hermitian, thus they have complex Wilson coefficients. However, $\mathcal{O}_{gt} + \mathcal{O}_{gt}^\dagger$ and $\mathcal{O}_{gQ} + \mathcal{O}_{gQ}^\dagger$ can be expressed as a combination of four-fermion operators (c.f. equations (7) and (8) from [4]), meaning that they are redundant. Once

306 we treat four-fermion operators separately in this work, $\mathcal{O}_{gt} + \mathcal{O}_{gt}^\dagger$ and $\mathcal{O}_{gQ} + \mathcal{O}_{gQ}^\dagger$ do not add
 307 new degrees of freedom. Their differences in turn, $\mathcal{O}_{gt} - \mathcal{O}_{gt}^\dagger$ and $\mathcal{O}_{gQ} - \mathcal{O}_{gQ}^\dagger$, are CP -odd and
 308 cannot be written as a combination of four-fermion operators. Thus, only the imaginary part of
 309 the Wilson coefficients from \mathcal{O}_{gt} and \mathcal{O}_{gQ} contains new degrees of freedom. These parameters
 310 will be encoded in \mathcal{O}_{-+}^g and \mathcal{O}_{-+}^q , as defined by [2], after restriction to the top-quark gluon
 311 sector. Here we show first how the latter can be constructed.

Note that the sum $\mathcal{O}_{gt} + \mathcal{O}_{gQ}$ restricted to the top-sector results in a non-hermitian operator with positive parity

$$\begin{aligned}\mathcal{O}_+ &\equiv \mathcal{O}_{gt} + \mathcal{O}_{gQ} \\ &= [\bar{t}_R \gamma^\mu T^A D^\nu t_R] G_{\mu\nu}^a + [\bar{t}_L \gamma^\mu T^A D^\nu t_L] G_{\mu\nu}^a \\ &= [\bar{t} \gamma^\mu T^A D^\nu t] G_{\mu\nu}^a,\end{aligned}\tag{91}$$

where in the last equality we used that $\bar{\psi} \gamma^\mu D^\nu \psi = \bar{\psi}_R \gamma^\mu D^\nu \psi_R + \bar{\psi}_L \gamma^\mu D^\nu \psi_L$ ³. Given the arguments on redundant operators stated before, only a combination of the operators $\mathcal{O}_{gt} - \mathcal{O}_{gt}^\dagger$ and $\mathcal{O}_{gQ} - \mathcal{O}_{gQ}^\dagger$ adds new degrees of freedom. They are encoded in the CP -odd, P -even hermitian operator defines as

$$\begin{aligned}\mathcal{O}_{-+} &\equiv i(\mathcal{O}_+ - \mathcal{O}_+^\dagger) \\ &= i[(\mathcal{O}_{gt} - \mathcal{O}_{gt}^\dagger) + (\mathcal{O}_{gQ} - \mathcal{O}_{gQ}^\dagger)],\end{aligned}\tag{92}$$

312 which takes care of one of the degrees of freedom.

The remaining degree of freedom can be isolated analogously. The difference $\mathcal{O}_{gt} - \mathcal{O}_{gQ}$ defines an operator with negative parity

$$\begin{aligned}\mathcal{O}_- &\equiv i[\mathcal{O}_{gt} - \mathcal{O}_{gQ}] \\ &= i[\bar{t}_R \gamma^\mu T^A D^\nu t_R] G_{\mu\nu}^a - i[\bar{t}_L \gamma^\mu T^A D^\nu t_L] G_{\mu\nu}^a \\ &= i[\bar{t}_R \gamma^\mu T^A D^\nu \gamma_5 t_R] G_{\mu\nu}^a + i[\bar{t}_L \gamma^\mu T^A D^\nu \gamma_5 t_L] G_{\mu\nu}^a \\ &= i[\bar{t} \gamma^\mu \gamma_5 T^A D^\nu t] G_{\mu\nu}^a.\end{aligned}\tag{93}$$

where, we again used eigenvalues relation to insert γ_5 . By the same type of arguments, only the combination of $\mathcal{O}_{gt} - \mathcal{O}_{gt}^\dagger$ and $\mathcal{O}_{gQ} - \mathcal{O}_{gQ}^\dagger$ have new degrees of freedom, which is given by the CP -Odd, P -Odd hermitian

$$\begin{aligned}\mathcal{O}_{--} &\equiv (\mathcal{O}_- + \mathcal{O}_-^\dagger), \\ &= i[(\mathcal{O}_{gt} - \mathcal{O}_{gt}^\dagger) - (\mathcal{O}_{gQ} - \mathcal{O}_{gQ}^\dagger)].\end{aligned}\tag{94}$$

313 At this point, it is important to highlight that \mathcal{O}_{-+} and \mathcal{O}_{--} , although containing new degrees
 314 of freedom are not implemented in `dim6top` or `SMEFT@NLO`, at least not directly. However,
 315 eq. (23) from [3] presents explicit relations for \mathcal{O}_{gt} and \mathcal{O}_{gQ} ⁴ as a combination of O_{CDM} , flavour
 316 changing neutral current (FCNC) and four-fermion operators. Considering that `dim6top` also
 317 implements some FCNC operators, where the stricter flavour conservation assumptions are
 318 relaxed, we attempt to derive a basis translation for \mathcal{O}_{-+} and \mathcal{O}_{--} as well.

³A general prove for such bilinears decomposition are given in 58

⁴In [3], they correspond to O_{uG}^{33} and O_{qG}^{33} , respectively.

In our notation, the expressions for \mathcal{O}_{gt} and \mathcal{O}_{gQ} in terms of the other operators [3] are⁵

$$\begin{aligned}\mathcal{O}_{gt} &= \frac{1}{4} \left[Y_{k3}^u O_{uG}^{k3} - Y_{3k}^u {}^\dagger (O_{uG}^{3k}) {}^\dagger \right] \\ &+ \frac{g_s}{4} \left[(\bar{t}_R \gamma^\mu T^A t_R) (\bar{q}_{Lk} \gamma_\mu T^A q_{Lk}) + (\bar{t}_R \gamma^\mu T^A t_R) (\bar{u}_{Rk} \gamma_\mu T^A u_{Rk}) + (\bar{t}_R \gamma^\mu T^A t_R) (\bar{d}_{Rk} \gamma_\mu T^A d_{Rk}) \right] \\ &= \frac{1}{4} \left[Y_{33}^u \mathcal{O}_{tG} - Y_{33}^u {}^\ast \mathcal{O}_{tG}^\dagger + Y_{a3}^u O_{uG}^{a3} - Y_{3a}^u {}^\dagger (O_{uG}^{a3}) {}^\dagger \right] + \frac{g_s}{4} \left[\mathcal{O}_{tq}^{(8)} + \mathcal{O}_{Qt}^{(8)} + \mathcal{O}_{tu}^{(8)} + \mathcal{O}_{tt}^{(8)} + \mathcal{O}_{td}^{(8)} + \mathcal{O}_{tb}^{(8)} \right],\end{aligned}\tag{95}$$

$$\begin{aligned}\mathcal{O}_{gQ} &= -\frac{1}{4} \left[Y_{3k}^u O_{uG}^{3k} + Y_{3k}^d O_{dG}^{3k} - Y_{k3}^u {}^\dagger (O_{uG}^{3k}) {}^\dagger - Y_{k3}^d {}^\dagger (O_{dG}^{3k}) {}^\dagger \right] \\ &+ \frac{g_s}{4} \left[(\bar{Q}_L \gamma^\mu T^A Q_L) (\bar{q}_{Lk} \gamma_\mu T^A q_{Lk}) + (\bar{Q}_L \gamma^\mu T^A Q_L) (\bar{u}_{Rk} \gamma_\mu T^A u_{Rk}) + (\bar{Q}_L \gamma^\mu T^A Q_L) (\bar{d}_{Rk} \gamma_\mu T^A d_{Rk}) \right] \\ &= -\frac{1}{4} \left[Y_{33}^u \mathcal{O}_{tG} - Y_{33}^u {}^\ast \mathcal{O}_{tG}^\dagger + Y_{3a}^u O_{uG}^{3a} - Y_{a3}^u {}^\dagger (O_{uG}^{3a}) {}^\dagger \right] + \frac{g_s}{4} \left[\mathcal{O}_{Qq}^{(8,1)} + \mathcal{O}_{QQ}^{(8)} + \mathcal{O}_{Qu}^{(8)} + \mathcal{O}_{Qt}^{(8)} + \mathcal{O}_{Qd}^{(8)} + \mathcal{O}_{Qb}^{(8)} \right],\end{aligned}\tag{96}$$

where k, a are the quark generation indices for the three generations ($k = 1, 2, 3$) and for the two lightest generations ($a = 1, 2$). Sum in k and a are implied. Observe that we disregard $O_{dG}^{(ij)}$ in \mathcal{O}_{gQ} because it does not contribute to top couplings. Also, observe that O_{uG}^{3a} and O_{uG}^{a3} are FCNC operators implemented in `dim6top`. Finally note that 5 operators: $\mathcal{O}_{QQ}^{(8)}, \mathcal{O}_{Qt}^{(8)}, \mathcal{O}_{Qb}^{(8)}, \mathcal{O}_{tt}^{(8)}, \mathcal{O}_{tb}^{(8)}$, were not considered in [2]. Most likely, they are not relevant for top studies because they contain only heavy quarks⁶. Nonetheless, as we shall see, including them will not change our final statements about \mathcal{O}_{+-} and \mathcal{O}_{--} . For simplicity, we disregard them from now on. Hence, the four-fermion operators left can be summarised by the definition of the so-called \mathcal{O}_{VV} and \mathcal{O}_{VA} (defined later in detail in this work study eqs. (136) and (139)). Using them to shorten our expressions

$$\mathcal{O}_+ = \mathcal{O}_{gt} + \mathcal{O}_{gq} = \frac{1}{4} \left[(Y_{a3}^u O_{uG}^{a3} - Y_{3a}^u {}^\dagger (O_{uG}^{a3}) {}^\dagger) - (Y_{3a}^u O_{uG}^{3a} - Y_{a3}^u {}^\dagger (O_{uG}^{3a}) {}^\dagger) \right] + \frac{g_s}{4} \mathcal{O}_{VV},\tag{97}$$

$$\mathcal{O}_- = i \left[\mathcal{O}_{gt} - \mathcal{O}_{gq} \right] = \frac{i}{4} \left[2(Y_{33}^u \mathcal{O}_{tG} - Y_{33}^u {}^\ast \mathcal{O}_{tG}^\dagger) + (Y_{a3}^u O_{uG}^{a3} - Y_{3a}^u {}^\dagger (O_{uG}^{a3}) {}^\dagger) \right.\tag{98}$$

$$\left. + (Y_{3a}^u O_{uG}^{3a} - Y_{a3}^u {}^\dagger (O_{uG}^{3a}) {}^\dagger) \right] + \frac{g_s}{4} i \mathcal{O}_{VA},\tag{99}$$

⁵Our notation is very similar to that of `dim6top` [8], but we write the chirality explicit in the sub-indices, *i.e.* $Q, q \rightarrow Q_L, q_L$ and $t, b, u, d \rightarrow t_R, b_R, u_R, d_R$

⁶For $\mathcal{O}_{tt}^{(8)}$, there is not even a `dim6top` implementation, most likely, for it being also expressed in terms of other four-heavy quark operators (c.f. eq. 67 in [8])

From that it is easy to see that all four-fermion operators vanishes in \mathcal{O}_{-+} and \mathcal{O}_{--} .

$$\begin{aligned}
\mathcal{O}_{-+} &= +\frac{i}{4} \left[(Y_{a3}^u O_{uG}^{a3} - Y_{3a}^u {}^\dagger (O_{uG}^{a3})^\dagger) - (Y_{3a}^u O_{uG}^{3a} - Y_{a3}^u {}^\dagger (O_{uG}^{3a})^\dagger) \right] \\
&\quad - \frac{i}{4} \left[(Y_{a3}^u O_{uG}^{a3} - Y_{3a}^u {}^\dagger (O_{uG}^{a3})^\dagger) - (Y_{3a}^u O_{uG}^{3a} - Y_{a3}^u {}^\dagger (O_{uG}^{3a})^\dagger) \right]^\dagger \\
&= \left[\frac{i}{4} (Y_{a3}^u O_{uG}^{a3} - (Y_{a3}^u O_{uG}^{a3})^\dagger) - \frac{i}{4} (Y_{3a}^u O_{uG}^{3a} - (Y_{3a}^u O_{uG}^{3a})^\dagger) \right] \\
&\quad + \left[\frac{i}{4} (Y_{a3}^u O_{uG}^{a3} - (Y_{a3}^u O_{uG}^{a3})^\dagger) - \frac{i}{4} (Y_{3a}^u O_{uG}^{3a} - (Y_{3a}^u O_{uG}^{3a})^\dagger) \right]^\dagger \\
&= 2 \left[\frac{i}{4} (Y_{a3}^u O_{uG}^{a3} - (Y_{a3}^u O_{uG}^{a3})^\dagger) - \frac{i}{4} (Y_{3a}^u O_{uG}^{3a} - (Y_{3a}^u O_{uG}^{3a})^\dagger) \right], \tag{100}
\end{aligned}$$

where we used the property that each subtraction inside the brackets multiplied by i , for example $i(Y_{a3}^u O_{uG}^{a3} - (Y_{a3}^u O_{uG}^{a3})^\dagger)$ is a hermitian matrix. Formally this comes from the fact that all term under brackets, e.g. $(Y_{a3}^u O_{uG}^{a3} - (Y_{a3}^u O_{uG}^{a3})^\dagger)$, define anti-hermitian matrices by construction⁷. Therefore the expression can be simplified to

$$\mathcal{O}_{-+} = \frac{i}{2} \left[(Y_{a3}^u O_{uG}^{a3} - (Y_{a3}^u O_{uG}^{a3})^\dagger) - (Y_{3a}^u O_{uG}^{3a} - (Y_{3a}^u O_{uG}^{3a})^\dagger) \right]. \tag{103}$$

Motivated by previous studies with FCNC, we can define $Y_{a3}^u = Y_{3a}^u = y_t$, where y_t is the Yukawa coupling of the top-quark[17]. Then, any deviations of Y_{a3}^u and Y_{3a}^u from y_t will be encoded in the Wilson coefficients. With that, (103) gives a tentative basis translation

$$c_{-+} \propto \frac{1}{2} \sum_a (c_{uG}^{I(a3)} - c_{uG}^{I(3a)}). \tag{104}$$

³¹⁹ Non-null c_{-+} would imply that that CP -odd, P -even effects are produced when $c_{uG}^{I(a3)} \neq c_{uG}^{I(3a)}$
³²⁰ and that at least one of them is non-null. This would also mean that, if that happens, at least
³²¹ one of the Yukawa terms, Y_{a3}^u and Y_{3a}^u , is complex and that their imaginary part is asymmetric
³²² between each other. Knowing that they are related with the CKM matrix⁸, it is not unrealistic
³²³ to think that such combinations will result in a complex CP -violating V_{CKM} .

⁷ Given an arbitrary matrix C an Hermitian matrix H and a anti-hermitian A can be constructed as

$$H = \frac{1}{2}(C + C^\dagger) \tag{101}$$

$$A = \frac{1}{2}(C - C^\dagger) \tag{102}$$

Moreover for every A , iA is hermitian.

⁸ The Y^u relates with the mass matrix by $M_{diag}^u = V_L^u Y^u V_R^{u\dagger} (\nu / \sqrt{2})$ and V_{CKM} is defined by $V_{CKM} = V_L^u V_L^{d\dagger}$.

We will do the analogous process for \mathcal{O}_{--} ,

$$\mathcal{O}_{--} = \left[\frac{i}{2} (Y_{33}^u \mathcal{O}_{tG} - Y_{33}^{u*} \mathcal{O}_{tG}^\dagger) + \frac{i}{4} (Y_{a3}^u O_{uG}^{a3} - Y_{3a}^{u\dagger} (O_{uG}^{a3})^\dagger) + \frac{i}{4} (Y_{3a}^u O_{uG}^{3a} - Y_{a3}^{u\dagger} (O_{uG}^{3a})^\dagger) \right] \quad (105)$$

$$+ \left[\frac{i}{2} (Y_{33}^u \mathcal{O}_{tG} - Y_{33}^{u*} \mathcal{O}_{tG}^\dagger) + \frac{i}{4} (Y_{a3}^u O_{uG}^{a3} - Y_{3a}^{u\dagger} (O_{uG}^{a3})^\dagger) + \frac{i}{4} (Y_{3a}^u O_{uG}^{3a} - Y_{a3}^{u\dagger} (O_{uG}^{3a})^\dagger) \right]^\dagger \quad (106)$$

$$= Y_{33}^u i (\mathcal{O}_{tG} - (\mathcal{O}_{tG})^\dagger) + \left[\frac{i}{4} (Y_{a3}^u O_{uG}^{a3} - (Y_{a3}^u (O_{uG}^{a3})^\dagger)) + \frac{i}{4} (Y_{3a}^u O_{uG}^{3a} - (Y_{3a}^u (O_{uG}^{3a})^\dagger)) \right] \quad (107)$$

$$+ \left[\frac{i}{4} (Y_{a3}^u O_{uG}^{a3} - (Y_{a3}^u (O_{uG}^{a3})^\dagger)) + \frac{i}{4} (Y_{3a}^u O_{uG}^{3a} - (Y_{3a}^u (O_{uG}^{3a})^\dagger)) \right]^\dagger, \quad (108)$$

that simplifies to

$$\mathcal{O}_{--} = Y_{33}^u i (\mathcal{O}_{tG} - (\mathcal{O}_{tG})^\dagger) + \frac{i}{2} \left[(Y_{a3}^u O_{uG}^{a3} - (Y_{a3}^u O_{uG}^{a3})^\dagger) + (Y_{3a}^u O_{uG}^{3a} - (Y_{3a}^u O_{uG}^{3a})^\dagger) \right]. \quad (109)$$

Defining again Wilson coefficients embedding Y_{ij}^u in their definitions, the translation is

$$c_{--} \propto c_{tG}^I + \frac{1}{2} \sum_a (c_{uG}^{I(a3)} + c_{uG}^{I(3a)}). \quad (110)$$

Because the respective PDFs suppress $t\bar{t}$ production by $q\bar{q}$ annihilation for $q = s, c, b$ as compared to $q = u, d$, only contributions with u, d in the initial states are accounted in [2], one could think that only $a = 1$ terms could contributes. However, this is not true, since we are concerned with $gg \rightarrow tbart$ processes, with no quarks in the initial state. Therefore, we should keep the two generations. Below, for facilitating comparisons, we will keep just one generation for pedagogical purposes. So, analysing only the $a = 1$ case and comparing it with eq. (3.4) from [2], our basis translation reads⁹

$$\frac{g_s^2}{m_t^2} \hat{c}_{-+} \propto \frac{1}{2} \left(\frac{c_{uG}^{I(13)}}{\Lambda^2} - \frac{c_{uG}^{I(31)}}{\Lambda^2} \right), \quad (111)$$

$$\frac{g_s^2}{m_t^2} \hat{c}_{--} \propto \frac{c_{tG}^I}{\Lambda^2} + \frac{1}{2} \left(\frac{c_{uG}^{I(13)}}{\Lambda^2} + \frac{c_{uG}^{I(31)}}{\Lambda^2} \right). \quad (112)$$

Considering the case where the couplings $c_{uG}^{I(13)}, c_{uG}^{I(31)}$ are normalised by g_s , as it is the case for c_{tG}^I , for consistency, we have our final translation

$$\hat{c}_{-+} = \frac{m_t^2}{2g_s} \left(\frac{c_{uG}^{I(13)}}{\Lambda^2} - \frac{c_{uG}^{I(31)}}{\Lambda^2} \right), \quad (113)$$

$$\hat{c}_{--} = \frac{m_t^2}{g_s} \frac{c_{tG}^I}{\Lambda^2} + \frac{m_t^2}{2g_s} \left(\frac{c_{uG}^{I(13)}}{\Lambda^2} + \frac{c_{uG}^{I(31)}}{\Lambda^2} \right). \quad (114)$$

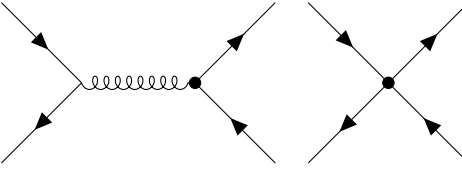


Figure 30: Feynman diagrams showing insertion of one dimension-6 operator in top pair production via $q\bar{q}$.

³²⁴ B.2 Four-fermion operators in $q\bar{q} \rightarrow t\bar{t}$

In the hadronic top pair production via $q\bar{q}$ initial states at leading order, EFT can be inserted in the $g\bar{t}t$ vertex as well as four-fermion vertices can be added as shown in Figure (30). The former was already discussed in the context of gluon fusion. The relevant four-fermion operators are presented in [2] as

$$\mathcal{O}_{VV} = (\bar{q}\gamma^\mu T^A q)(\bar{t}\gamma_\mu T^A t), \quad (115)$$

$$\mathcal{O}_{VA} = (\bar{q}\gamma^\mu T^A q)(\bar{t}\gamma_\mu \gamma_5 T^A t), \quad (116)$$

$$\mathcal{O}_{AV} = (\bar{q}\gamma^\mu \gamma_5 T^A q)(\bar{t}\gamma_\mu T^A t), \quad (117)$$

$$\mathcal{O}_{AA} = (\bar{q}\gamma^\mu \gamma_5 T^A q)(\bar{t}\gamma_\mu \gamma_5 T^A t), \quad (118)$$

$$\mathcal{O}_1^1 = (\bar{q}\gamma^\mu T^A \sigma_3 q)(\bar{t}\gamma_\mu T^A t) + (\bar{q}\gamma^\mu \gamma_5 T^A \sigma_3 q)(\bar{t}\gamma_\mu T^A t), \quad (119)$$

$$\mathcal{O}_2^1 = (\bar{q}\gamma^\mu \gamma_5 T^A \sigma_3 q)(\bar{t}\gamma_\mu \gamma_5 T^A t) - (\bar{q}\gamma^\mu \gamma_5 T^A \sigma_3 q)(\bar{t}\gamma_\mu T^A t), \quad (120)$$

$$\mathcal{O}_3^1 = (\bar{q}\gamma^\mu T^A \sigma_3 q)(\bar{t}\gamma_\mu \gamma_5 T^A t) + (\bar{q}\gamma^\mu \gamma_5 T^A \sigma_3 q)(\bar{t}\gamma_\mu T^A t), \quad (121)$$

³²⁵ where in [2] $q = (u, d)$ corresponds only to the light quarks of the first generation.

Such operators can be obtained by combinations of operators implemented by `dim6top`, SMEFT@NLO. Here we try to find their translation. We start by selecting all four-fermion operators containing top pairs together with light quarks that can interfere with SM QCD amplitudes at tree level. There are seven independent two-heavy-two-light degrees of freedom that can be obtained via the Warsaw Basis under the $U(2)_q \times U(2)_u \times U(2)_d$ flavour assumption. Besides forming colour octets, these operators can be organised following their chiral structure:

$\bar{L}L\bar{L}L$:

$$\mathcal{O}_{Qq}^{(8,1)} = (\bar{Q}_L \gamma^\mu T^A Q_L)(\bar{q}_L \gamma_\mu T^A q_L), \quad (122)$$

$$\mathcal{O}_{Qq}^{(8,3)} = (\bar{Q}_L \gamma^\mu T^A \sigma^A Q_L)(\bar{q}_L \gamma_\mu T^A \sigma^A q_L), \quad (123)$$

$\bar{L}L\bar{R}R$:

$$\mathcal{O}_{Qu}^{(8)} = (\bar{Q}_L \gamma^\mu T^A Q_L)(\bar{u}_R \gamma_\mu T^A u_R), \quad (124)$$

$$\mathcal{O}_{Qd}^{(8)} = (\bar{Q}_L \gamma^\mu T^A Q_L)(\bar{d}_R \gamma_\mu T^A d_R), \quad (125)$$

$$\mathcal{O}_{tq}^{(8)} = (\bar{q}_L \gamma^\mu T^A q_L)(\bar{t}_R \gamma_\mu T^A t_R), \quad (126)$$

$\bar{R}R\bar{R}R$:

$$\mathcal{O}_{tu}^{(8)} = (\bar{t}_R \gamma^\mu T^A t_R)(\bar{u}_R \gamma_\mu T^A u_R), \quad (127)$$

$$\mathcal{O}_{td}^{(8)} = (\bar{t}_R \gamma^\mu T^A t_R)(\bar{d}_R \gamma_\mu T^A d_R). \quad (128)$$

³²⁶ where $Q_L = (t_L, b_L)$ are the left-handed weak doublets of the third quark generation, $q_L = (u_L, d_L)$ are those of the first two generations, t_R is the right-handed top quark and, finally,

⁹There could be a sign difference between [2] and `dim6top`, need a check.

³²⁸ u_R, d_R are the right-handed singlets of the first two generations. Moreover, σ^A are the Pauli
³²⁹ matrices (normalised to $\text{tr}(\sigma^A \sigma^B) = 2\delta^{AB}$) and T^A are the generators of SU(3) in the fundamental
³³⁰ representation (normalised to $\text{tr}(T^A T^b) = \delta^{ab}/2$).

³³¹ B.2.1 Isospin-0 operators

They can be combined to have definite $SU(2)$ isospin symmetry. In the isospin-0 sector, vector-like and axial-vector-like combinations are possible[4]. The right-handed part is given by

$$\mathcal{O}_{Rv} = \mathcal{O}_{tu}^{(8)} + \mathcal{O}_{td}^{(8)} + \mathcal{O}_{tq}^{(8)}, \quad \mathcal{O}_{Ra} = \mathcal{O}_{tu}^{(8)} + \mathcal{O}_{td}^{(8)} - \mathcal{O}_{tq}^{(8)}, \quad (129)$$

while the left-handed by

$$\mathcal{O}_{Lv} = \mathcal{O}_{Qu}^{(8)} + \mathcal{O}_{Qd}^{(8)} + \mathcal{O}_{Qq}^{(8,1)}, \quad \mathcal{O}_{La} = \mathcal{O}_{Qu}^{(8)} + \mathcal{O}_{Qd}^{(8)} - \mathcal{O}_{Qq}^{(8,1)}. \quad (130)$$

We check that explicitly using eqs. (122)-(128)

$$\mathcal{O}_{Rv} = (\bar{t}_R \gamma^\mu T^A t_R) (\bar{u}_R \gamma_\mu T^A u_R + \bar{d}_R \gamma_\mu T^A d_R + \bar{q}_L \gamma^\mu T^A q_L), \quad (131)$$

$$= (\bar{t}_R \gamma^\mu T^A t_R) (\bar{q} \gamma_\mu T^A q), \quad (132)$$

$$\mathcal{O}_{Lv} = (\bar{Q}_L \gamma^\mu T^A Q_L) (\bar{u}_R \gamma_\mu T^A u_R + \bar{d}_R \gamma_\mu T^A d_R + \bar{q}_L \gamma_\mu T^A q_L), \quad (133)$$

$$= (\bar{Q}_L \gamma^\mu T^A Q_L) (\bar{q} \gamma_\mu T^A q), \quad (134)$$

³³² where in eqs. (132) and (134), $\bar{\psi} \gamma^\mu \psi = \bar{\psi}_L \gamma^\mu \psi_L + \bar{\psi}_R \gamma^\mu \psi_R$ ¹⁰ was used.

Note that the reason for the separation in axial-vector and vector combinations is that they have well-defined discrete symmetries that affect spin observables (P,CP)¹¹. In turn, they can be also combined in terms of axial- and vector-like behaviour for the heavy quarks par

$$\begin{aligned} \mathcal{O}_{Rv} + \mathcal{O}_{Lv} &= (\bar{t}_R \gamma^\mu T^A t_R + \bar{Q}_L \gamma^\mu T^A Q_L) (\bar{q} \gamma_\mu T^A q), \\ &= \left((\bar{t}_R \quad 0) \gamma^\mu T^A \begin{pmatrix} t_R \\ 0 \end{pmatrix} + (\bar{t}_L \quad \bar{b}_L) \gamma^\mu T^A \begin{pmatrix} t_L \\ b_L \end{pmatrix} \right) (\bar{q} \gamma_\mu T^A q), \\ &= (\bar{t} \gamma^\mu T^A t) (\bar{q} \gamma_\mu T^A q) + (\bar{b}_L \gamma^\mu T^A b_L) (\bar{q} \gamma_\mu T^A q) \equiv \mathcal{O}_{Vv}. \end{aligned} \quad (135)$$

¹⁰One can see that this holds by writing

$$\bar{\psi} \gamma^\mu \psi = (\bar{\psi}_L + \bar{\psi}_R) \gamma^\mu (\psi_L + \psi_R) = \bar{\psi}_L \gamma^\mu \psi_L + \bar{\psi}_R \gamma^\mu \psi_R + \bar{\psi}_L \gamma^\mu \psi_R + \bar{\psi}_R \gamma^\mu \psi_L,$$

and inserting the projection operators,

$$P_L = (1 - \gamma_5)/2 \text{ and } P_R = (1 + \gamma_5)/2,$$

to see that each crossing term vanishes:

$$\bar{\psi}_R \gamma^\mu \psi_L = \bar{\psi} P_L \gamma^\mu P_L \psi_L = \bar{\psi} \gamma^\mu P_R P_L \psi_L = 0$$

$$\bar{\psi}_L \gamma^\mu \psi_R = \bar{\psi} P_R \gamma^\mu P_R \psi_R = \bar{\psi} \gamma^\mu P_L P_R \psi_R = 0.$$

More general calculation of this type are shown in the Appendix A.1.

¹¹For instance, axial operators are asymmetric under exchange of a quark and an antiquark (C-odd)

$$\bar{\psi}(k_1) \gamma_\mu \gamma_5 T^A \psi(k_2) = -\bar{\psi}^c(k_2) \gamma_\mu \gamma_5 T^A \psi^c(k_1),$$

while the vector operators are symmetric:

$$\bar{\psi}(k_1) \gamma_\mu T^A \psi(k_2) = \bar{\psi}^c(k_2) \gamma_\mu T^A \psi^c(k_1).$$

When we are interested in final states where the initial partons have given rise to top quarks only, the b_L -dependent term vanishes. Hence

$$\begin{aligned}\mathcal{O}_{Vv} &= \mathcal{O}_{tu}^{(8)} + \mathcal{O}_{td}^{(8)} + \mathcal{O}_{tq}^{(8)} + \mathcal{O}_{Qu}^{(8)} + \mathcal{O}_{Qd}^{(8)} + \mathcal{O}_{Qq}^{(8,1)}, \\ &= \mathcal{O}_{VV},\end{aligned}\quad (136)$$

³³³ with \mathcal{O}_{VV} given in (136).

Differences between those same operators are asymmetric under heavy quarks exchange.

$$\begin{aligned}\mathcal{O}_{Rv} - \mathcal{O}_{Lv} &= (\bar{t}_R \gamma^\mu T^A t_R - \bar{Q}_L \gamma^\mu T^A Q_L) (\bar{q} \gamma_\mu T^A q), \\ &= (\bar{t} \gamma^\mu T^A (t_R - t_L)) (\bar{q} \gamma_\mu T^A q) - (\bar{b}_L \gamma^\mu T^A b_L) (\bar{q} \gamma_\mu T^A q), \\ &= (\bar{t} \gamma^\mu T^A \gamma_5 t) (\bar{q} \gamma_\mu T^A q) + (\bar{b}_L \gamma^\mu T^A \gamma_5 b_L) (\bar{q} \gamma_\mu T^A q) \equiv \mathcal{O}_{Av},\end{aligned}\quad (137)$$

where we use that ψ_L and ψ_R are the eigenvectors of γ_5 , with eigenvalues $-1, 1$ respectively.¹² If the b_L -dependent contribution is, again, disregarded

$$\begin{aligned}\mathcal{O}_{Av} &= \mathcal{O}_{tu}^{(8)} + \mathcal{O}_{td}^{(8)} + \mathcal{O}_{tq}^{(8)} - \mathcal{O}_{Qu}^{(8)} - \mathcal{O}_{Qd}^{(8)} - \mathcal{O}_{Qq}^{(8,1)}, \\ &= \mathcal{O}_{VA},\end{aligned}\quad (139)$$

³³⁴ with \mathcal{O}_{VA} given by (139). Observe though, that [2] is misleading, pointing to the wrong equivalence between \mathcal{O}_{Av} and \mathcal{O}_{AV} .

The same procedure can be made for the asymmetric combination of light quarks

$$\mathcal{O}_{Ra} = \mathcal{O}_{tu}^{(8)} + \mathcal{O}_{td}^{(8)} - \mathcal{O}_{tq}^{(8)} \quad (140)$$

$$= (\bar{t}_R \gamma^\mu T^A t_R) (\bar{q} \gamma_\mu \gamma_5 T^A q), \quad (141)$$

$$\mathcal{O}_{La} = \mathcal{O}_{Qu}^{(8)} + \mathcal{O}_{Qd}^{(8)} - \mathcal{O}_{Qq}^{(8,1)} \quad (142)$$

$$= (\bar{Q}_L \gamma^\mu T^A Q_L) (\bar{q} \gamma_\mu \gamma_5 T^A q). \quad (143)$$

And they can also be combined in symmetric and antisymmetric combinations of heavy quarks:

$$\mathcal{O}_{Va} \equiv \mathcal{O}_{Ra} + \mathcal{O}_{La} = ((\bar{t} \quad \bar{b}_L) \gamma^\mu T^A \begin{pmatrix} t \\ b_L \end{pmatrix}) (\bar{q} \gamma_\mu \gamma_5 T^A q), \quad (144)$$

$$\mathcal{O}_{Aa} \equiv \mathcal{O}_{Ra} - \mathcal{O}_{La} = ((\bar{t} \quad \bar{b}_L) \gamma^\mu \gamma_5 T^A \begin{pmatrix} t \\ b_L \end{pmatrix}) (\bar{q} \gamma_\mu \gamma_5 T^A q), \quad (145)$$

which, when ignoring the b_L terms defines the operators \mathcal{O}_{AV} (117) and \mathcal{O}_{AA} (118), which associate to

$$\mathcal{O}_{AV} = \mathcal{O}_{tu}^{(8)} + \mathcal{O}_{td}^{(8)} - \mathcal{O}_{tq}^{(8)} + \mathcal{O}_{Qu}^{(8)} + \mathcal{O}_{Qd}^{(8)} - \mathcal{O}_{Qq}^{(8,1)}, \quad (146)$$

$$\mathcal{O}_{AA} = \mathcal{O}_{tu}^{(8)} + \mathcal{O}_{td}^{(8)} - \mathcal{O}_{tq}^{(8)} - \mathcal{O}_{Qu}^{(8)} - \mathcal{O}_{Qd}^{(8)} + \mathcal{O}_{Qq}^{(8,1)}. \quad (147)$$

¹² In order to see that, one just need to use the projection operators

$$\gamma_5 \psi_L = \frac{\gamma_5 - (\gamma_5)^2}{2} \psi = -\psi_L \text{ and } \gamma_5 \psi_R = \frac{\gamma_5 + (\gamma_5)^2}{2} \psi = \psi_R = . \quad (138)$$

Because the relation between the operators in the two basis are known, their contribution to each observable can be proportional to the sum of their Wilson Coefficients (presumably averaged over the number of flavours and generation)

$$c_{Vv} = c_{Rv} + c_{Lv}, \quad (148)$$

$$c_{Av} = c_{Rv} - c_{Lv}, \quad (149)$$

where [4]

$$c_{Rv} = \frac{1}{2}((c_{tu} + c_{td})/2 + c_{tq}), \quad (150)$$

$$c_{Lv} = \frac{1}{2}((c_{Qu} + c_{Qd})/2 + c_{Qq}^{(8,1)}). \quad (151)$$

But in [2] only the first generation of light quarks are considered, therefore, the correct expression might be

$$c_{Rv} = (c_{tu} + c_{td})/2 + c_{tq}, \quad (152)$$

$$c_{Lv} = (c_{Qu} + c_{Qd})/2 + c_{Qq}^{(8,1)}. \quad (153)$$

And

$$c_{Va} = c_{Ra} + c_{La}, \quad (154)$$

$$c_{Aa} = c_{Ra} - c_{La}, \quad (155)$$

where

$$c_{Ra} = \frac{1}{2}((c_{tu} + c_{td})/2 - c_{tq}), \quad (156)$$

$$c_{La} = \frac{1}{2}((c_{Qu} + c_{Qd})/2 - c_{Qq}^{(8,1)}). \quad (157)$$

or

$$c_{Ra} = (c_{tu} + c_{td})/2 - c_{tq}, \quad (158)$$

$$c_{La} = (c_{Qu} + c_{Qd})/2 - c_{Qq}^{(8,1)}. \quad (159)$$

This gives

$$c_{VV} = 2 \times \frac{1}{4} (c_{tu} + c_{Qu} + c_{td} + c_{Qd} + 2c_{tq} + 2c_{Qq}^{(8,1)}), \quad (160)$$

$$c_{VA} = 2 \times \frac{1}{4} (c_{tu} - c_{Qu} + c_{td} - c_{Qd} + 2c_{tq} + 2c_{Qq}^{(8,1)}), \quad (161)$$

$$c_{VA} = 2 \times \frac{1}{4} (c_{tu} + c_{Qu} + c_{td} + c_{Qd} - 2c_{tq} - 2c_{Qq}^{(8,1)}), \quad (162)$$

$$c_{AV} = 2 \times \frac{1}{4} (c_{tu} - c_{Qu} + c_{td} - c_{Qd} - 2c_{tq} + 2c_{Qq}^{(8,1)}). \quad (163)$$

When this is compared compare with the adimensional definitions given at [2], and correcting for their typo $c_{AV} \leftrightarrow c_{VA}$, the translation is

$$\hat{c}_{VV} = \frac{m_t^2}{g_s^2 \Lambda^2} \left[\left(c_{tq}^8 + c_{Qq}^{(8,1)} \right) / 2 + \left(c_{tu}^8 + c_{td}^8 + c_{Qu}^8 + c_{Qd}^8 \right) / 4 \right], \quad (164)$$

$$\hat{c}_{AA} = \frac{m_t^2}{g_s^2 \Lambda^2} \left[-\left(c_{tq}^8 - c_{Qq}^{(8,1)} \right) / 2 + \left(c_{tu}^8 + c_{td}^8 - c_{Qu}^8 - c_{Qd}^8 \right) / 4 \right], \quad (165)$$

$$\hat{c}_{AV} = \frac{m_t^2}{g_s^2 \Lambda^2} \left[\left(c_{tq}^8 - c_{Qq}^{(8,1)} \right) / 2 + \left(c_{tu}^8 + c_{td}^8 - c_{Qu}^8 - c_{Qd}^8 \right) / 4 \right], \quad (166)$$

$$\hat{c}_{VA} = \frac{m_t^2}{g_s^2 \Lambda^2} \left[-\left(c_{tq}^8 + c_{Qq}^{(8,1)} \right) / 2 + \left(c_{tu}^8 + c_{td}^8 + c_{Qu}^8 + c_{Qd}^8 \right) / 4 \right]. \quad (167)$$

³³⁶ B.2.2 Isospin-1 operators

The translation for the isospin-1 sector is pointed in [2] as

$$\hat{c}_1 = \frac{m_t^2}{g_s^2 \Lambda^2} \left[\left(c_{tu}^8 - c_{td}^8 \right) / 2 + \left(c_{Qu}^8 - c_{Qd}^8 \right) / 2 + c_{Qq}^{(8,3)} \right], \quad (168)$$

$$\hat{c}_2 = \frac{m_t^2}{g_s^2 \Lambda^2} \left[\left(c_{tu}^8 - c_{td}^8 \right) / 2 - \left(c_{Qu}^8 - c_{Qd}^8 \right) / 2 + c_{Qq}^{(8,3)} \right], \quad (169)$$

$$\hat{c}_3 = \frac{m_t^2}{g_s^2 \Lambda^2} \left[\left(c_{tu}^8 - c_{td}^8 \right) / 2 - \left(c_{Qu}^8 - c_{Qd}^8 \right) / 2 - c_{Qq}^{(8,3)} \right]. \quad (170)$$

And from that we can also find another combination used in [2]

$$\hat{c}_1 - \hat{c}_2 + \hat{c}_3 = \frac{m_t^2}{g_s^2 \Lambda^2} \left[\left(c_{tu}^8 - c_{td}^8 \right) / 2 + \left(c_{Qu}^8 - c_{Qd}^8 \right) / 2 - c_{Qq}^{(8,3)} \right]. \quad (171)$$

Here we will find the expression for the corresponding operator

$$\mathcal{O}_1^1 - \mathcal{O}_2^1 + \mathcal{O}_3^1 = (\bar{q} \gamma^\mu T^A \sigma_3 q) (\bar{t} \gamma_\mu T^A t + \bar{t} \gamma_\mu \gamma_5 T^A t) \quad (172)$$

$$- (\bar{q} \gamma^\mu \gamma_5 T^A \sigma_3 q) (\bar{t} \gamma_\mu \gamma_5 T^A t) + 3(\bar{q} \gamma^\mu \gamma_5 T^A \sigma_3 q) (\bar{t} \gamma_\mu T^A t) \quad (173)$$

$$= (\bar{q} \gamma^\mu T^A \sigma_3 q - q \gamma^\mu \gamma_5 T^A \sigma_3 q) (\bar{t} \gamma_\mu \gamma_5 T^A t) \quad (174)$$

$$+ (\bar{q} \gamma^\mu T^A \sigma_3 q) (\bar{t} \gamma_\mu T^A t) + 3(\bar{q} \gamma^\mu \gamma_5 T^A \sigma_3 q) (\bar{t} \gamma_\mu T^A t) \quad (175)$$

$$= (\bar{q} \gamma^\mu T^A \sigma_3 q - q \gamma^\mu \gamma_5 T^A \sigma_3 q) (\bar{t} \gamma_\mu \gamma_5 T^A t + \bar{t} \gamma_\mu T^A t - \bar{t} \gamma_\mu T^A t) \quad (176)$$

$$+ (\bar{q} \gamma^\mu T^A \sigma_3 q) (\bar{t} \gamma_\mu T^A t) + 3(\bar{q} \gamma^\mu \gamma_5 T^A \sigma_3 q) (\bar{t} \gamma_\mu T^A t) \quad (177)$$

$$= (\bar{q} \gamma^\mu T^A \sigma_3 q - q \gamma^\mu \gamma_5 T^A \sigma_3 q) (\bar{t} \gamma_\mu \gamma_5 T^A t + \bar{t} \gamma_\mu T^A t) \quad (178)$$

$$+ (\bar{q} \gamma^\mu \gamma_5 T^A \sigma_3 q) (\bar{t} \gamma_\mu T^A t) + 3(\bar{q} \gamma^\mu \gamma_5 T^A \sigma_3 q) (\bar{t} \gamma_\mu T^A t) \quad (179)$$

$$= 2(\bar{q} \gamma^\mu T^A \sigma_3 P_L q) 2(\bar{t} \gamma_\mu T^A P_R t) \quad (180)$$

$$+ 4(\bar{q} \gamma^\mu \gamma_5 T^A \sigma_3 q) (\bar{t} \gamma_\mu T^A t) \quad (181)$$

$$(182)$$

³³⁷ B.3 Basis validation via Monte Carlo generation

³³⁸ B.3.1 Validation via total inclusive cross-section

When using only u and d as initial states quarks:

$$c'_{VV} = \frac{1}{2} \left[\left(c_{tq}^8 + c_{Qq}^{(8,1)} \right) / 2 + \left(c_{tu}^8 + c_{td}^8 + c_{Qu}^8 + c_{Qd}^8 \right) / 4 \right], \quad (183)$$

	c'_{VV} ($= \hat{c}_{VV}/(2m_t^2/g_s^2)$)	c'_1 ($= \hat{c}_1/(2m_t^2/g_s^2)$)	c_{tG} ($= \hat{u}_t/(2m_t^2)$)
σ_{lin} [pb]	28.064 ± 0.078	2.626 ± 0.060	147.767 ± 0.079
σ_{quad} [pb]	6.800 ± 0.016	3.007 ± 0.012	26.360 ± 0.016

Table 5: Cross-section interpolation parameters for different EFT operators, using samples with Wilson Coefficients equal 0 (SM), 4.0 and 8.0 to perform a quadratic interpolation.

	\hat{c}_{VV}	\hat{c}_1	\hat{u}_t
σ_{lin} [pb]	692.49 ± 1.9	64.798 ± 1.5	2458.9 ± 1.3
σ_{quad} [pb]	4140.4 ± 9.7	1830.9 ± 7.3	7299.4 ± 4.4

Table 6: Cross-section interpolation parameters re-scaled to match the operators definitions of arXiv:1508.05271

with

$$\hat{c}_{VV} = \frac{m_t^2}{g_s^2 \Lambda^2} c'_{VV} \quad (184)$$

we had a linear term of $\sigma'_{lin} = 45.18 \pm 0.03043$ pb for $c_{VV} = 1$. That corresponds to

$$\sigma_{lin} = (45.18 \pm 0.03043) \times \left(\frac{m_t^2}{g_s^2 \Lambda^2} \right)^{-1} = 555.20 \pm 0.36 \text{ pb} \quad (185)$$

³³⁹ This differs from Bernreuther's for about 4.5 percent level.

Using the translation

$$\hat{c}_{VV-1gen} = 2 \frac{m_t^2}{g_s^2 \Lambda^2} \left[\left(c_{tq}^8 + c_{Qq}^{(8,1)} \right) / 2 + \left(c_{tu}^8 + c_{td}^8 + c_{Qu}^8 + c_{Qd}^8 \right) / 4 \right] \quad (186)$$

³⁴⁰ we got to equivalent results.

On the other hand, when we use the first two generation of quarks, the correct translation is

$$\hat{c}_{VV-2gen} = \frac{m_t^2}{g_s^2 \Lambda^2} \left[\left(c_{tq}^8 + c_{Qq}^{(8,1)} \right) / 2 + \left(c_{tu}^8 + c_{td}^8 + c_{Qu}^8 + c_{Qd}^8 \right) / 4 \right] \quad (187)$$

and this gives

$$\sigma_{lin} = 694 \pm 0.6538 \quad (188)$$

a similar result is obtained when we calculate the linear term via 183 $\sigma'_{lin} = 28.14 \pm 0.01849$ pb, which, using the conversion:

$$\sigma_{lin} = (28.14 \pm 0.01849) \times \left(\frac{m_t^2}{2g_s^2 \Lambda^2} \right)^{-1} = 694.37 \pm 0.46 \text{ pb} \quad (189)$$

Now we look at the operator c_1 , for the basis translation we use

$$c'_1 = \frac{1}{2} \left[\left(c_{tu}^8 - c_{td}^8 \right) / 2 + \left(c_{Qu}^8 - c_{Qd}^8 \right) / 2 + c_{Qq}^{(8,3)} \right], \quad (190)$$

when we account only for u and d in the initial state. This has resulted in a cross-section of $\sigma'_{lin} = 1.585 \pm 0.005835$ pb. When we apply the conversion

$$\sigma_{lin} = (1.585 \pm 0.005835 \text{ pb}) \times \left(\frac{m_t^2}{4g_s^2 \Lambda^2} \right)^{-1} = 78.22 \pm 0.28 \text{ pb} \quad (191)$$

And equivalent results were recovered when using directly

$$\hat{c}_{1,1gen} = \frac{m_t^2}{2g_s^2\Lambda^2} \left[(c_{tu}^8 - c_{td}^8)/2 + (c_{Qu}^8 - c_{Qd}^8)/2 + c_{Qq}^{(8,3)} \right]. \quad (192)$$

³⁴¹ for the translation.

On the other hand, if we calculate c'_1 for the $pp \rightarrow t\bar{t}$ we get $\sigma'_{lin} = 2.623 \pm 0.01171$ pb which, when we apply the conversion

$$\sigma_{lin} = (2.623 \pm 0.011 pb) \times \left(\frac{m_t^2}{2g_s^2\Lambda^2} \right)^{-1} = 64.74 \pm 0.29 \text{pb} \quad (193)$$

we can also be achieved by using the basis translation

$$\hat{c}_{1,2gen} = \frac{m_t^2}{g_s^2\Lambda^2} \left[(c_{tu}^8 - c_{td}^8)/2 + (c_{Qu}^8 - c_{Qd}^8)/2 + c_{Qq}^{(8,3)} \right]. \quad (194)$$



DRAFT

342 **C Additional Information**

343 **C.1 Additional Spin Observables**

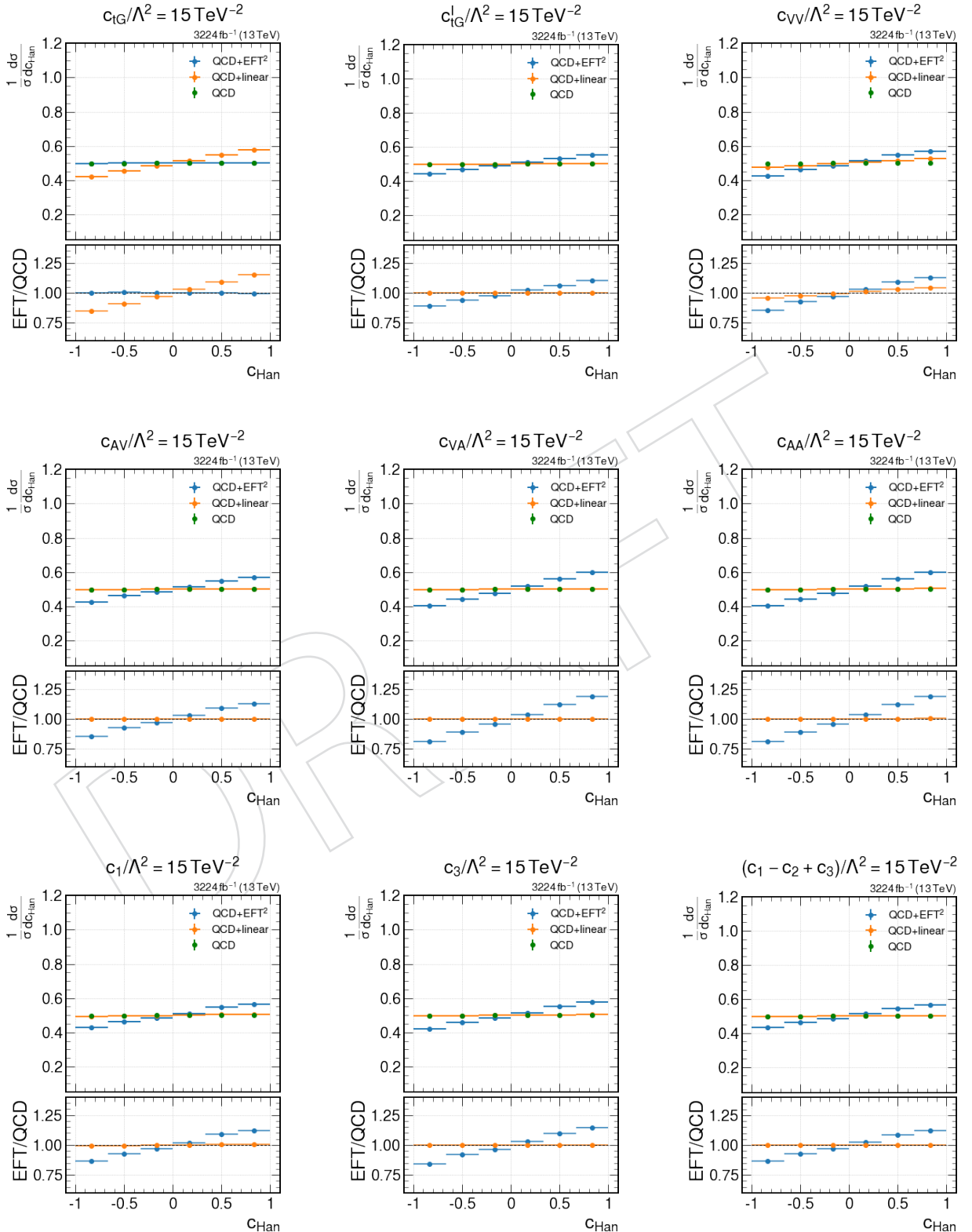


Figure 31: Lepton angular distribution showing the linear and quadratic contributions of each experiment-based EFT coefficients compared to the LO-SM contribution.

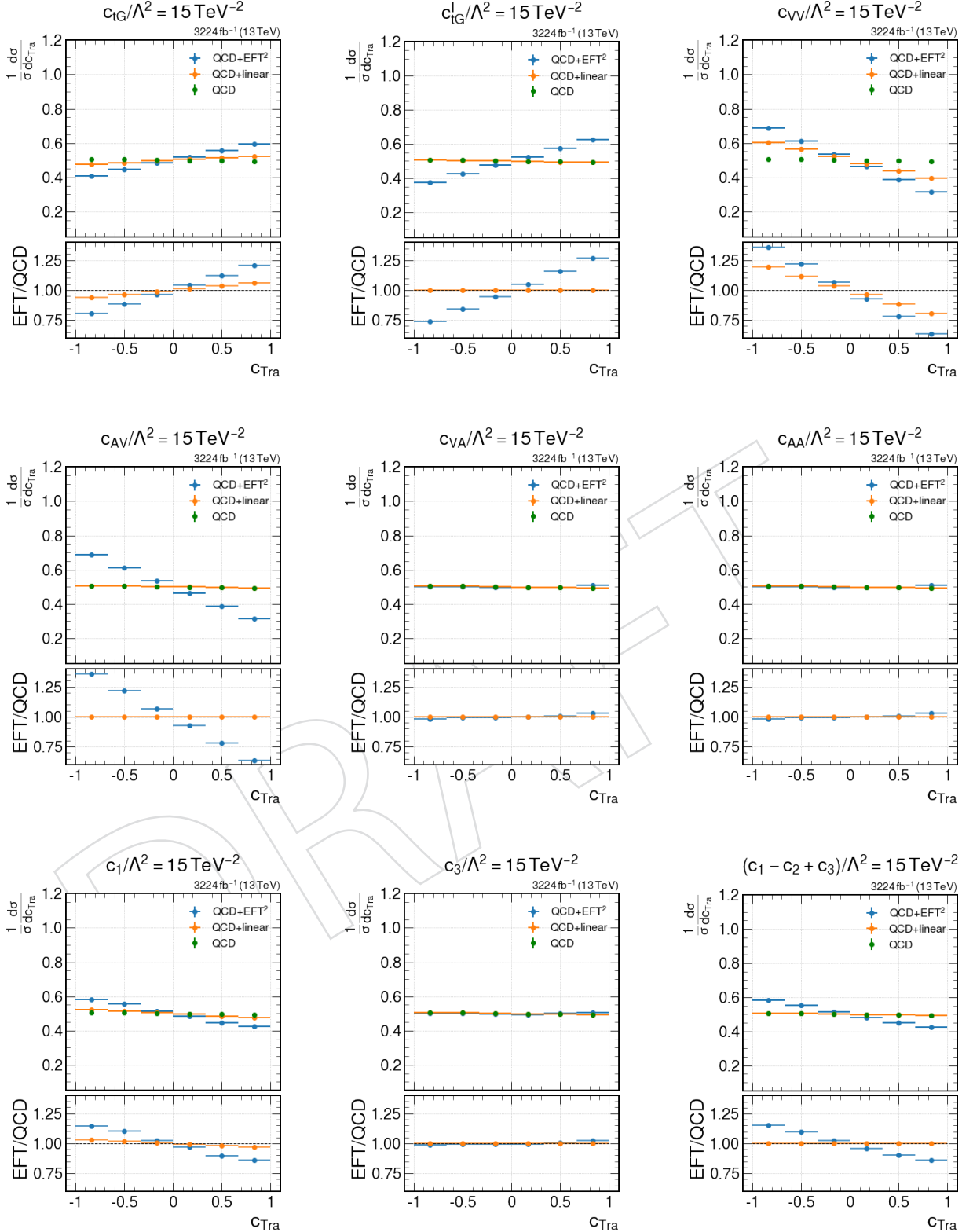


Figure 32: Lepton angular distribution showing the linear and quadratic contributions of each experiment-based EFT coefficients compared to the LO-SM contribution.

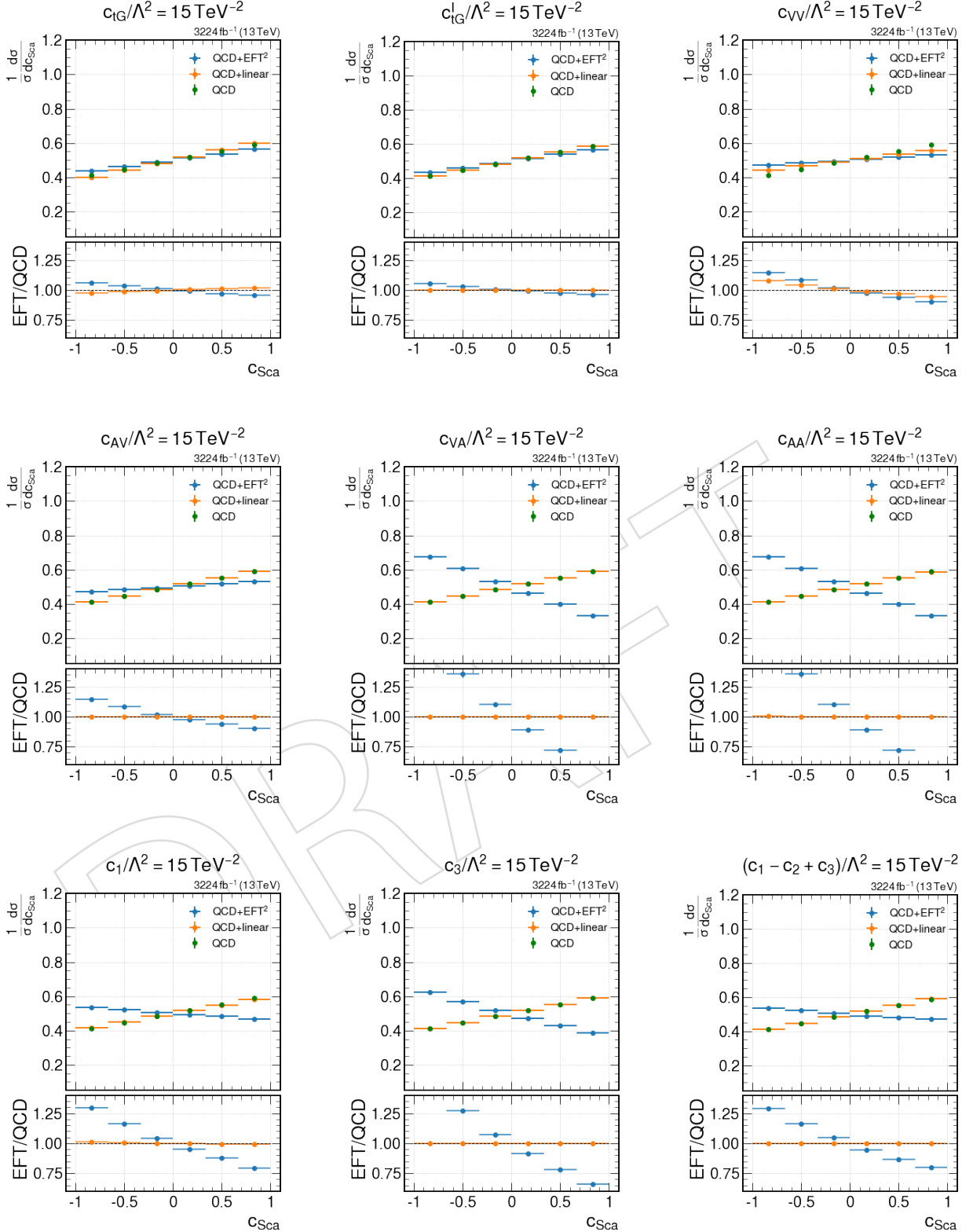


Figure 33: Lepton angular distribution showing the linear and quadratic contributions of each experiment-based EFT coefficients compared to the LO-SM contribution.

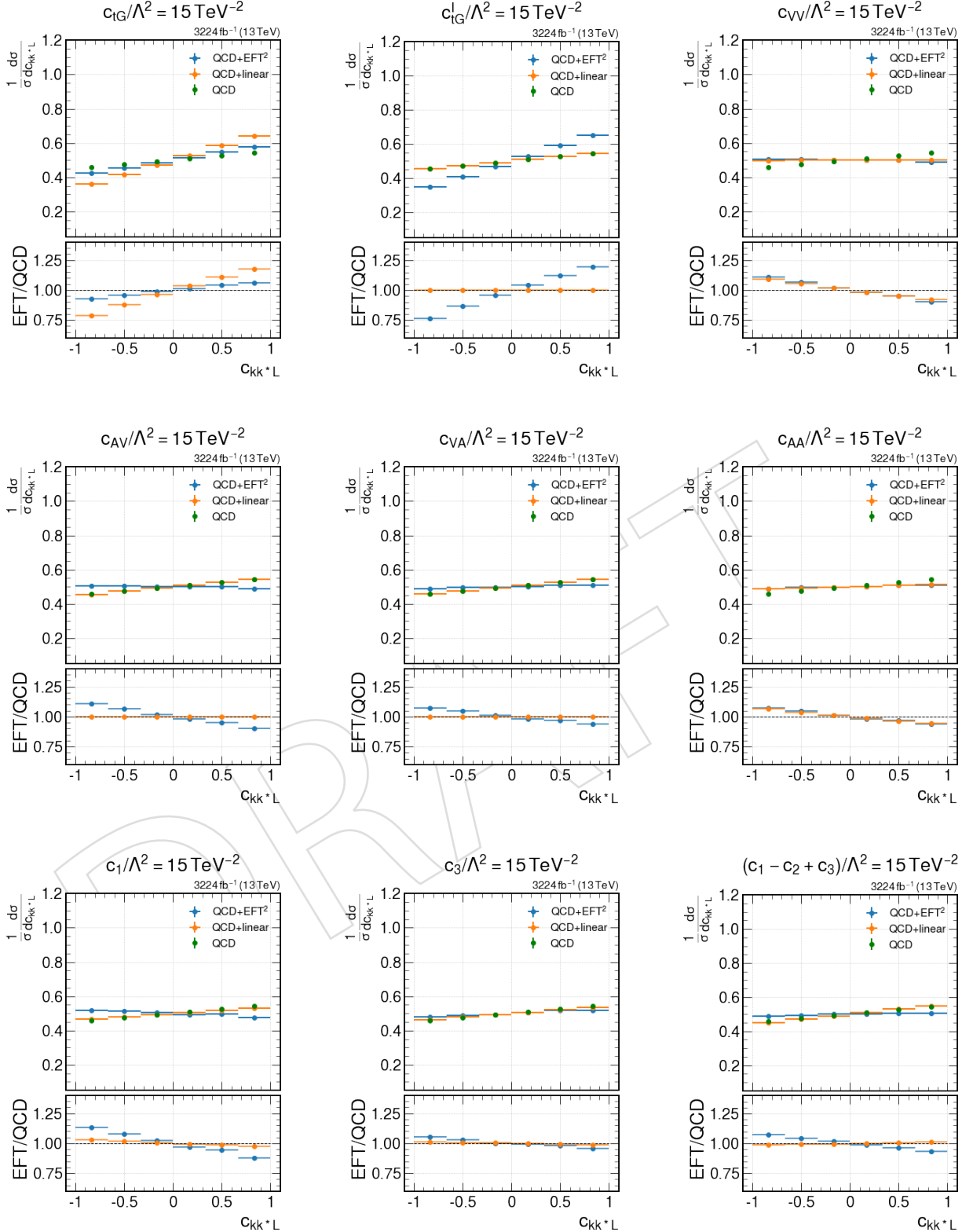


Figure 34: Lepton angular distribution showing the linear and quadratic contributions of each experiment-based EFT coefficients compared to the LO-SM contribution.

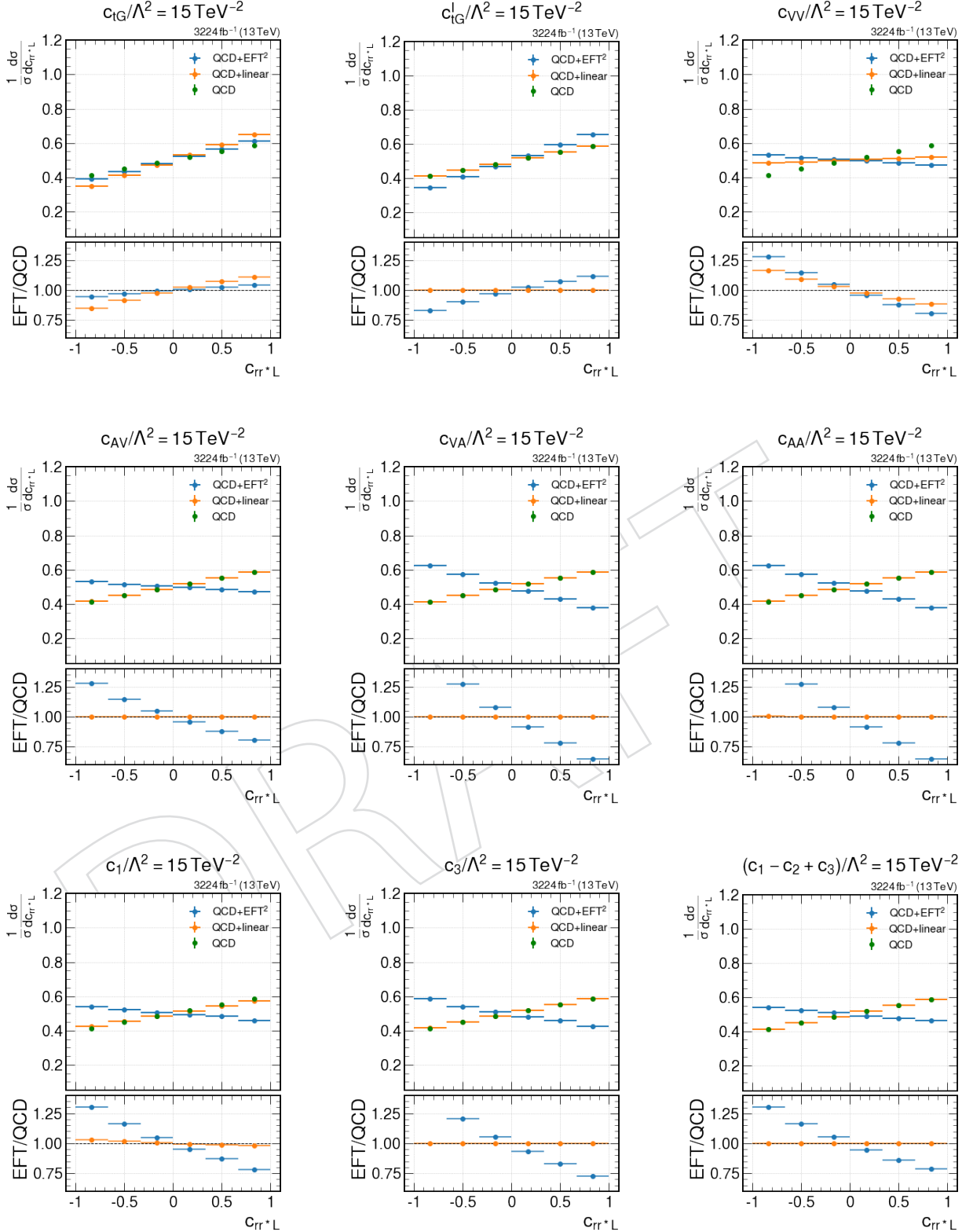


Figure 35: Lepton angular distribution showing the linear and quadratic contributions of each experiment-based EFT coefficients compared to the LO-SM contribution.

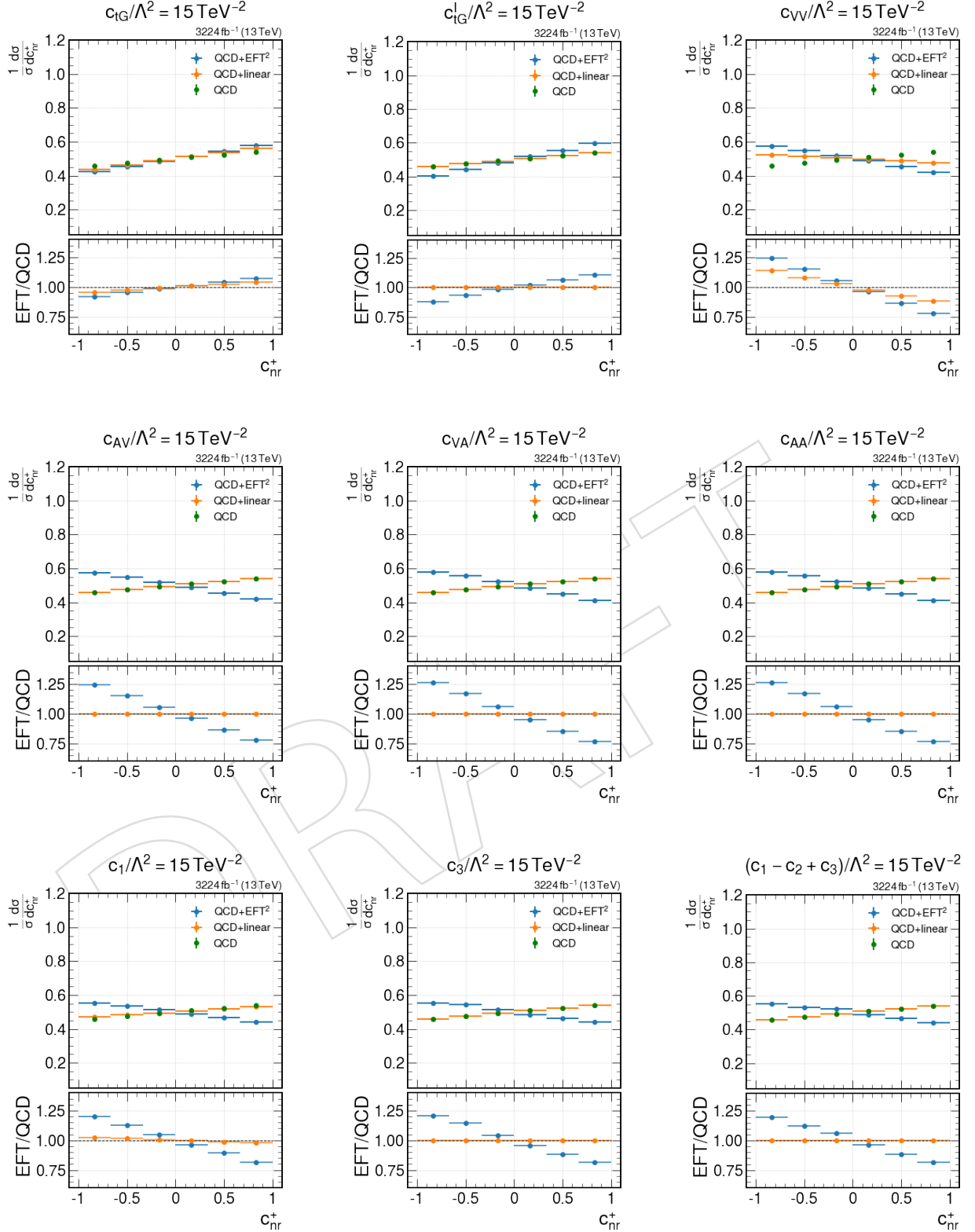


Figure 36: Lepton angular distribution showing the linear and quadratic contributions of each experiment-based EFT coefficients compared to the LO-SM contribution.

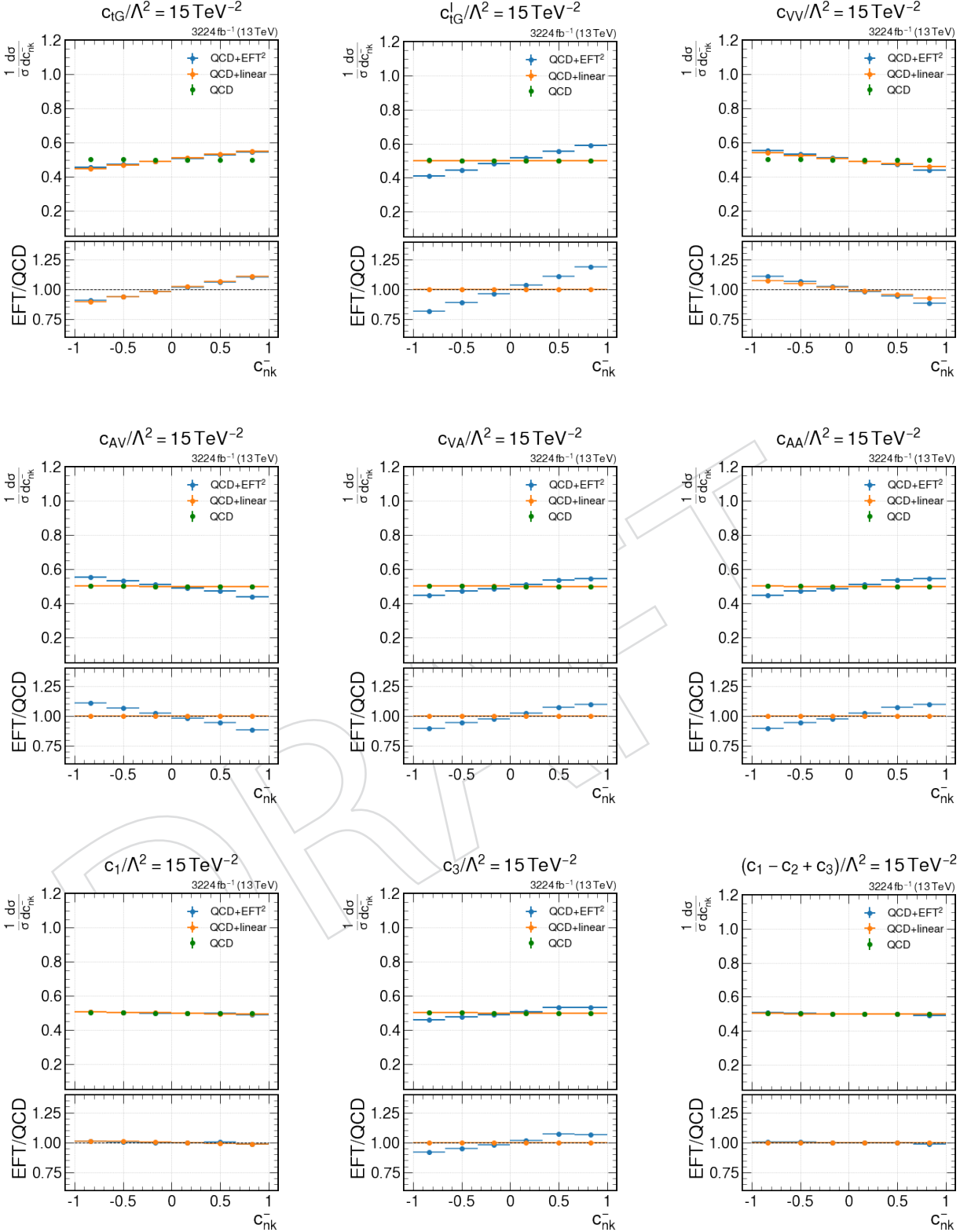


Figure 37: Lepton angular distribution showing the linear and quadratic contributions of each experiment-based EFT coefficients compared to the LO-SM contribution.

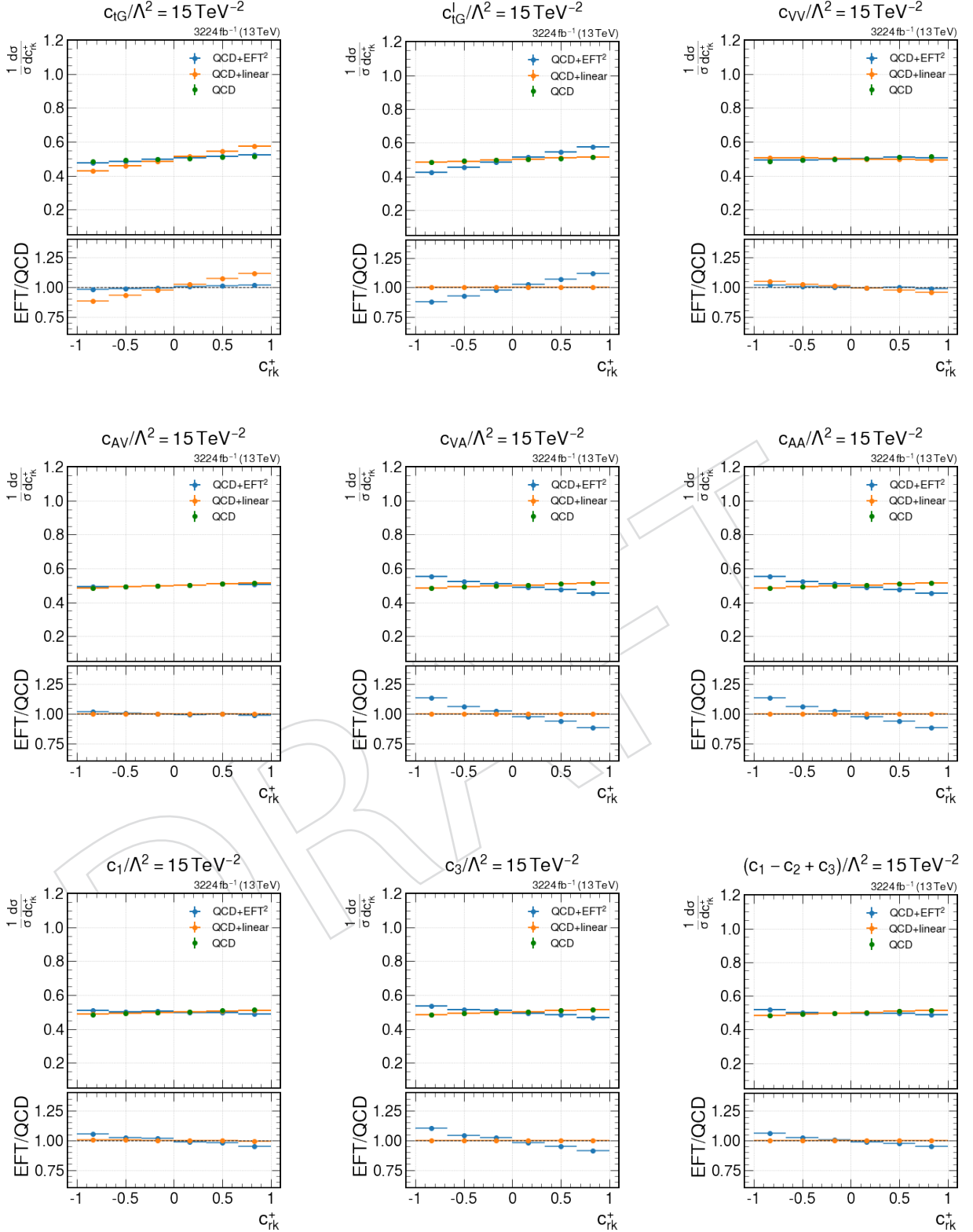


Figure 38: Lepton angular distribution showing the linear and quadratic contributions of each experiment-based EFT coefficients compared to the LO-SM contribution.

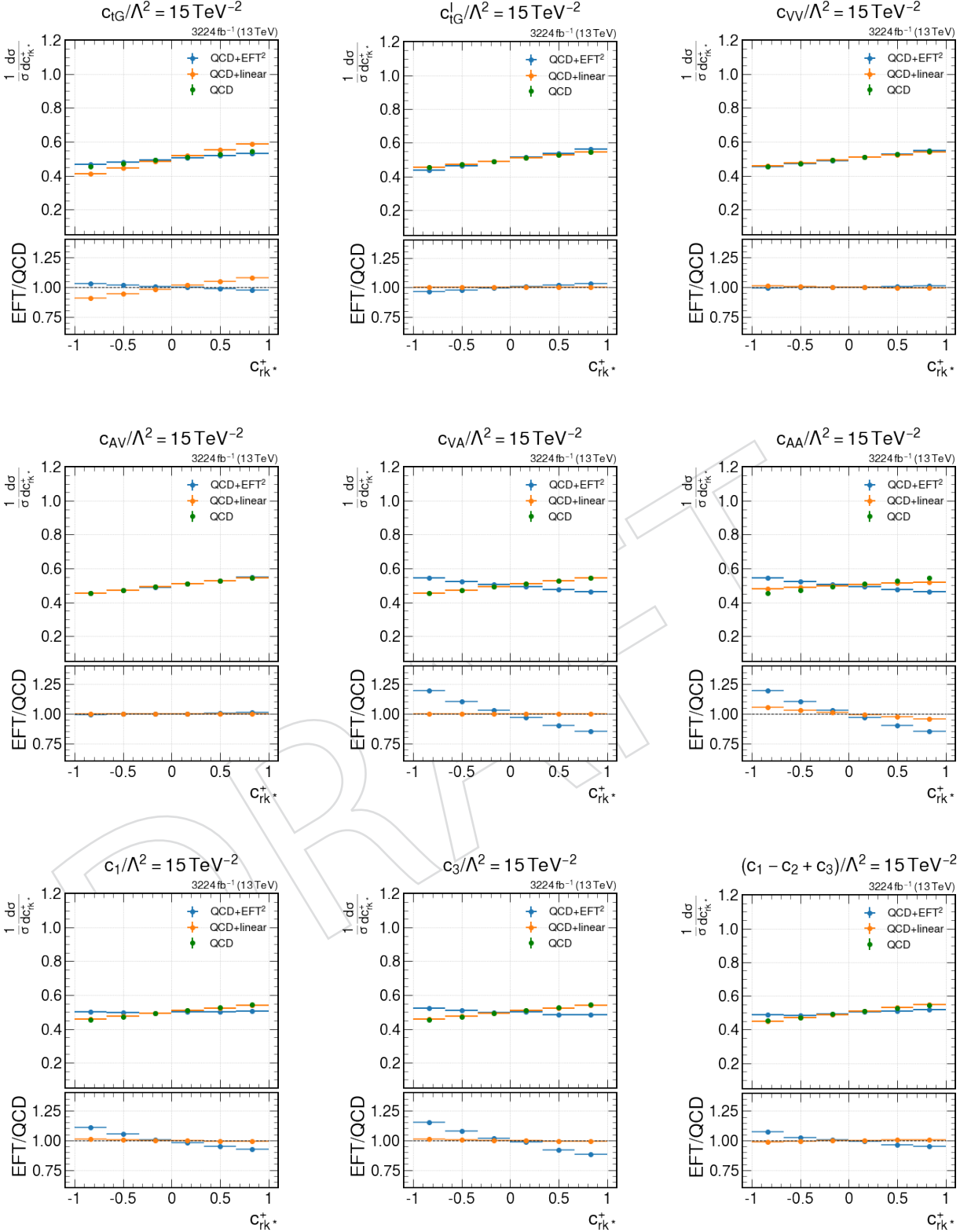


Figure 39: Lepton angular distribution showing the linear and quadratic contributions of each experiment-based EFT coefficients compared to the LO-SM contribution.

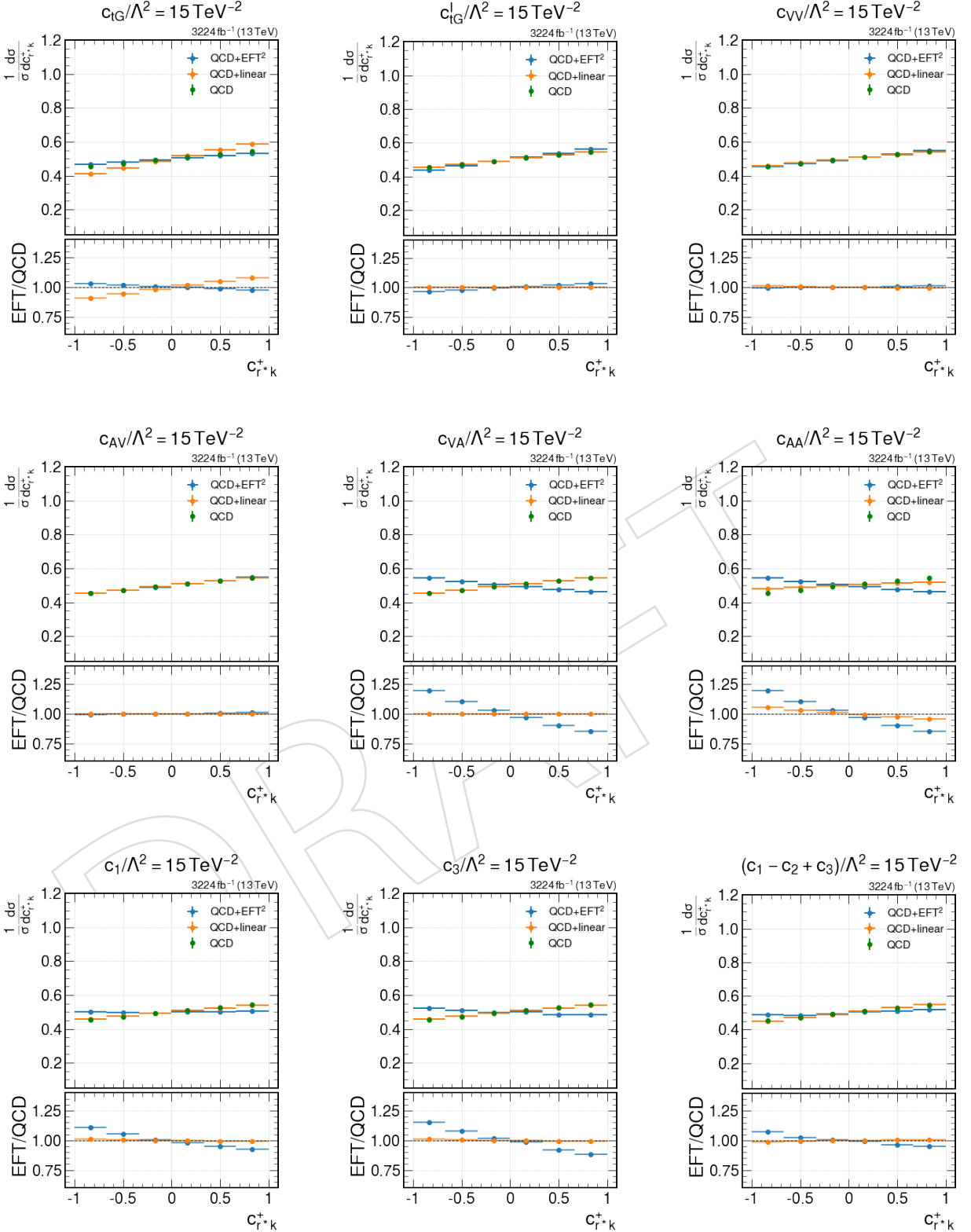


Figure 40: Lepton angular distribution showing the linear and quadratic contributions of each experiment-based EFT coefficients compared to the LO-SM contribution.

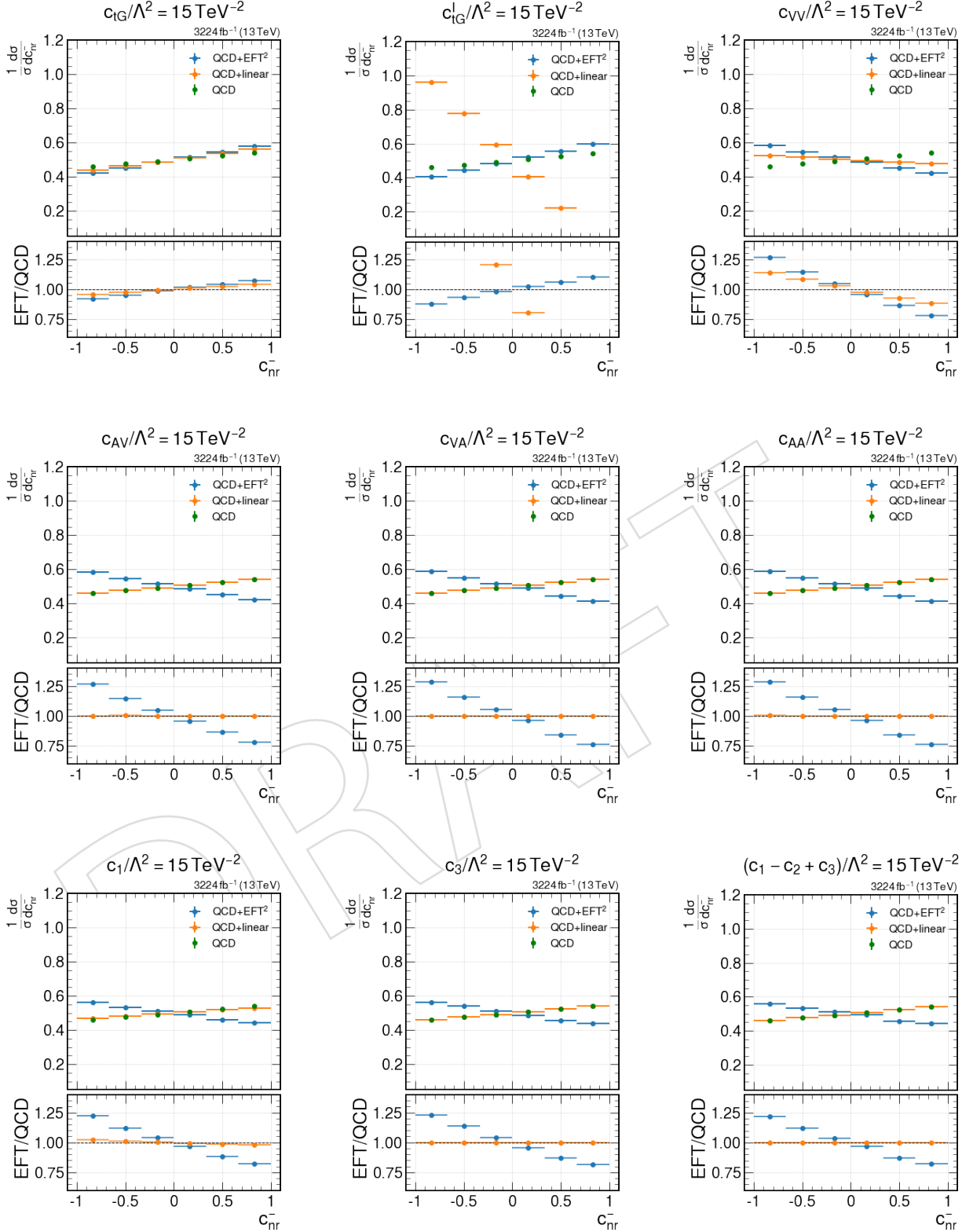


Figure 41: Lepton angular distribution showing the linear and quadratic contributions of each experiment-based EFT coefficients compared to the LO-SM contribution.

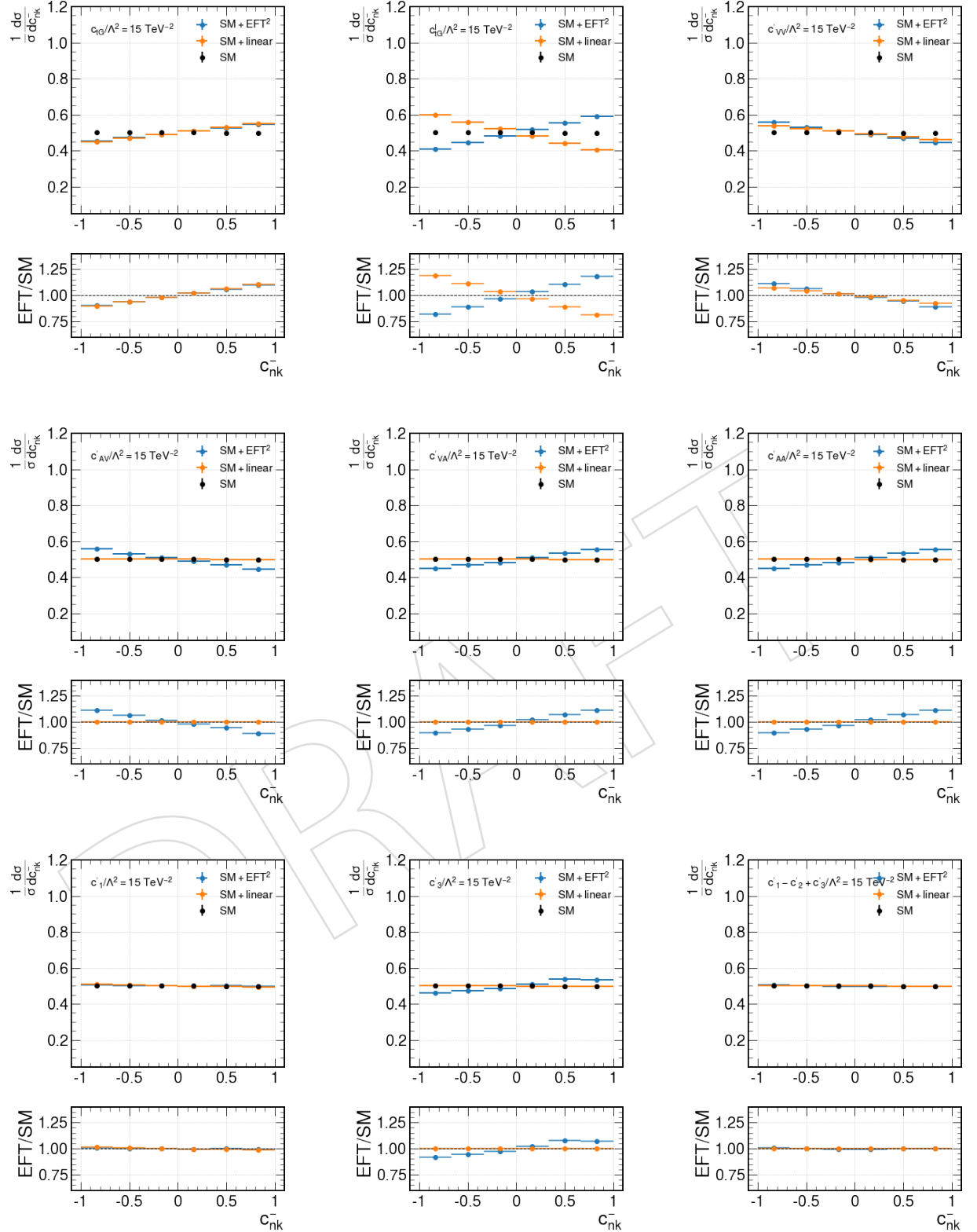


Figure 42: Lepton angular distribution showing the linear and quadratic contributions of each experiment-based EFT coefficients compared to the LO-SM contribution.

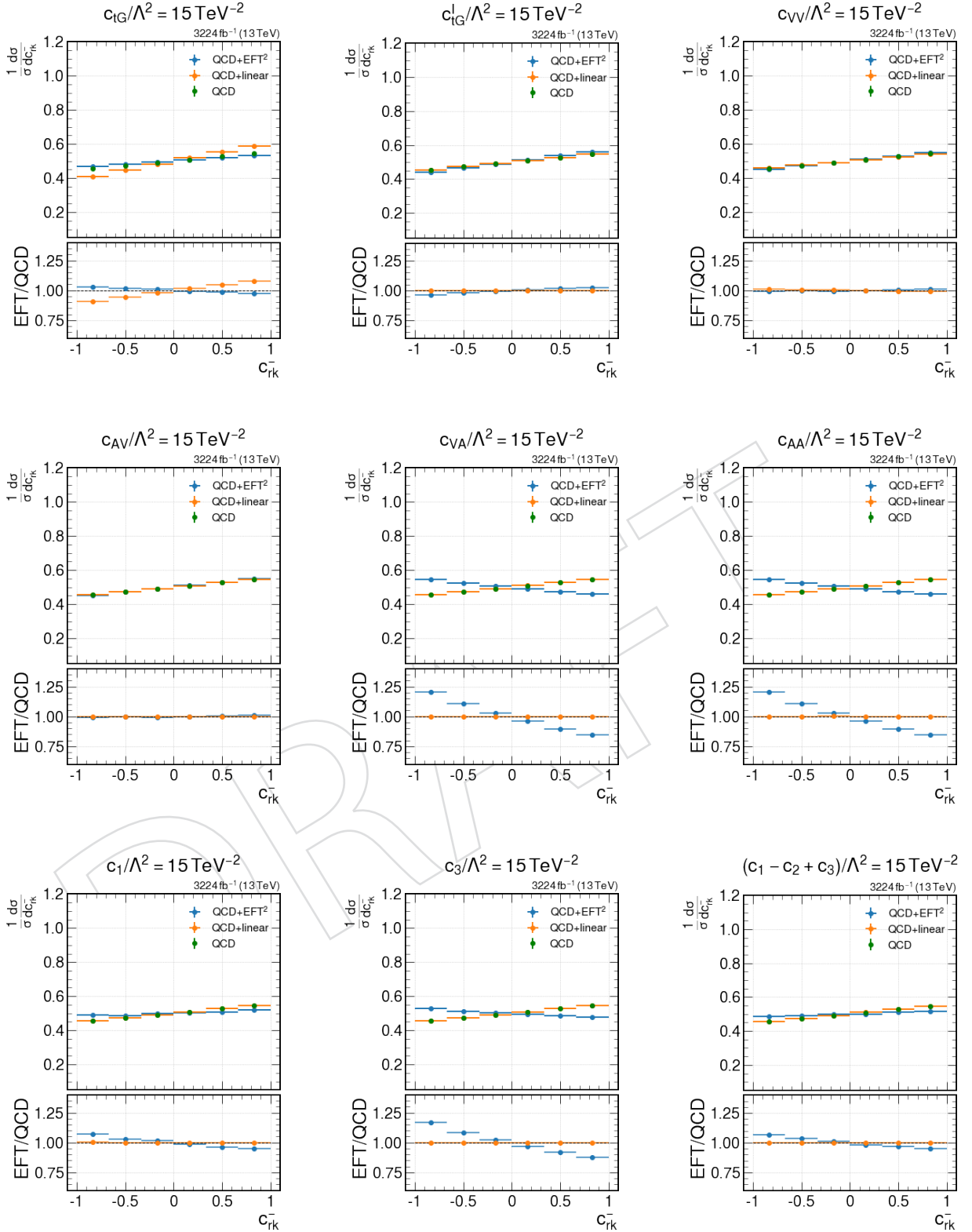


Figure 43: Lepton angular distribution showing the linear and quadratic contributions of each experiment-based EFT coefficients compared to the LO-SM contribution.

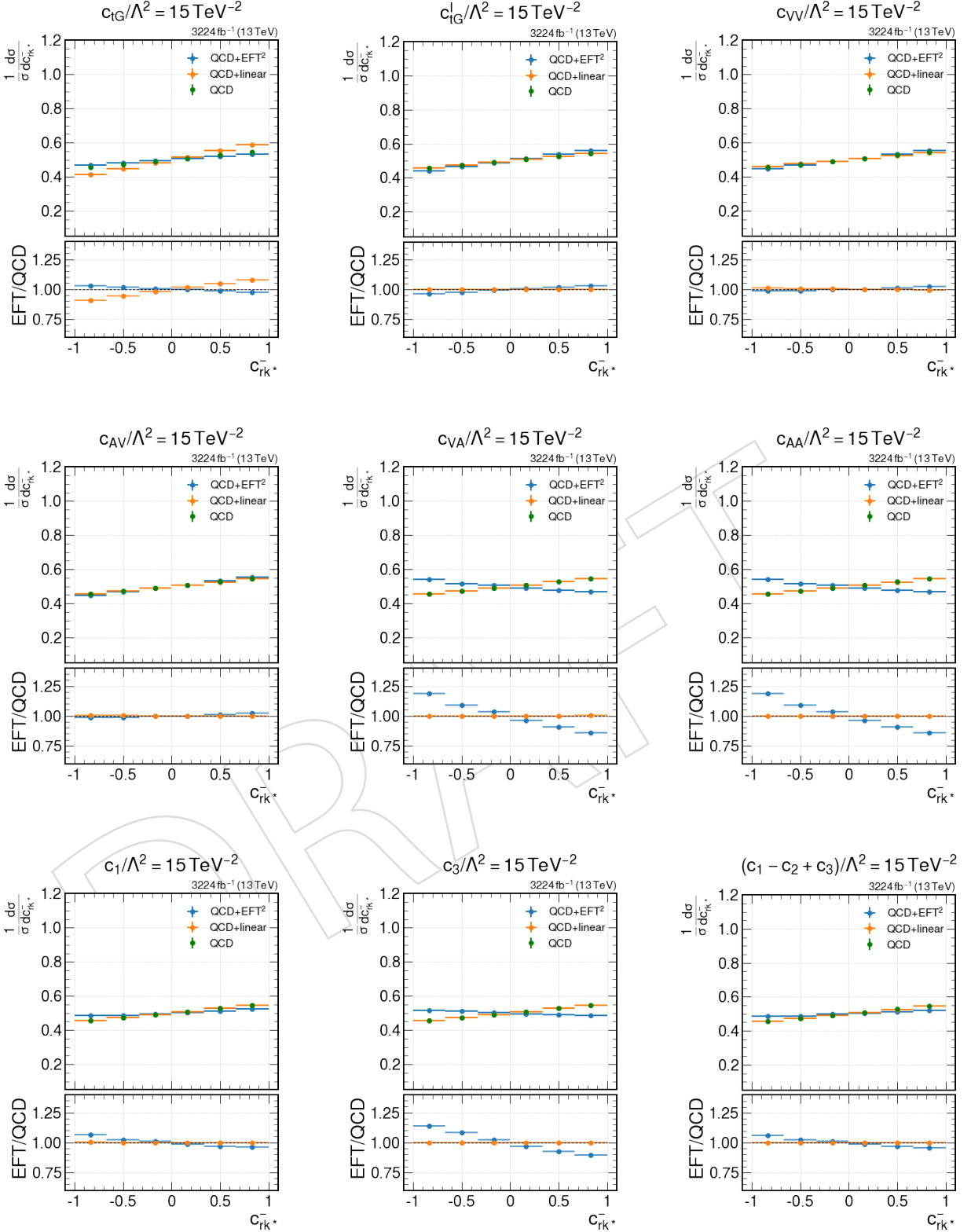


Figure 44: Lepton angular distribution showing the linear and quadratic contributions of each experiment-based EFT coefficients compared to the LO-SM contribution.

344 **C.2 Interpolation weights**

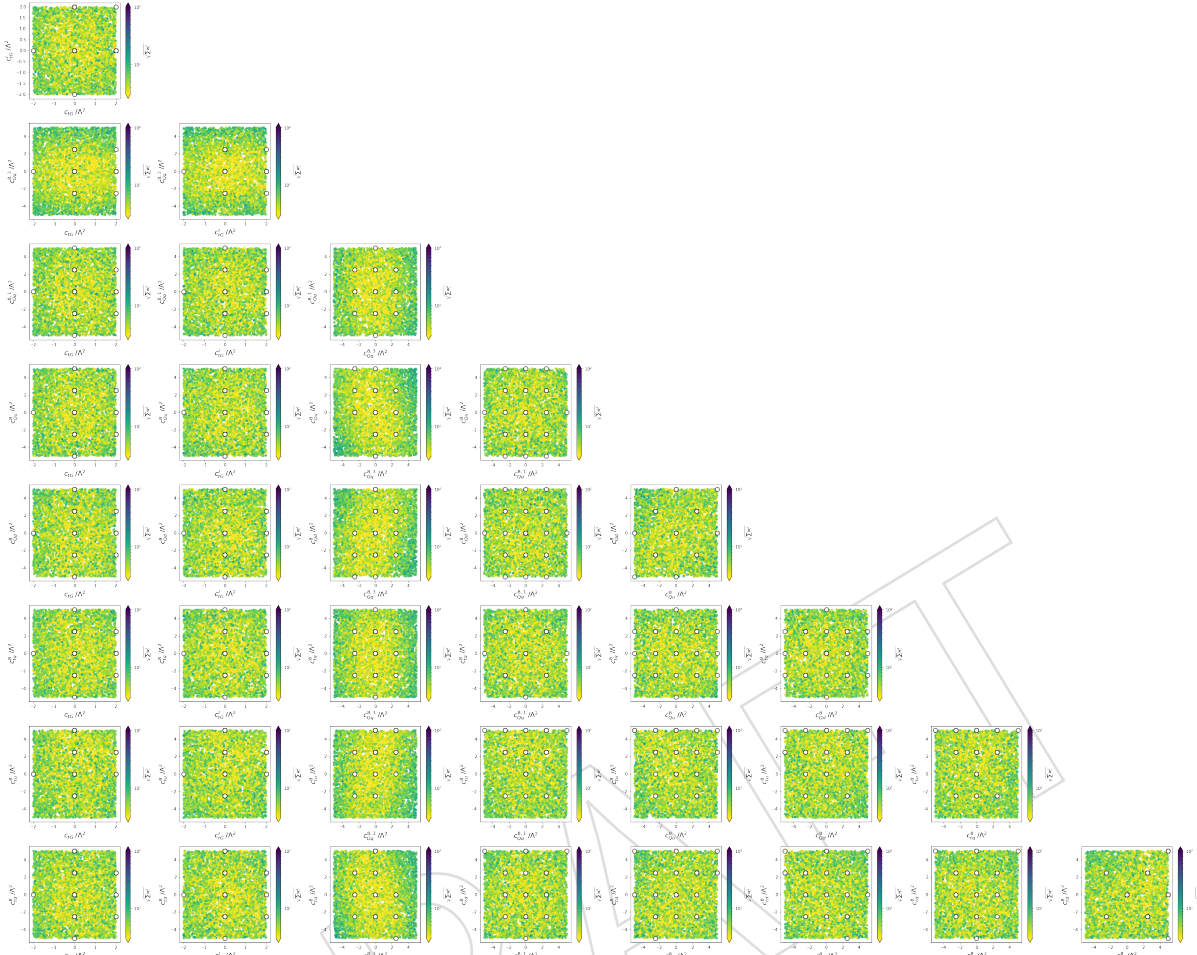


Figure 45: Interpolation weights for 1000 random test EFT hypothesis shown as a function of every 2 EFT parameters used in this study.

345 **References**

- 346 [1] CMS Collaboration Collaboration, "Measurement of the top quark polarization and $t\bar{t}$
347 spin correlations using dilepton final states in proton-proton collisions at $\sqrt{s} = 13$ TeV",
348 *Phys. Rev. D* **100** (Oct, 2019) 072002, doi:10.1103/PhysRevD.100.072002.
- 349 [2] W. Bernreuther, D. Heisler, and Z.-G. Si, "A set of top quark spin correlation and
350 polarization observables for the lhc: Standard model predictions and new physics
351 contributions", *Journal of High Energy Physics* **2015** (2015), no. 12, 1–36,
352 doi:10.1007/jhep12(2015)026, arXiv:1508.05271.
- 353 [3] J. Aguilar-Saavedra, "A minimal set of top anomalous couplings", *Nuclear Physics B* **812**
354 (2009), no. 1–2, 181–204, doi:10.1016/j.nuclphysb.2008.12.012,
355 arXiv:0811.3842.
- 356 [4] C. Degrande et al., "Non-resonant new physics in top pair production at hadron
357 colliders", *Journal of High Energy Physics* **2011** (2011), no. 3,
358 doi:10.1007/jhep03(2011)125, arXiv:1010.6304.

- [5] A. Buckley et al., "LHAPDF6: parton density access in the LHC precision era", *The European Physical Journal C* **75** (mar, 2015) doi:10.1140/epjc/s10052-015-3318-8.
- [6] C. Bierlich et al., "A comprehensive guide to the physics and usage of pythia 8.3", 2022. doi:10.48550/ARXIV.2203.11601, <https://arxiv.org/abs/2203.11601>.
- [7] J. Alwall et al., "The automated computation of tree-level and next-to-leading order differential cross sections, and their matching to parton shower simulations", *Journal of High Energy Physics* **2014** (jul, 2014) doi:10.1007/jhep07(2014)079.
- [8] J. A. Saavedra et. al, "Interpreting top-quark lhc measurements in the standard-model effective field theory", 2018.
- [9] A. Aize, "EFTFitter".
- [10] A. Anuar et al., "AN-18-288".
- [11] C. Degrande et al., "Automated one-loop computations in the standard model effective field theory", *Physical Review D* **103** (2021), no. 9, doi:10.1103/physrevd.103.096024, arXiv:2008.11743.
- [12] F. Krauss, S. Kuttmalai, and T. Plehn, "Lhc multijet events as a probe for anomalous dimension-six gluon interactions", *Phys. Rev. D* **95** (2017) 035024, doi:10.1103/PhysRevD.95.035024, arXiv:1611.00767.
- [13] V. Hirschi, F. Maltoni, I. Tsinikos, and E. Vryonidou, "Constraining anomalous gluon self-interactions at the lhc: a reappraisal", *Journal of High Energy Physics* **93** (2018) 93, doi:10.1007/JHEP07(2018)093, arXiv:1611.00767.
- [14] A. collaboration, "Measurement of the top-quark mass in $t\bar{t} + 1$ -jet events collected with the atlas detector in pp collisions at $\sqrt{s} = 8$ tev", *Journal of High Energy Physics* **2019** (2019), no. 11, doi:10.1007/jhep11(2019)150, arXiv:1905.02302.
- [15] C. Collaboration, "Measurement of the top quark mass with lepton+jets final states using p p collisions at $\sqrt{s} = 13$ TeV", *The European Physical Journal C* **78** (2018), no. 11, doi:10.1140/epjc/s10052-018-6332-9, arXiv:1805.01428.
- [16] C. Collaboration, "Measurement of the top quark yukawa coupling from $t\bar{t}$ kinematic distributions in the dilepton final state in proton-proton collisions at $\sqrt{s} = 13$ tev", *Physical Review D* **102** (2020), no. 9, doi:10.1103/physrevd.102.092013, arXiv:2009.07123.
- [17] G. Durieux, F. Maltoni, and C. Zhang, "Global approach to top-quark flavor-changing interactions", *Physical Review D* **91** (2015), no. 7, doi:10.1103/physrevd.91.074017, arXiv:1412.7166.